



CTU

**CZECH TECHNICAL
UNIVERSITY
IN PRAGUE**

Faculty of Electrical Engineering
Department of Measurement

Master's thesis

Autonomous Sensor Signal Acquisition System

Bc. Marta Křepelková

May 2017

Thesis supervisor: doc. Ing. Radislav Šmíd, Ph.D.



ZADÁNÍ DIPLOMOVÉ PRÁCE

Student: **Bc. Marta Křepelková**

Studijní program: **Kybernetika a robotika**
Obor: **Senzory a přístrojová technika**

Název tématu česky: **Autonomní systém pro záznam signálů ze senzorů**

Název tématu anglicky: **Autonomous Sensor Signal Acquisition System**

Pokyny pro vypracování:

Navrhněte a realizujte autonomní systém pro záznam signálů ze senzorů založený na mikrokontroléru STM32F4. Systém by měl umožňovat připojení analogových vstupů, tenzometrů, akcelerometrů, senzorů teploty a dalších senzorů s rozhraním I2C/SPI. V režimu autonomního měření bude po spuštění digitalizovat a ukládat data do paměti realizované SD kartou. V režimu přenosu bude umožňovat bezdrátový přenos dat do PC a nabíjení akumulátoru. Zvažte možnost bezdrátového nabíjení.

Seznam odborné literatury:

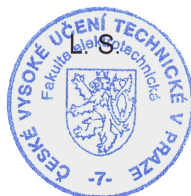
- [1] firemní literatura STMicroelectronics
- [2] Ganssle, J.: The Art of Designing Embedded Systems, Newnes 2008
- [3] Kester, W.: The Data Conversion Handbook, Newnes 2005

Vedoucí diplomové práce: doc. Ing. Radislav Šmíd, Ph.D.

Datum zadání diplomové práce: 21. prosince 2016

Platnost zadání do¹: 30. září 2018

Prof. Ing. Jan Holub, Ph.D.
vedoucí katedry



Prof. Ing. Pavel Ripka, CSc.
děkan

V Praze dne 21. 12. 2016

¹ Platnost zadání je omezena na dobu tří následujících semestrů.



Statutory Declaration

I declare that I worked out the presented thesis independently and I quoted all used sources of information in accord with Methodical instructions about ethical principles for writing an academic thesis.

In Prague 26. 5. 2017



Acknowledgements

I would first like to thank Radislav Šmíd for his guidance, supervision and inspiring discussions.

I would especially like to thank Honza Sixta who was giving me great ideas around all the hardware and software problems, was bringing my thoughts in the right direction when I got stuck and was also my big psychological support.

I would also like to thank Ondřej Hruška for his WiFi module software, as well as his devotion to help me apply it to the device.

I would like to thank the company STMicroelectronics for access to their laboratories. It would be impossible to create such complex device without full-time access to laboratory equipment, which was not provided to us.

Many thanks also go to Martin Korábečný for his comments on the English grammar.

At last but not least I would like to thank my family and boyfriend for a big support during my studies and writing this thesis. They were able to give me psychological support when I was breaking down, they were trying to make my studies easier and give me new motivation and energy. I would also like to thank my boyfriend for useful comments to my English text and its correction.

Abstrakt

Tato práce se zabývá návrhem a realizací autonomního systému pro záznam signálů ze senzorů pro měření na malých a těžce přístupných místech. Zařízení podporuje připojení osmi analogových vstupů, tří digitálních I2C vstupů, čtyř univerzálních binárních vstupů a obsahuje vestavěný digitální akcelerometr. Zařízení dále poskytuje programovatelné proudové zdroje pro napájení analogových senzorů a obvody pro zesílení signálů z analogových vstupů.

Zařízení podporuje dva módy. V režimu autonomního měření jsou po uživatelem nastavený čas zaznamenávána data z jednotlivých senzorů. Naměřená data jsou ukládána na interní microSD kartu. V režimu přenosu mohou být skrze webovou stránku konfigurovány parametry měření a stahovány soubory s naměřenými daty. Možnost připojení indukční nabíječky zajišťuje kompletní bezdrátovost celého zařízení.

Práce se zabývá hardwarovým řešením a návrhem firmwaru do mikrokontroléru STM32F411VE sloužícímu k ovládání celého zařízení a do mikrokontroléru ESP8266 obsaženém uvnitř Wi-Fi modulu.

Abstract

This thesis discusses the concept and the realisation of the autonomous sensor signal acquisition system for measurement in small and hardly accessible places. The device supports eight analog inputs, onboard digital accelerometer, three I2C digital inputs and four universal binary inputs. The device also provides programmable power sources for analog sensors and signal conditioners for amplification of the measured analog signal.


The device provides two modes. In the stand-alone mode, the system with specified settings records data for given time. The measured data are stored to the microSD card. In transfer mode, the system can be configured through the web page, and the files with measured data can be downloaded. The possibility of using inductive charging ensures the complete wireless device operation.

This text considers the hardware solutions and the firmware design for the STM32F411VE microcontroller used to control the device and for the ESP8266 microcontroller included in the Wi-Fi module.

Contents

1	Introduction	1
2	Related work	4
2.1	Analysis of existing concepts	4
2.2	Examples of existing acquisition systems	5
3	Technology overview	7
3.1	Interfacing electronic circuits	7
3.1.1	Signal conditioners	7
3.1.2	Analog-to-digital converters	7
3.1.2.1	Architectures of ADCs	7
3.1.2.2	ADC errors	10
3.2	Strain gauges	11
3.2.1	Classification of strain gauges	11
3.2.2	Strain gauges parameters	12
3.2.3	Measuring circuits for strain gauges	13
3.3	Accelerometers	14
3.3.1	Specification of accelerometers	15
3.4	Temperature sensors	15
3.4.1	Thermistor	16
3.4.2	Infrared temperature sensor	16
3.5	Serial buses	18
3.5.1	Serial Peripheral Interface (SPI)	18
3.5.2	Secure Digital Input Output (SDIO)	19
3.5.3	Inter-Integrated Circuit (I2C)	20
3.6	Wireless communication	20
3.7	Wireless charging	21
4	Realisation	22
4.1	Device concept	22
4.2	Components selection	24
4.2.1	Analog-to-digital converter	24
4.2.2	Signal conditioner	26
4.2.3	Programmable current source	27
4.2.4	Infrared temperature sensor	27
4.2.5	Accelerometer	30
4.2.6	Universal inputs and outputs	31
4.2.7	Memory card	31
4.2.8	Wireless link	32

4.2.9	Microcontroller	33
4.2.10	Real Time Clock	33
4.2.11	Lithium-Ion battery	34
4.2.12	Power supply	35
4.3	Testing board	36
4.3.1	Power supply board of the testing device	37
4.3.2	Testing board with analog and digital components	38
4.3.3	External components connected to the testing boards	40
4.4	Final board	42
4.4.1	Power part	43
4.4.2	MicroSD memory card	45
4.4.3	Accelerometer LIS2DH12	45
4.4.4	Wi-Fi module ESP-07	46
4.4.5	Microcontroller STM32F411VE	47
4.4.6	ADC AD7606	48
4.4.7	Signal conditioners LTC6915 and current sources	49
4.4.8	User connectors	51
4.4.9	Photo of the final board	52
4.5	STM32F411VE microcontroller's firmware	53
4.5.1	The AD7606 converter	57
4.5.2	The LTC6915 signal conditioners and the MAX335 programmable switch	58
4.5.3	The microSD card	58
4.5.4	The real time clock	59
4.5.5	Battery percentage measurement	59
4.5.6	The LIS2DH12 digital accelerometer	59
4.5.7	The IR temperature sensor TMP006	59
4.5.8	Placeholders for the custom code	60
4.5.9	The Wi-Fi module	60
4.6	The ESP8266 microcontroller's firmware	61
4.6.0.1	The TinyFrame library	61
4.6.0.2	Implementation of the TinyFrame library	63
5	Results	65
5.1	Format of the output data	67
5.2	LEDs usage	68
5.3	Measured data	69
6	Conclusion	73
	References	75



Appendix	79
A Testing board schematic and layout	79
A.1 Power supply board of the testing device	79
A.2 Testing board with analog and digital components	82
B TMP006 schematic and layout	86
C Final device schematic and layout	87
D Content of the CD	95

List of Figures

1	Application of strain gauges to measure the stress applied on the ski during ski jumping.	2
2	Simplified block diagram of the device.	3
3	Operation concepts of acquisition systems.	4
4	Electronic Arrow tip construction (source: [1]).	5
5	The SensorTag (source: [2]).	6
6	Data Acquisition System 7000 from Micro-Measurements (source: [3]).	6
7	Technology of the data transfer IR Telemetrics (source: [4]).	6
8	Successive approximation ADC: block diagram and principle (source: [7]).	8
9	Sample and hold circuit.	8
10	Dual-slope ADC output waveforms (source: [6]).	9
11	Strain gauges categorisation (source: [9]).	11
12	Meandering of the strain gauge.	12
13	Basic rosette types, classified by grid orientation: (a) tee; (b) 45-rectangular; (c) 60 delta (source: [10]).	12
14	Half-Bridge circuit (source: [11]).	13
15	Dummy strain gauge for temperature compensation (source: [11]).	13
16	Full-Bridge circuit (source: [11]).	13
17	Inverting charge amplifier.	14
18	SPI bus with Master and two independent Slaves.	19
19	Inductive charging principle (source: [27]).	21
20	Block diagram of the final device.	23
21	AD7606 functional block diagram (source: [28]).	25
22	Typical INL of AD7606 (source: [28]).	25
23	Typical DNL of AD7606 (source: [28]).	25
24	SNR vs. Input frequency for different oversampling rates of AD7606 (source: [28]).	26
25	PSRR of AD7606 (source: [28]).	26
26	Block diagram of LTC6915 in 16-SSOP package (source: [31]).	27
27	TMP006 IR Temperature Sensor from Texas Instruments Incorporated.	28
28	TMP006 functional block diagram (source: [33]).	28
29	Percentage of IR Signal Absorbed by Sensor versus Angle of Incidence (source: [33]).	29
30	LIS2DH12 3-axis accelerometer from STMicroelectronics. .	30
31	LIS2DH12 3-axis accelerometer's functional block diagram.	31
32	Wi-Fi module CC3100 from Texas Instruments Incorporated.	32
33	Wi-Fi module ESP-07 based on ESP8266 from Espressif Systems.	32

34	Pin usage of STM32F411VE microcontroller.	34
35	The inductive power receiver and transmitter.	36
36	The AD7606 connected to STM32F411RE.	36
37	Power supply testing board.	37
38	Schematic of inverting DC-DC step-down converter.	38
39	Testing board with analog and digital components.	38
40	MAX1454 signal conditioner and 74HC4051 multiplexer electrical schematic.	39
41	Electrical schematic of LTC6916 signal conditioner.	40
42	STEVAl-MKII105V1 adapter board with LIS3DH ac- celerometer from STMicroelectronics (source: [48]).	40
43	All parts of the testing device connected together.	41
44	The TOP and the BOTTOM side of the final device's PCB.	42
45	Final PCB's block diagram.	43
46	Battery charging circuit with power ON/OFF switch.	43
47	Voltage divider for battery voltage measuring.	44
48	Electrical schematic of 3.3 V voltage regulator TS1117BCW33.	45
49	Electrical schematic of the microSD card.	45
50	Electrical schematic of the LIS2DH12 accelerometer.	46
51	Electrical schematic of the ESP-07 Wi-Fi module.	46
52	Electrical schematic of the STM32F411VE microcontroller.	47
53	SWD pin arrangement on the final board.	48
54	Electrical schematic of the analog-to-digital converter	49
55	Electrical schematic of the first LTC6915 signal conditioner.	50
56	Electrical schematic of the current sources, which are switched using the MAX335 programmable switch.	51
57	Electrical schematic of the user connectors.	52
58	PWM pin arrangement on the final board.	52
59	Assembled final board.	53
60	Cyclic buffer for the measurement.	54
61	Main flow chart.	55
62	Measurement flow chart.	56
63	AD7606 ADC timing – reading after a conversion.	57
64	AD7606 ADC final timing diagram.	57
65	The web user interface.	64
66	The TinyFrame structure.	64
67	The developed sensors acquisition system.	65
68	Example of the measured data.	68
69	LEDs configurable by the firmware.	68
70	Measurement with the strain gauges connected to the ac- quisition system.	69
71	Electrical schematic of the strain gauges connected to the acquisition system.	69
72	Measured strain applied on the beam.	70

73	Measurement with the onboard accelerometer.	71
74	Measured acceleration on the rotating chair.	72
75	Measured acceleration caused by hand movement.	72
76	Real-size PCB image of the power supply board.	79
77	Real-size PCB image of the testing board.	82
78	Real-size PCB image of the TMP006 board.	86
79	Real-size PCB image of the final board - TOP side.	87
80	Real-size PCB image of the final board - BOTTOM side (mirrored).	87
81	Final device: the TOP layer of the PCB.	87
82	Final device: the second layer of the PCB.	88
83	Final device: the third layer of the PCB.	88
84	Final device: the BOTTOM layer of the PCB.	88

Chapter 1

Introduction

Testing devices are needed in many industries. They can be used for testing of engineering products, building materials, in sports and other sectors. These devices usually include many sensors to measure strain, acceleration, temperature, etc. Some applications require measuring in remote and heavily accessible places. The application restricts the device's implementation. For example measurement in hardly accessible places disallows frequent physical access. Measuring a moving object (like a wheel) cannot use wires. The data rate can be high during such testing, caused by high sampling rates for measuring fast dynamic changes.

The multi-sensors data loggers have a variety of uses. One of them is in research and development of combustion engines. The connecting rod, which converts together with the crank reciprocating motion into rotating motion, is exposed to strain. Thus, it is important to perform strain tests to avoid accidental damage. Another application can be for the development of forklift trucks. Their wheels are exposed to big stresses. However, the data logger for such applications has many constraints. The device with sensors has to be placed into a limited space, so the device's size is crucial. Another limitation may come from the device's materials. The metal objects could cause a loss in Wi-Fi communication. Therefore, the sensors have to be connected by wires and not through Wi-Fi. Once the device is installed, all the connectors are usually hardly accessible. Hence, there is a requirement to operate the device remotely through Wi-Fi. However, such device is a battery device, so the battery needs to be regularly charged. As connecting a wire to charge the device could be difficult, inductive charging is an important feature.

Also, the data loggers are applicable in sports. The inspiration can be a miniaturised arrow ballistic measurement system [1]. The disadvantage of the presented device is that it does not allow wireless data transmission. So, the arrow has to be connected to USB, when the data needs to be read. The data logger can also be used in curling or ski jumping. The curling broom must have a certain flexibility and strength to sweep the ice in the path of the curling stone properly. In ski jumping, the ski must be light and flexible, but also strong enough not to break during the flight and landing. In both applications, it would be necessary to measure the stressed object with a strain gauge, as shown in Figure 1. These dynamic signals are not required to transfer and proceed online. The data can be stored during the measurement inside the memory. The user can download and evaluate the data after the measurement is completed.

1.0 INTRODUCTION



Figure 1: Application of strain gauges to measure the stress applied on the ski during ski jumping.

It is impossible to use the concept where the data from the sensor go directly through the Wi-Fi module to the central unit if all the requirements mentioned above have to be met. The existing data loggers usually allow either online data transmission with low sampling rates or offline data storage without wireless configuration. The devices with online data transmission usually have a low sampling rate, and they are not suitable for measurement of dynamic signals. Their use is usually for temperature measurement. The devices with offline data storing must usually be disconnected before any parameter change because they do not contain any wireless link. The disconnection is unsuitable for devices mounted in heavily accessible places. The device introduced in this thesis has to be able to measure autonomously without physical contact with the user. It is necessary to measure dynamic effects using high sampling rates. Fortunately, the device does not have to interact with the environment during the measurement. The measured data can be stored in the memory and sent to the user after the measurement. Therefore, the concept with offline data logging was chosen. The device can be placed into hardly accessible places, and the wireless communication allows to operate the device.

This thesis presents a small unique device, which allows multi-rate processing, offline data storage with a large memory, support for multiple sensor types, high sampling rate and user interface accessible through a Wi-Fi. The simplified block diagram is shown in Figure 2. The device allows a complete wireless operation including the possibility to charge the battery using the inductive charger.

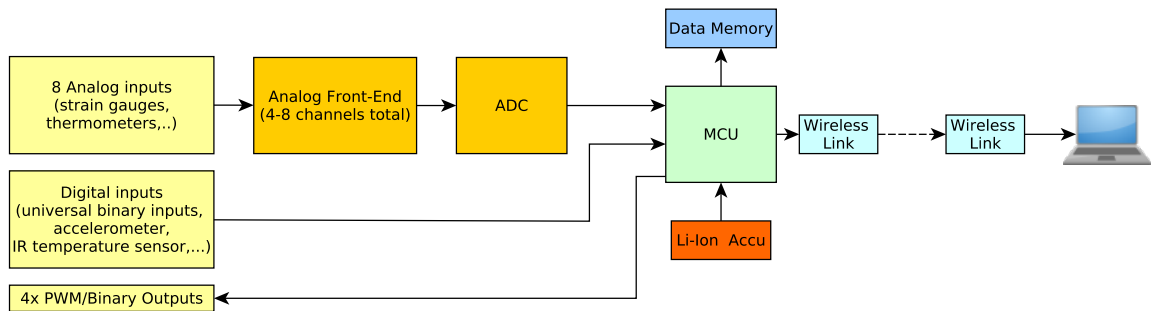


Figure 2: Simplified block diagram of the device.

The following chapter introduces the reader deeper into the issue. Already existing solutions are presented, and their advantages and disadvantages are described. The Chapter "Related work" is followed by the Chapter "Technology overview" which summarises the used technologies. The final device concept and selection of the components are described in the Chapter "Realisation". This chapter also includes an explanation of the components schematics. Two boards are described, the first one was used for testing the selected components. The second, final board, is a practical realisation of the proposed device. The important part of the device is firmware, the explanation of which is also included in this chapter. The following Chapter "Results" involves measured results and a user manual. In the attachments, there are complete schematics and PCB designs for the future production.

Chapter 2

Related work

2.1 Analysis of existing concepts

The data acquisition system, sometimes called a data logger, is a device for measuring and recording the measured data. The data can be stored either into memory or sent through a wireless link to the user. On the market, there are available many various data loggers using different operation concepts. The selection of possible concepts is in Figure 3.

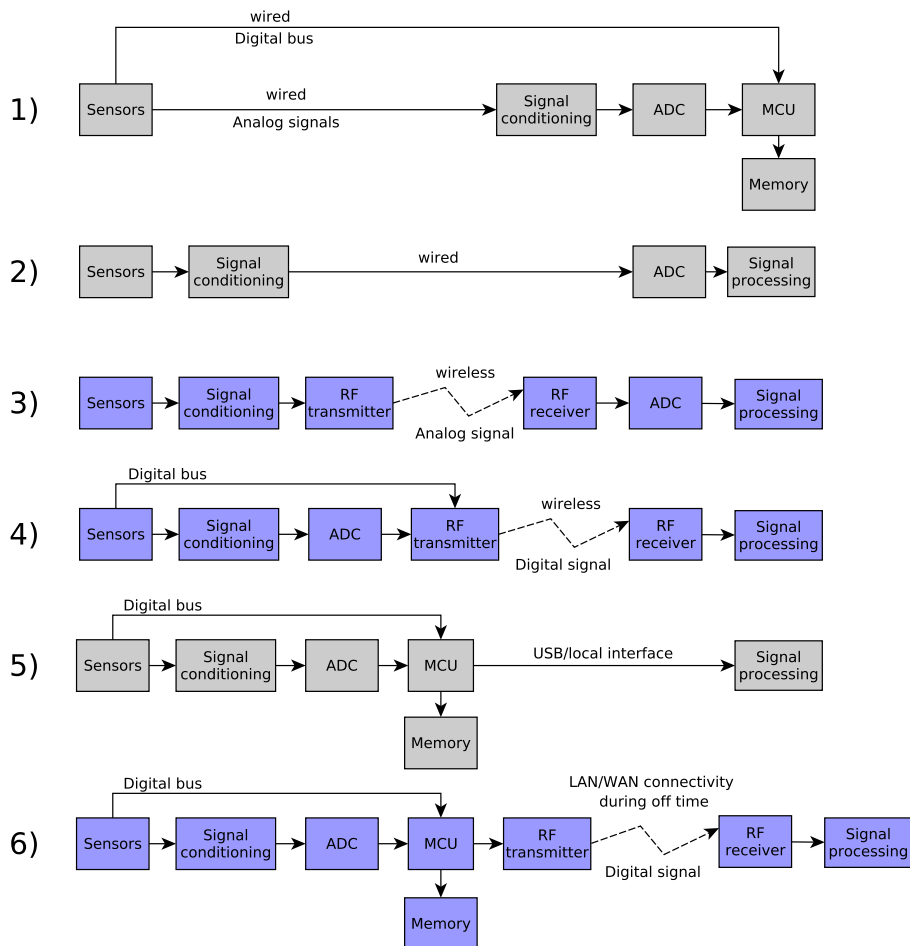


Figure 3: Operation concepts of acquisition systems.

The concepts one and two allow making a small device for measuring dynamic effects using high sampling rate. However, when the device has to be mounted into hardly accessible places, these solutions without remote control would not fit the requirements. The concepts three and four allow to mount the device into hardly accessible places, but wireless transmission speed limits the sampling rate. The solution five allows high sampling rates, but without wireless communication. Hence, the solution number six allowing two running modes was chosen. The stand-alone mode allows measuring the data with high sampling rates. In the transfer mode can be the device configured and measured data transferred to the user's device.

■ 2.2 Examples of existing acquisition systems

Many different acquisition systems have been developed so far. The systems listed in the following text are selected based on either their interesting properties or their similarity to the goals of this work's device. The devices are firstly introduced, then their purpose is stated, and finally, their advantages and disadvantages for the goals of this works are presented.

One of the existing acquisition systems is a miniaturised arrow ballistic measurement system [1]. The system allows measuring an arrow's in-flight characteristics. This system is using concept four in the Figure 3, so it is not designed to use wireless communication. It is a miniaturised sensor data acquisition system mounted into the arrow tip. The main advantages of this system are size, operation from battery and possibility to record fast dynamic effects on internal memory. The main parts of the system are 3-axis accelerometer, microprocessor and EEPROM memory. The disadvantage is that the device has to be removed from the arrow tip when the data needs to be read. Due to limitations of the internal EEPROM memory, the device can record only four shots, so the inconvenient dismounting is required.



Figure 4: Electronic Arrow tip construction (source: [1]).

Another existing device is SensorTag [2] shown in Figure 5. This IoT kit is small, battery powered, supports various type of sensors, includes amplifiers and comparators and provides wireless connectivity. However, the device uses the concept five in the Figure 3, so it does not include the internal memory to measure and save the data with high sampling rate. Another disadvantage is the missing support for strain gauges.

2.2 EXAMPLES OF EXISTING ACQUISITION SYSTEMS



Figure 5: The SensorTag (source: [2]).

The market provides plenty of the strain gauges acquisition systems which are stable, accurate and with selectable parameters. However, these systems are usually very large, and they are unusable for application in small places. These acquisition systems should be located remotely from the measured object. These sensors have to be connected by wires, being a disadvantage for applications in hardly accessible places or rotating objects. The example of the large acquisition system from Micro-Measurements is in Figure 6. These devices are using concept five in the Figure 3.



Figure 6: Data Acquisition System 7000 from Micro-Measurements (source: [3]).

There are devices similar to the large acquisition systems mentioned above which are suitable for measuring rotating objects. The large system size is compensated by the fast wireless communication, which is shown in Figure 7. These systems use the concept number four from Figure 3. However, such systems are custom work, so their price is high.

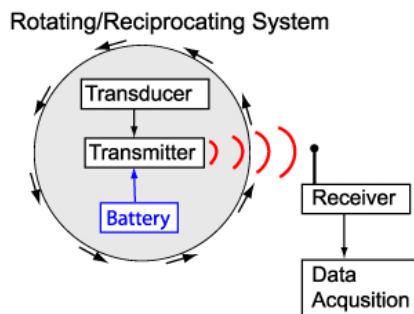


Figure 7: Technology of the data transfer IR Telemetry (source: [4]).

Chapter 3

Technology overview

the device consists of several types of sensors, interfacing circuits and various types of digital buses. This part introduces these sensors, circuits, buses and other technologies.

■ 3.1 Interfacing electronic circuits

Analog signal usually needs to be adapted. For example, the signal from sensors such as strain gauges and thermometers has to be amplified before digitalisation. This functionality provides signal conditioners. An analog-to-digital converter then digitalises the modified signal and sends it into the microcontroller through a digital interface, such as SPI or I2C.

■ 3.1.1 Signal conditioners

Circuit for signal conditioning is responsible for adapting the signal from the sensor to format compatible with following device, usually ADC. The signal conditioner must be compatible with the output signal of the sensor and also the input of the ADC. The input part is specified by input impedance, offset voltage, input bias current, leakage current. The input of such conditioner can be AC/DC voltage or current, frequency or electric charge. The output can be voltage, current, resistance, etc.

■ 3.1.2 Analog-to-digital converters

The analog output of the sensors has to be converted to a digital signal as a microcontroller input. The conversion is provided using an analog-to-digital converter (ADC). It is a system converting input analog voltage (or current) to a digital number. The analog to digital conversion is a discretization in amplitude and time.

■ 3.1.2.1 Architectures of ADCs

The main part of every ADC is a comparator, which is a 1-bit converter. The output has a high logic value when the input signal is above defined threshold, and a low logic value when the input signal is below the threshold. Every ADC consists of at least one comparator. Some of the most important architectures are discussed below.

3.1 INTERFACING ELECTRONIC CIRCUITS

The Flash ADC is the fastest type of the ADC. Flash ADC is also named as parallel ADC because it consists of $2^N - 1$ comparators arranged in parallel, where N is a number of bits. There are 2^N resistors providing a reference voltage to comparators. The flash ADC usually has eight bits, and the sampling frequency is in hundreds of MHz. The disadvantage of the flash converter is a big complexity, higher consumption and higher input capacity.

The Successive Approximation ADC (SAR ADC) is a compensating ADC, and its principle is shown in the Figure 8. The conversion is made in N steps starting from the MSB. The input voltage U_X is compared with the U_{DAC} voltage from DAC feedback. If the U_{DAC} is greater than U_X , then the relevant bit in SAR is set to logic zero. Otherwise, it is set to logic one. This process is repeated until the LSB is set to a logic value. The SAR ADC has a resolution usually 16 bits or higher, and the sampling frequency is up to 1 MHz. The disadvantage of the SAR ADC is that the input voltage must be constant during the conversion. For this purpose the sample-and-hold circuit (S&H) shown in Figure 9 is used. It is a short time analog memory. The circuit samples and stores the input signal as an AC or DC voltage for required time. This converter makes a good compromise between speed and accuracy.

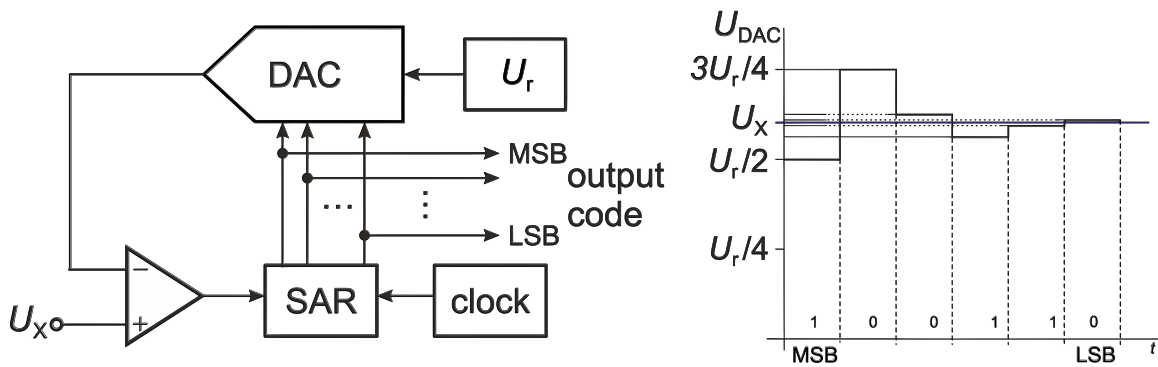


Figure 8: Successive approximation ADC: block diagram and principle (source: [7]).

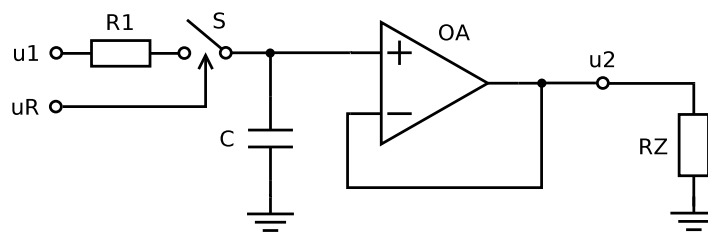


Figure 9: Sample and hold circuit.

The Dual-Slope/Multi-Slope ADC use the integrator for the conversion. The input voltage V_{IN} is integrated for a fixed time T . After this time is applied a reference voltage V_{REF} , which has the opposite polarity than V_{IN} voltage. The V_{REF} voltage is integrated for unknown time t_X down until it reaches zero (see Figure 10). The ratio between input voltage V_{IN} and reference voltage V_{REF} is a ratio between measured time t_X and fixed T and is represented by Equation (1). The advantages of this converter are high resolution (14 bits and more), low cost, low power consumption, low offset and gain errors, independence of integrating capacitor and resistor, etc. The disadvantage is slower conversion because the conversion takes more steps than other architectures.

$$\frac{V_{IN}}{V_{REF}} = \frac{t_X}{T} \quad (1)$$

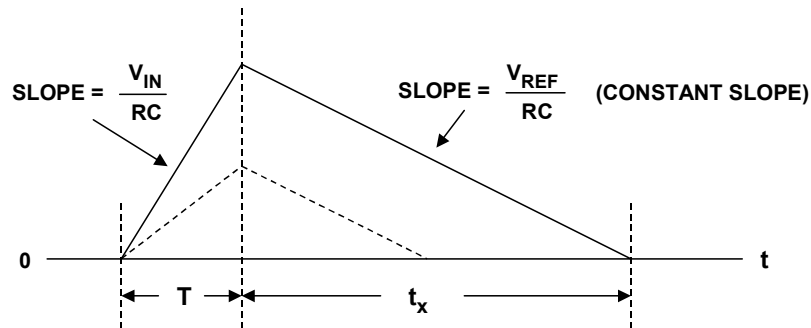


Figure 10: Dual-slope ADC output waveforms (source: [6]).

The Sigma-delta (Σ - Δ) ADC use a sigma-delta modulator. The input analog signal is converted to pulses. The oversampled input voltage passes into the integrator, and the integrated signal is compared with GND and resampled in D-latch. The digital filter behind the D-latch counts these pulses for a chosen interval N and gives a mean analog voltage during the interval. The number of bits is typically 12-24, dependent on the number of clock pulses N . The sampling time is around hundreds or tens of ms . The advantage of this ADC is a high resolution; the disadvantage is slow sampling due to oversampling.

3.1 INTERFACING ELECTRONIC CIRCUITS

■ 3.1.2.2 ADC errors

The analog to digital converters quantise the input signal, which causes some errors. The most common ADC specifications are discussed below. The essential characteristics of the ADC are speed, stability, price and ADC errors, which are described further.

Static parameters affect the DC signal conversion accuracy.

Integral Nonlinearity (INL) is a deviation from a straight line passing through the endpoints of the ADC transfer function.

Differential Nonlinearity (DNL) is the deviation between the actual and the ideal step width of the one LSB.

Offset error is a difference between the nominal and the actual offset points.

Gain Error is a difference between the nominal and the actual gain points on the transfer function. It is defined after the correction of the offset error to zero.

Total Error includes INL, DNL, offset error and gain error. It is a maximum difference between an analog and ideal midstep value.

Temperature, time and voltage reference drifts.

Dynamic parameters in a time domain include sampling time, an uncertainty of sampling time, collection time and conversion time. In a frequency domain are the most common parameters following.

Signal-to-noise ratio (SNR) is a ratio of the signal power and the background noise power.

Signal-to-noise and distortion ratio (SINAD) is a ratio of the total signal power level including signal, noise and distortion to the power of noise and distortion.

Effective number of bits (ENOB) is a dynamic range of the ADC.

Total Harmonic Distortion (THD) is a ratio of the sum of all harmonic components powers to the power of fundamental frequency.

Intermodulation distortion (IMD) is a ratio between the power of fundamental frequency and third-order distortion products. The IMD quantifies the non-harmonic frequencies added to the input signal.

Power Supply Rejection Ratio (PSRR) is a ratio of the change in supply voltage to the produced output voltage.

■ 3.2 Strain gauges

Strain gauges are sensors for measuring mechanical quantities, which can be transformed into a change in length, such as bend, torsion, force, torque, pressure, etc. The amount of strain in the device is in proportion to the strain gauge's electrical resistance. When the conductive wire is positively tensed, its length is increasing, the cross-section is decreasing, and also its electrical resistance is increasing based on the Equation (2).

$$R = \rho \frac{l}{S}, \quad (2)$$

where ρ is the electrical resistivity of the material, l is the length of the wire and S the cross-section of the wire.

■ 3.2.1 Classification of strain gauges

The strain gauges can be categorised by material and construction as shown in Figure 11).

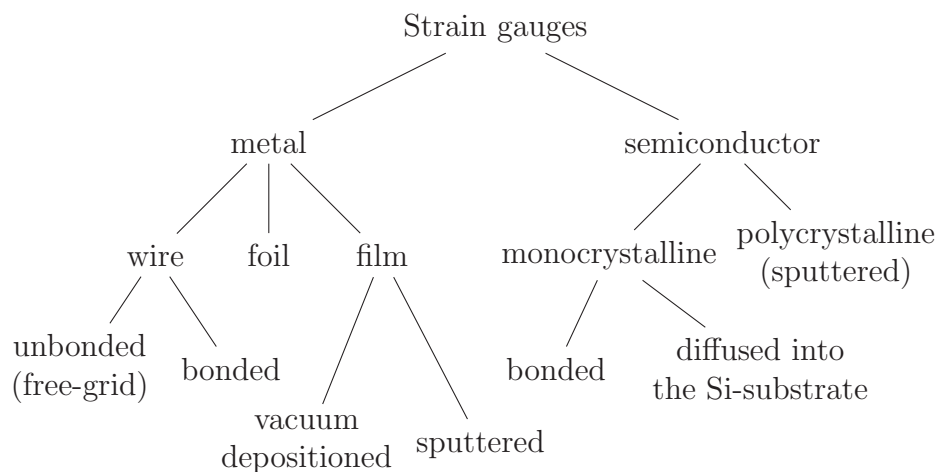


Figure 11: Strain gauges categorisation (source: [9]).

Both, metal and semiconductor strain gauges, have bias resistance 120, 350 or 1000 Ω . The metal wire and foil strain gauges are mostly used for sensors of force and pressure. Their conductive layer is meandering, as shown in the Figure 12. Semiconductor strain gauges use a piezoresistive effect and are mostly made from monocrystalline and diffused into the Si-substrate.

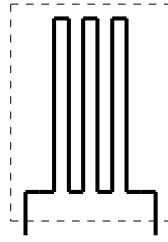


Figure 12: Meandering of the strain gauge.

3.2.2 Strain gauges parameters

The significant strain gauge parameter is the gauge factor (GF) determining its sensitivity to the strain. It is represented by the Equation (3).

$$GF = \frac{\Delta R/R}{\Delta l/l} = \frac{\Delta R/R}{\epsilon}, \quad (3)$$

where $\Delta R/R$ is a relative change in electrical resistance and $\Delta l/l$ is a relative change in length, which can be represented by strain ϵ . The temperature dependence of the strain gauge sensitivity can be compensated.

The dependence of measured deformation and resistance of the strain gauge is not linear and is also dependent on the temperature. The temperature dependence is characterised by the temperature coefficient.

Another important characteristic of the strain gauge is a directional sensitivity. It is defined as a ratio between vertical and horizontal direction. For measuring strains along different directions is usually used a combination of three strain gauges configured to strain rosettes, as shown in the Figure 13.

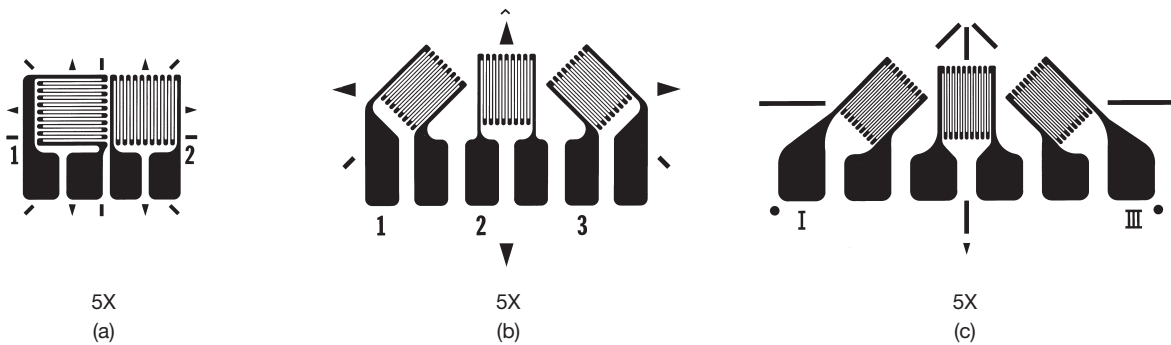


Figure 13: Basic rosette types, classified by grid orientation: (a) tee; (b) 45-rectangular; (c) 60 delta (source: [10]).

On the terminal between a measurement circuit and strain gauge arises thermo-electric effect causing a disturbance. It can be compensated by choosing a proper measurement method.

3.2.3 Measuring circuits for strain gauges

For measuring small changes in resistance is commonly used Wheatstone bridge circuit. Depending on the measured subject, one or more strain gauges are connected. For one active strain gauge is usually used quarter-bridge. However, the resistance can change with temperature change. Therefore we connect also temperature compensating strain gauge to a half-bridge circuit as shown in Figures 14 and 15, which is placed in 90 degrees rotation against measuring strain gauge. Equation (4) can describe this half-bridge configuration and strain resistance change can be expressed by Equation (5).

$$\frac{V_0}{V_{EX}} = -\frac{GF \cdot \varepsilon}{2} \tag{4}$$

$$\Delta R = R_G \cdot GF \cdot \varepsilon \tag{5}$$

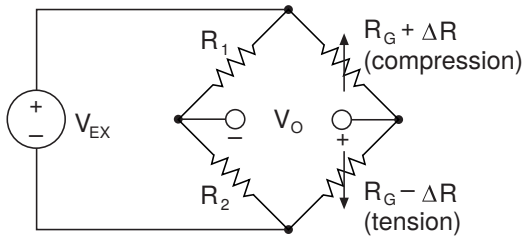


Figure 14: Half-Bridge circuit (source: [11]).

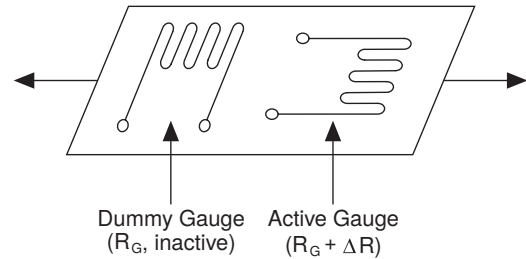


Figure 15: Dummy strain gauge for temperature compensation (source: [11]).

For better sensitivity, we can use the full-bridge circuit, as shown in Figure 16. The sensitivity of the bridge with four strain gauges is four times higher than the sensitivity of the bridge with just one strain gauge. The full-bridge is described in Equation (6).

$$\frac{V_0}{V_{EX}} = -GF \cdot \varepsilon \tag{6}$$

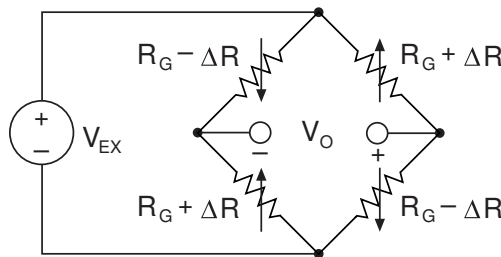


Figure 16: Full-Bridge circuit (source: [11]).

3.3 Accelerometers

The accelerometer is a device for measuring linear acceleration, which is the velocity change of the measured object. The accelerometer senses static and dynamic forces of acceleration, such as orientation, vibrations, shocks, etc. Acceleration \mathbf{a} is dependent on the initial force \mathbf{F} and the mass m of the moving object and is described by the Newton's second law in Equation (7). The acceleration direction is the same as the direction of the force. The units of acceleration are meters per squared second (m/s^2) or G-forces (g).

$$\mathbf{a} = \frac{\mathbf{F}}{m} \quad (7)$$

Accelerometers are typically made with micro-electro-mechanical systems (MEMS) technology, providing low cost and small size sensor. Accelerometers usually consist of movable (seismic) mass, which is attached to a frame. The seismic mass is moving according to applied acceleration and can be measured for example through a capacitive divider between frame and mass.

The mostly used types of accelerometers and their signal processing are following [14]:

Piezoelectric Accelerometers: the piezoelectric sensing element generates a high-impedance charge signal. The charge amplifier is used to convert the generated charge into a usable low-impedance voltage signal. The Equation (8) applies for the inverting charge amplifier in Figure 17.

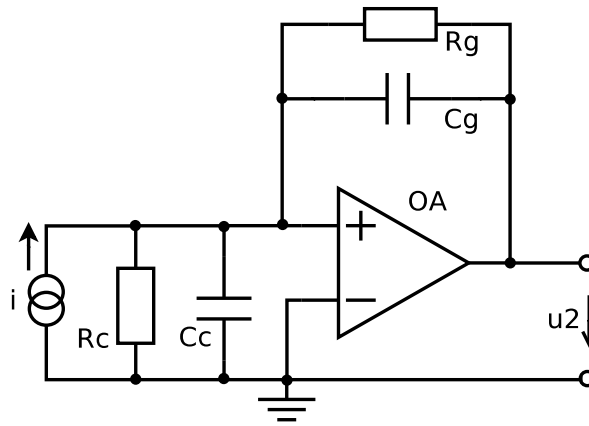


Figure 17: Inverting charge amplifier.

$$u_2 = -\frac{1}{C_g} \int i \cdot dt = -\frac{Q}{C_g} \quad (8)$$

Piezoresistive Accelerometers: the change of resistance reflects the acceleration. Therefore, for example, the Wheatstone bridge mentioned in Section 3.2.3 can be used.

Capacitive Accelerometers: the change of capacitance reflects the acceleration. They usually consist of a built-in circuit, which converts the capacitance change into a usable voltage signal. MEMS integrated accelerometers usually integrate electronics for conversion to digital output.

Servo (Force Balance) Accelerometers: the acceleration is measured directly using a piezoelectric, piezoresistive or capacitive technology. These types of accelerometers use a feedback current to keep the mass in a default position. A servo circuit derives an error signal from the mass motion. A current sent through a coil generates a torque, which is proportional to the acceleration and keeps the mass in a default position.

■ 3.3.1 Specification of accelerometers

Various use cases need different types of accelerometers, and it is important to choose the right one which meets the necessary specifications. The following list describes the most important parameters.

Digital accelerometer Sensitivity is expressed in mg/LSB , and it is the ratio of acceleration change to change of the output signal.

Measurement Range is expressed in $\pm g$, and it is the maximum acceleration, which can be measured and represented as an output signal.

Output type can be either digital or analog.

Axis of accelerometers can be either 1-axis, 2-axis or 3-axis.

Noise of accelerometer is a deviation from the ideal output signal and is expressed in $mg - RMS$.

■ 3.4 Temperature sensors

Temperature measurement utilises multiple types of temperature sensors. Some of them measure the temperature using physical contact, and some are remote (non-contact temperature sensors). In this text will be introduced just one type of the contact temperature sensor – thermistor, and one type of the non-contact temperature sensor – IR temperature sensor. The temperature is expressed in Kelvins (K), degrees Celsius ($^{\circ}C$), degrees Fahrenheit ($^{\circ}F$) and degrees Rankine ($^{\circ}R$). Temperature sensors are divided into two groups: absolute sensors, which measure the temperature referenced to absolute zero or another fixed temperature; and relative sensors, which measure thermal gradient or the temperature difference between two objects. Absolute sensors are for example thermistors and resistance temperature detectors (RTDs), a relative sensor is for example thermocouple.

3.4 TEMPERATURE SENSORS

■ 3.4.1 Thermistor

The thermistor is a thermally sensitive resistor, so its resistance R [Ω] changes with temperature change T [K]. The transfer characteristic can be expressed by Steinhart Equation (9).

$$\frac{1}{T} = A + B \cdot \ln R + C \cdot (\ln R)^3, \quad (9)$$

where A, B, C are diagram constants.

Thermistors are usually made from oxides of nickel, cobalt or manganese. They are split into two categories: with positive temperature coefficient (PTC), so their resistance is increasing with a temperature rise, and negative temperature coefficient (NTC), so the resistance decreases with a temperature rise.

Thermistors ability to detect small temperature changes is a significant advantage over RTDs and thermocouples. On the other hand, thermistors have a strong non-linearity.

■ 3.4.2 Infrared temperature sensor

We use pyrometers for contactless temperature measurement. They are based on the radiation observation. The contactless technology can be applied to measure moving objects, catch fast temperature changes and view the entire surface of measuring object. On the other hand, there is uncertainty in the determination of the emissivity, and there are errors due reflection and throughput of some materials.

The infrared (IR) sensors are part of pyrometers. The wavelength of infrared radiation is longer than visible light wavelengths and shorter than microwaves, so it is invisible to human eyes. The most important pyrometers specifications are the following:

Photosensitivity or Responsivity is a ratio of output signal and radiant flux [W] falling on sensors' sensitive part Equation (10)).

$$K = \frac{U}{\Phi} \quad [V \cdot W^{-1}] \quad (10)$$

Noise Equivalent Power (NEP) indicates the radiant flux, when the amount of output signal is equal to effective spectral density of voltage noise.

$$NEP = \Phi \frac{\sqrt{u_s^2}}{U} \quad [W \cdot Hz^{-\frac{1}{2}}], \quad (11)$$

where $\sqrt{u_s^2}$ is a spectral density of voltage noise.

Detectivity (D , D^*) is a photosensitivity per unit area of a detector and can be written as inverted value of NEP: $D = NEP^{-1}$. It is often related to the sensitive area of the radiation sensor and is marked as D^* .

$$D^* = \frac{\sqrt{S}}{NEP}, \quad (12)$$

where S is a relative spectral sensitivity.

Temperature measurement with an IR sensor is based on blackbody radiation. All bodies with a temperature above $0^\circ K$ radiate infrared energy. The IR radiation travels from a source through obstacles, which can partially absorb and partially reflect the IR radiation. For material effectivity in emitting energy as thermal radiation, we use term emissivity ε . Different materials with various emissivity emit IR energy with different intensity at the same temperature. The emissivity is important for IR measurement because of the differences.

The main equations for contactless measurement are following.

Kirchhoff's Law of Radiation states that the emissivity ε of a surface is equal to its absorptance α at a given temperature T and wavelength λ . The reflectivity ρ is then in relation to emissivity ε by the Equation (13).

$$\rho = 1 - \varepsilon \quad (13)$$

Stefan-Boltzmann Law states that the thermal energy radiated by a blackbody radiator is proportional to the fourth power of absolute temperature (eq. 14). For non-ideal objects we can rewrite the Equation (14) by Equation (15).

$$E_0 = \frac{P}{A} = \sigma T^4 \quad (14)$$

$$\frac{P}{A} = \varepsilon \sigma T^4, \quad (15)$$

where $\sigma = 5.67 \cdot 10^{-8} W/m^2 \cdot K^4$ is Stefan-Boltzmann constant, A is the geometry factor, and ε is emissivity.

Wien's Displacement Law states that with increasing blackbody radiator temperature the overall radiated energy is increasing and the peak of the radiation curve moves to shorter wavelengths. So the hotter the object, the shorter the wavelength at which it will emit most of its radiation. The temperature can be computed from the wavelength of the peak of the blackbody radiation curve by Equation (15).

$$\lambda_{peak} \cdot T = 2.898 \cdot 10^{-3} mK, \quad (16)$$

where T is the temperature in K and λ_{peak} is in μm and it is a wavelength where the most of the radiant power is concentrated.

3.5 SERIAL BUSES

Planck's Radiation Law says that the radiant flux density is a power of electromagnetic radiation per unit of wavelength.

$$W_\lambda = \frac{\varepsilon(\lambda)C_1}{\pi\lambda^5 (e^{C_2/\lambda T} - 1)}, \quad (17)$$

where $\varepsilon(\lambda)$ is the emissivity of the surface, $C_1 = 3.74 \cdot 10^{12} \text{ W} \cdot \text{cm}^2$, $C_2 = 1.44 \text{ cm} \cdot \text{K}$, and e is the base of the natural logarithm.

The IR sensor uses lens to collect the emitted thermal radiation. The detector then converts the thermal radiation into an electrical signal. The device usually includes the emissivity correction, effective signal filtering, linearisation and other useful features.

■ 3.5 Serial buses

The serial communication sends the digital data over the communication channel sequentially, always one bit per clock. There are multiple advantages of serial buses, such as that fewer cables decrease the price of the bus, and also remove inconvenience with synchronisation, as with parallel buses. The serial buses with differential serial links are less susceptible to noise. Therefore they can transmit information over a longer distance than parallel buses. With a higher number of pins for the parallel bus also increases the price of the integrated circuits. Serial buses used in this device are the most common used and standardised buses and will be briefly described in the text below. All the mentioned buses can use DMA for data transmission, which allows access the main memory independently on a microcontroller.

■ 3.5.1 Serial Peripheral Interface (SPI)

The Serial Peripheral Interface is a four-wire synchronous serial bus which allows a Master device initiate communication with a Slave device. The SPI communication usually consists of the following signals:

MOSI (Master Output, Slave Input) is used for data out of the SPI Master device and data in of the SPI Slave device.

MISO (Master Input, Slave Output) is used for data in of the SPI Master device and data out of the SPI Slave device.

SCK (Serial Clock) is used to output clock signal for the SPI transfers.

$\overline{\text{SS}}$ (Slave Select) is used to select the Slave device with which the Master device communicates. The Slave Select is active low, so it should be coupled to the power supply to avoid accidental activation of the slave device.

The SPI configuration uses five registers, which are described in Motorola SPI specification [19]. The data transmission is synchronised by the serial clock, where phase and polarity should be configured in the Master device registers depending on the Slave device requirements.

The SPI bus is usually configured with one Master and many independent Slaves as shown in Figure 18. SPI Master communicates (receives or sends data) with one Slave in time by pulling his \overline{SS} low.

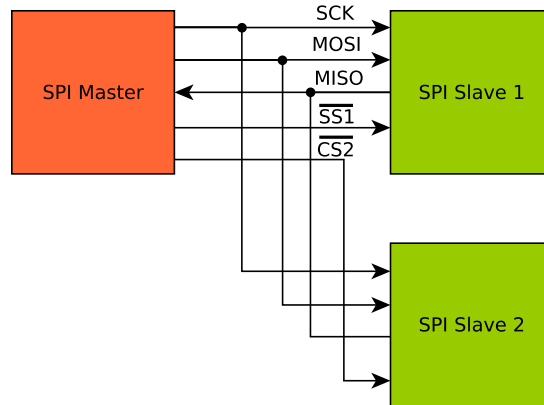


Figure 18: SPI bus with Master and two independent Slaves.

The second option of SPI connection is the Daisy chain configuration. In this configuration all the Slaves have the same Slave Select, which is set low before the transmission start. The first slave output (MISO) is not connected to the Master but to the next Slave input (MOSI). The MISO of the second Slave is again connected to the MOSI of the next Slave. The MISO of the last Slave can be connected to the MISO of the Master. This configuration is usually used to set parameters in Slave devices. The data are sent to the first Slave with a group of clock pulses. The first slave shifts the data to the next Slave with the next group of clock pulses. The process can be likened to a communication shift register. The data are stored in the Slaves when the slave select is set high.

The advantages of the SPI bus is the support of the full duplex synchronous communication. The data rate is higher than 1 Mbps (up to 100 Mbps) and has a low noise sensitivity compare to the I2C bus (see Section 3.5.3). The disadvantages of SPI bus are an inability of multi-Master communication and a requirement of four wires.

■ 3.5.2 Secure Digital Input Output (SDIO)

The Secure Digital Input Output is an interface for Secure Digital (SD) cards. The SDIO provides high-speed data rate over 10 MB/s. The SDIO cards can be configured in three signal modes: SPI bus mode, 1-bit SD Data Transfer Mode and 4-bit SD Data Transfer Mode. For more information about SD and SDIO standards see the specifications [20], [21]. The four-bit SD Data Transfer Mode cards can have up to 11 pins, depending on their type (MMC, SD, miniSD, microSD). Four pins are used for data transmission, one pin as a serial clock, one pin for command response, two or three pins for power supply and the remaining two pins are reserved and not used.

■ 3.5.3 Inter-Integrated Circuit (I2C)

The Inter-Integrated Circuit is a two-wire bidirectional serial multi-Master bus. The I2C bus consists of following signals:

SDA (Serial Data line) is used for data in and out and should be coupled to a power supply.

SCL (Serial Clock) is used to an output clock signal for I2C transfers.

The I2C standard is described in NXP Semiconductors specification [22]. Each device is identified by a unique address. The device which initiates the data transfer on the bus is also generating the clock signal and is considered as Master. Multi-Master bus configuration is controlled by one Master, who initiates the data transmission and configures all other Masters as slaves until the transmission is completed. When more than one Master wants to start transmission at one time, the arbitration is required. The arbitration proceeds bit by bit on SDA signal. When one of the Masters tries to send high on the SDA signal and simultaneously detects SDA level low, he loses the arbitration.

The advantages of the I2C bus are an easy connection of a new device on the bus, usage of only two pins, multi-Master support and acknowledgement of each transfer. The disadvantages are low data rate (between 100 kbps and 3.4 Mbps) compared to SPI bus, half duplex synchronous communication and high noise sensitivity compared to SPI bus.

■ 3.6 Wireless communication

The wireless communication is used for information transmission on large distances (between few meters to thousands of kilometres) without physical connection (wires, cables, etc). Devices, such as a data logger, use for wireless communication mainly Bluetooth, Wi-Fi and sometimes also ZigBee. The comparison of mainly used technologies is in Table 1.

Feature(s)	IEEE 802.11 b/g/n	Bluetooth	ZigBee
Power Profile	Hours	Days	Years
Complexity	Very Complex	Complex	Simple
Nodes/Master	32	7	64000
Latency	Enumeration up to 3 s	Enum. up to 10 s	Enum. 30 ms
Range	100 m	10 m	10 m - 300 m
Data Rate	11/54/600 Mbps	1 Mbps	250 kbps
Stack size	100+ kbyte	100+ kbyte	8-60 kbyte
Security	WEP, WPA/WPA2	64 bit, 128 bit	128 bit AES and Application Layer user defined

Table 1: Comparison of different wireless technology specifications. Based on [23], [24].

3.7 Wireless charging

The wireless charging is a technology for energy transfer between two objects using electromagnetic field and electromagnetic induction. There are two technologies for wireless transmission, inductive and resonant. The main differences are coil distance and if the coils are in resonance with each other. The wireless charging is used in many portable devices such as electrical toothbrushes and modern smartphones.

Inductive power transfer: the transmitting coil is connected to a power source and creates an alternating electromagnetic field. The field is collected by receiving coil, where it induces an alternating current. The current is rectified, filtered to DC and used to power the device. The efficiency of inductive chargers drops with the distance and the coil diameter. Efficiency above 90% can be achieved only if the distance is ten times lower than the coil diameter and both coils have similar size. For more information about inductive charging proceed to the Wireless Power Consortium website [27]. The Wireless Power Consortium developed the standard called Qi, which allows transfers up to 40 mm distance.

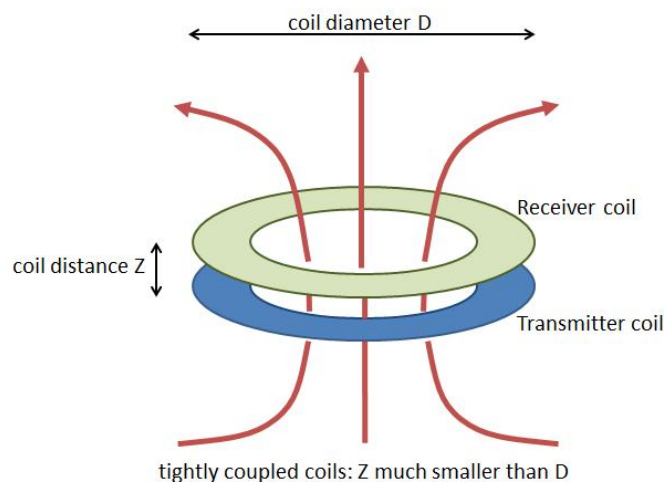


Figure 19: Inductive charging principle (source: [27]).

Resonant power transfer the transmitting and receiving coil can be almost ten times further unlike for inductive power transfer. The resonant power transfer works on a principle of a magnetic resonance between the transmitting and receiving coil. The transmitter includes a resonant circuit, which contains a coil, capacitor and resistors. The alternating current is applied to the resonant circuit, so the oscillation occurs, and an alternating oscillating magnetic field is created. The field is taken by the receiving coil, which also consists of a resonant circuit. The receiver converts the field to an alternating current, which is rectified, filtered to DC and used to power the device.

Chapter 4

Realisation

the project's realisation took place in several steps. The first essential task was to study the specification and decide what the possibilities are. It was necessary to devise a working solution, which also meets the most requirements. The next step was a selection of usable components to design the concept of a testing device. Besides, schematic and the layout were created for the testing board. A big part of the work on the device is a development of the firmware, such that fulfils the requirements. The procedure of the firmware development usually required to search for interesting ways how to solve commonly simple problems. At the same time, it was necessary to decide, which Wi-Fi module will be used, and how to apply it so that it will be the most efficient. The module was programmed so it connects to the firmware in the microcontroller. After experimenting with the testing device, it was necessary to design the final block concept and choose the final components usage. Subsequently, the final schematic and final board layout were created. As a part of firmware finalisation, the firmware was extended to control all the components, because the prototype board did not contain all the components from the final board. In the end, it was also necessary to make the device fail-safe and user-friendly.

4.1 Device concept

The block diagram of the final device is in the Figure 20 and it is divided into three sections: Analog, Digital and Power part. The core is a microcontroller, which collects all the data from sensors, saves the measured data to the memory card and provides the data exchange with a wireless module. The Analog Part consists of analog components for conditioning and digitalisation of the signals. These signals come from analog sensors, such as strain gauges and thermometers. The Digital part includes the microcontroller, universal digital inputs and outputs and digital sensors, such as an accelerometer or IR temperature sensor. The memory card and wireless link also belong to the Digital part. All the components need a power supply for their operation. The Power supply part provides three voltage levels necessary for the implemented components. This section also covers power for Real Time Clock and Lithium-Ion accumulator. The accumulator has two possible ways of charging: a common power source and inductive charger. The following text explains the blocks in detail and describe the used components and their connection.

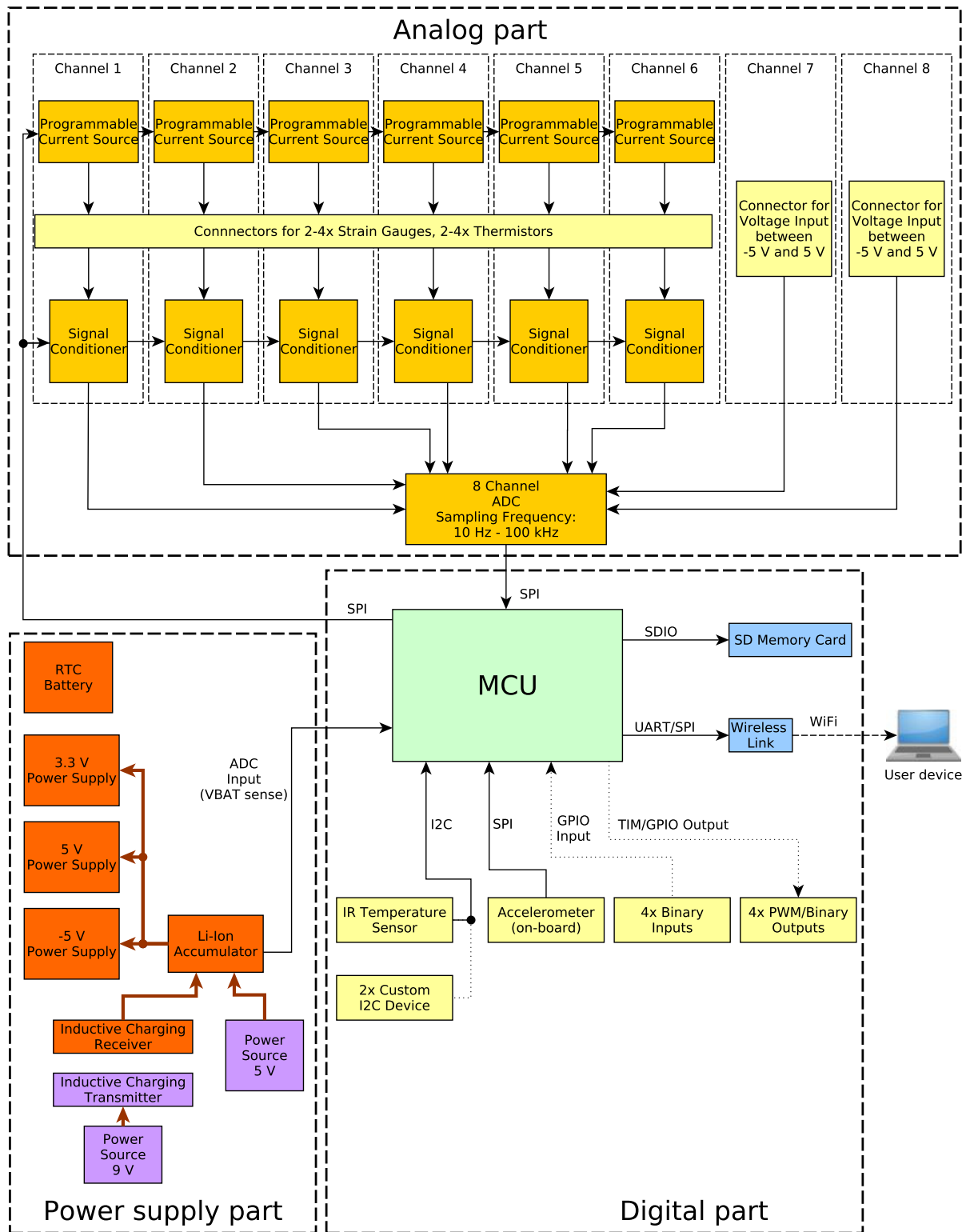


Figure 20: Block diagram of the final device.

■ 4.2 Components selection

The components selection began with the election of an analog-to-digital converter and other analog components. Later digital sensors, memory card and Wi-Fi module were chosen. The selected components have to be controlled by a microcontroller, and the device has to be powered by a power supply. This section describes the chosen components and their parameters, advantages and disadvantages.

■ 4.2.1 Analog-to-digital converter

The Analog-to-digital converter has to fulfil strict requirements for sampling frequency, which needs to be up to 100 kHz. There are eight intended analog inputs, so it was beneficial to find a multi-channel converter. Three converters have been taken into account: AD7709, MAX1300 and AD7606.

The AD7709 converter from Analog Devices, Inc. contains a 16-bit sigma delta ADC with PGA. The sampling rate is from 5.4 ksp/s to 105 ksp/s. This converter is inexpensive in comparison to the others. However, it contains only four channels.

The MAX1300 converter from Maxim Integrated contains a 16-bit successive approximation ADC. The sampling rate is up to 115 ksp/s, and it has eight channels. However, it is difficult to buy this converter.

The final and chosen ADC was the AD7606 [28] converter from Analog Devices, Inc. It is a successive approximation ADC with eight 16-bit channels and the sampling rate up to 200 ksp/s for all eight channels. The price is high compared to converters described above, but the converter provides many advantages. The component contains analog input clamp protection, anti-aliasing filter, track and hold amplifier, internal 2.5 V reference and high-speed serial and parallel interfaces. The functional block diagram is shown in Figure 21.

The converter is in the 64-LQFP package and has an adjustable, input range (± 5 V or ± 10 V), reference selection (internal or external) and type of the interface (parallel or serial). The internal digital filter can be configured through oversampling pins. Change of the oversampling ratio yields to better SNR and lower sampling frequency.

The interface selection affects the possible sampling rate of the converter. The parallel 16-bit interface can be connected to a parallel interface of the microcontroller, such as flexible static memory controller (FSMC) [29] included in many STMicroelectronics microcontrollers. The advantage is possible high sampling rate up to 200 ksp/s, the disadvantage is the occupation of 16 pins of the microcontroller, so it is space consuming. Moreover, not all microcontrollers have an FSMC bus. The requirement for the sampling rate of the device is up to 100 ksp/s, so the SPI interface is sufficient. The SPI data rate is from the AD7606 side limited to 12.5 MHz for V_{DRIVE} above 2.7 V and 15 MHz for V_{DRIVE} above 3.3 V. In the final device this pin is connected to a 3.3 V power supply.

4.2 COMPONENTS SELECTION

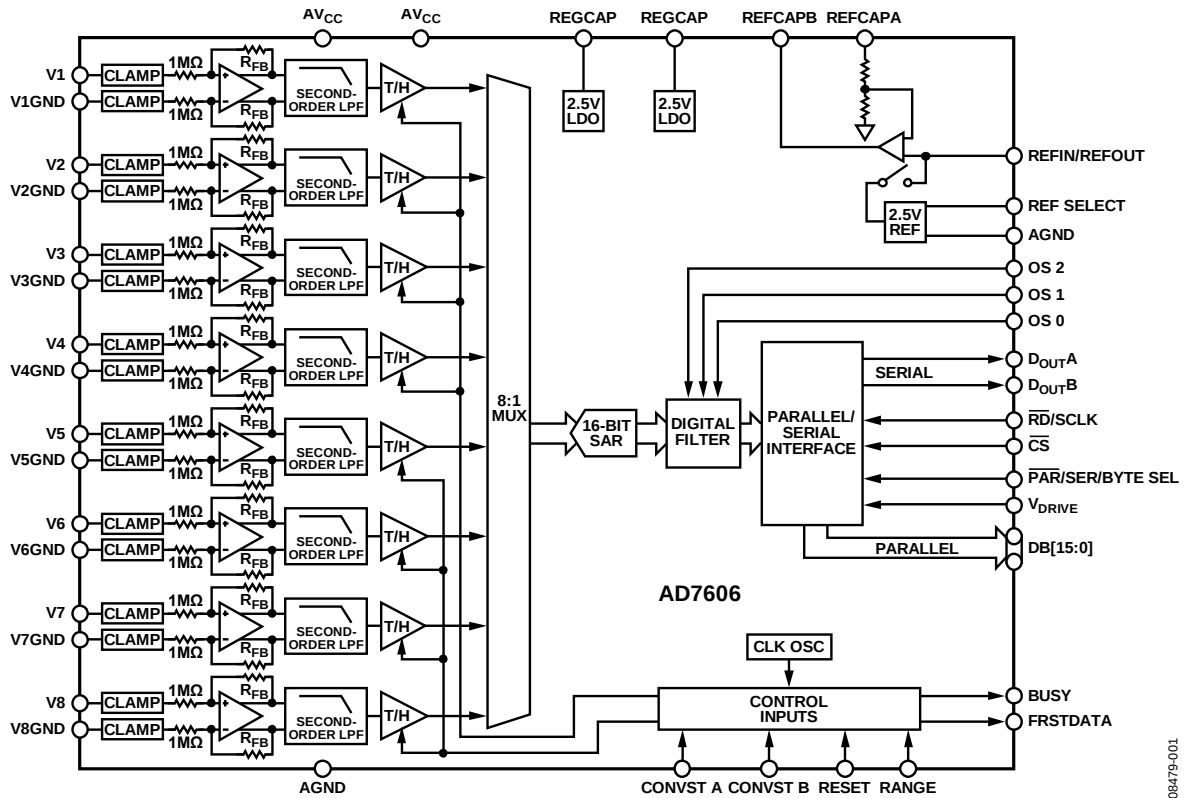


Figure 21: AD7606 functional block diagram (source: [28]).

Each ADC is subject to static and dynamic errors, so those parameters are always listed. They are described in Section 3.1.2.2. Some of AD7606 performance characteristics are in Figures 22 to 25.

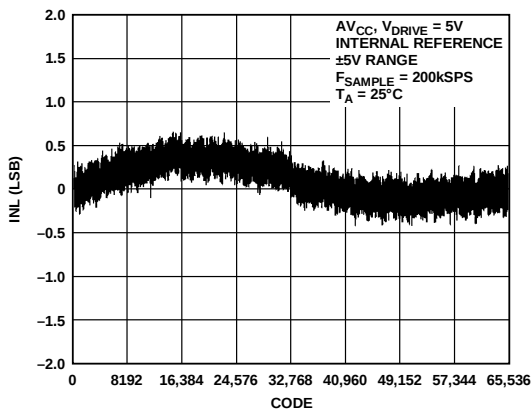


Figure 22: Typical INL of AD7606 (source: [28]).

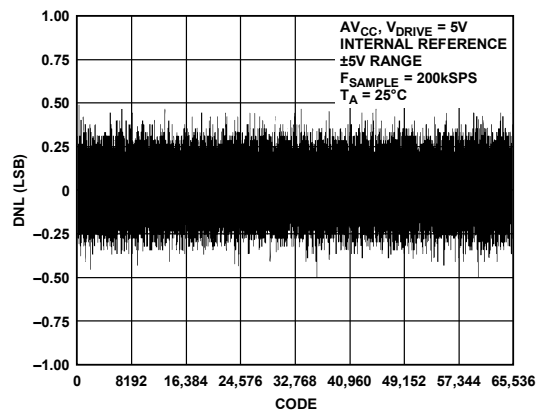


Figure 23: Typical DNL of AD7606 (source: [28]).

4.2 COMPONENTS SELECTION

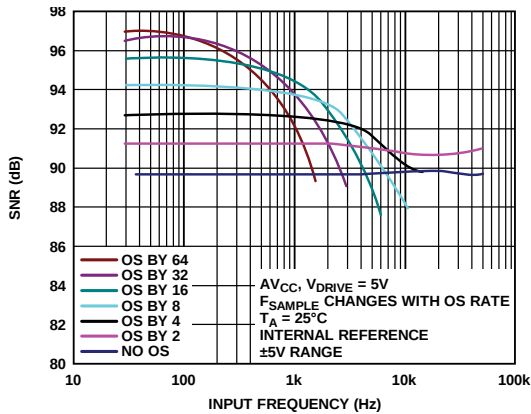


Figure 24: SNR vs. Input frequency for different oversampling rates of AD7606 (source: [28]).

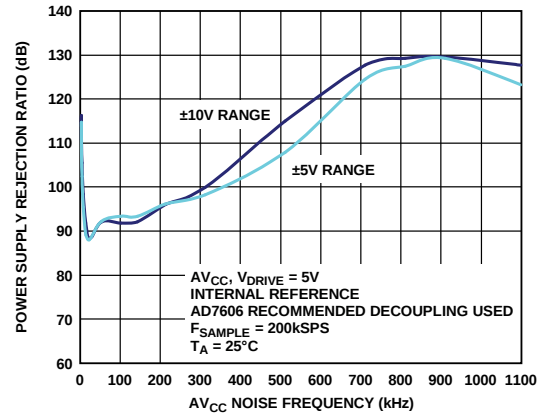


Figure 25: PSRR of AD7606 (source: [28]).

4.2.2 Signal conditioner

The main requirement for the signal conditioner was a programmable gain for signals from strain gauges and thermistors. The MAX1454 [30] signal conditioner from Maxim Integrated in the 16-TSSOP package was selected and tested on the testing board. The MAX1454 is a conditioner for automotive application, recommended for pressure sensors, resistive element sensors, strain gauges and others. The conditioner provides amplification, calibration and temperature compensation. The overvoltage and reverse voltage protection are also included. The gain is programmable in 32 steps, and the power supply for sensors is included. The disadvantage of this component is a low input signal frequency up to 1 kHz, power supply 5 V without symmetrical power supplies and complex configuration. Based on the datasheet, the configuration of the internal registers is complicated, and it uses a serial interface similar to UART.

Therefore, the MAX1454 was substituted by the LTC6915 [31] from Linear Technology. It was tested on testing board and used in the final device. This conditioner provides easy configuration through SPI interface, and a $\pm 5V$ symmetrical power supply. It allows measure signals which are altering along zero voltage. The gain can be programmed to multiply the signal by 0, 1, 2, 4, 8, 16, 32, 64, 128, 256, 512, 1024, 2048 or 4096. The LTC6915 does not include any protection and does not contain a power supply for sensors, so more external components are needed. The circuit has internal sampling frequency 3 kHz, so the frequency bandwidth of the input signal is also low. The component can be bought in the 12-DFN package or 16-SSOP package. The block diagram of LTC6915 in the 16-SSOP package is in Figure 26.

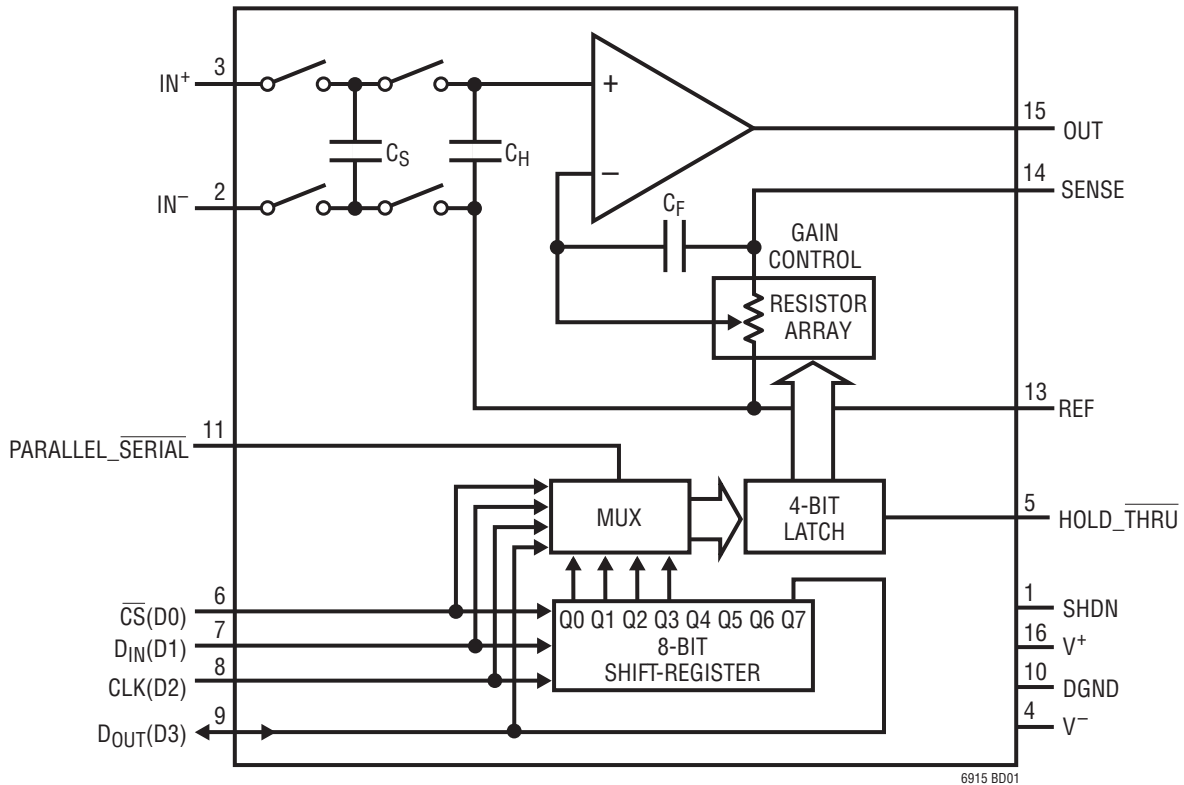


Figure 26: Block diagram of LTC6915 in 16-SSOP package (source: [31]).

■ 4.2.3 Programmable current source

The LTC6915 mentioned above does not provide the power supply for sensors, so the external programmable current source has to be used. The source was made from a linear regulator XC6206P182MR from Torex Semiconductor Ltd. connected as a current source. The resistors in the source feedback can be changed using a programmable switch MAX335 [32] in the 24-TSSOP package from Maxim Integrated. The component consists of eight separately controlled switches programmable through SPI interface. As the SPI configuration is the same as for LTC6915, it can be connected with them to a daisy chain. The switch allows setting the source current to 0.2 mA or 0.5 mA on each channel.

■ 4.2.4 Infrared temperature sensor

The device is using two temperature sensors. The first of them is infrared, and it is integrated on the board, while the second is a thermistor, which is external and so it is chosen by the user. Therefore only the integrated one is described here.

The temperature is measured by TMP006 Infrared Thermopile Contactless Temperature Sensor [33]. It is produced by Texas Instruments Incorporated, and it uses WCSP Package. The principle of such sensors is described in Section 3.4.2. The advantage

4.2 COMPONENTS SELECTION

of this MEMS fully integrated IR sensor is its small $1.6\text{ mm} \times 1.6\text{ mm} \times 0.625\text{ mm}$ DSBGA package shown in Figure 27. The tiny package size makes it possible to place the sensor in small spaces. The disadvantage is complicated soldering, which requires a special machine.

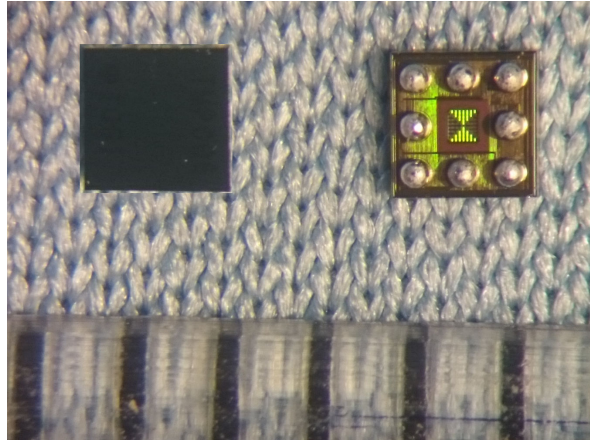


Figure 27: TMP006 IR Temperature Sensor from Texas Instruments Incorporated. A mm scale is for the reference at the bottom of the picture.

The TMP006 communicates through I2C or SMBus serial interface and supports up to eight programmable addresses. It provides high supply voltage range between 2.2V and 5.5V. The current in an active state is typically $240\ \mu\text{A}$. The operating temperature is between -40°C and $+125^\circ\text{C}$. The wavelengths for absorbing passive IR energy are between $4\ \mu\text{m}$ and $16\ \mu\text{m}$.

The TMP006 sensor has integrated temperature sensor, thermopile sensor, 16-Bit ADC and other blocks, as is shown in the functional block diagram in the Figure 28. The target object temperature should be calculated from the voltage change across the thermopile and the die temperature.

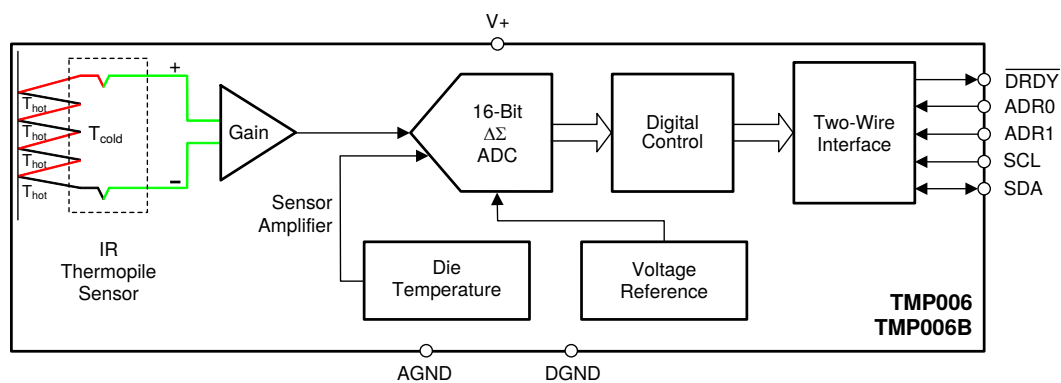


Figure 28: TMP006 functional block diagram (source: [33]).

The field of view of the TMP006 sensor is almost 180°. The calculation of the target temperature is dependent on the ability of the IR sensor to capture the signal from the target. The IR sensor capture efficiency depends on the angle at which the target temperature is scanned and the distance. In the Figure 29 is a dependence of the IR sensor absorption and the angle between IR sensor and target.

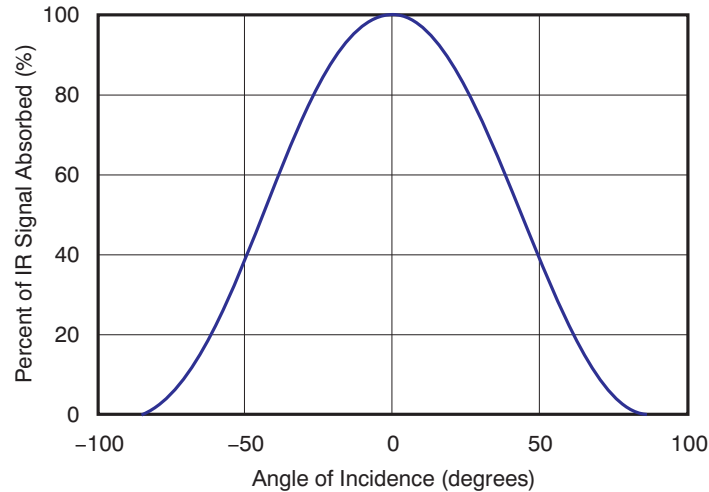


Figure 29: Percentage of IR Signal Absorbed by Sensor versus Angle of Incidence (source: [33]).

The equation for temperature computation is explained in the TMP006 User Guide SBOU107 downloadable from the TMP006 product page [33].

The Equation (18) represents the sensitivity of the thermopile sensor and how it changes over temperature.

$$S = S_0 [1 + a_1(T_{DIE} - T_{REF}) + a_2(T_{DIE} - T_{REF}^2)], \quad (18)$$

where S_0 is a calibration factor, which is described in detail in SBOU107 User Guide. The parameters a_1 , a_2 and T_{REF} are constants: $a_1 = 1.75 \cdot 10^{-3}$, $a_2 = -1.678 \cdot 10^{-5}$, $T_{REF} = 298.15$ K. The T_{DIE} parameter is a die temperature read from the sensor.

The offset voltage is represented by Equation (19). This voltage arises due to the slight self-heating caused by the non-zero thermal resistance of the package.

$$V_{OS} = b_0 + b_1(T_{DIE} - T_{REF}) + b_2(T_{DIE} - T_{REF})^2, \quad (19)$$

where b_0 , b_1 and b_2 are coefficients: $b_0 = -2.94 \cdot 10^{-5}$, $b_1 = -5.7 \cdot 10^{-7}$, $b_2 = 4.63 \cdot 10^{-9}$.

The Seebeck coefficients change over temperature is described by Equation (20). The Seebeck effect, also known as the thermoelectric effect, is a conversion of temperature difference to electrical voltage.

$$f(V_{OBJ}) = (V_{OBJ} - V_{OS}) + c_2(V_{OBJ} - V_{OS})^2, \quad (20)$$

where c_2 is a constant: $c_2 = 13.4$.

4.2 COMPONENTS SELECTION

The temperature of the target object can be expressed by Equation (21) and the result is in Kelvins.

$$T_{OBJ} = \sqrt[4]{T_{DIE}^4 + \left(\frac{f(V_{OBJ})}{S}\right)} \quad (21)$$

■ 4.2.5 Accelerometer

The chosen accelerometer is LIS2DH12 [34] from STMicroelectronics. The advantage is its small $2\text{ mm} \times 2\text{ mm} \times 1\text{ mm}$ LGA-12 package shown in Figure 30, which does not occupy much space on the PCB. The disadvantage is complicated soldering, as for IR temperature sensor described in Section 4.2.4. The LIS2DH12 is a MEMS capacitive accelerometer. The principle of accelerometers is described in Section 3.3

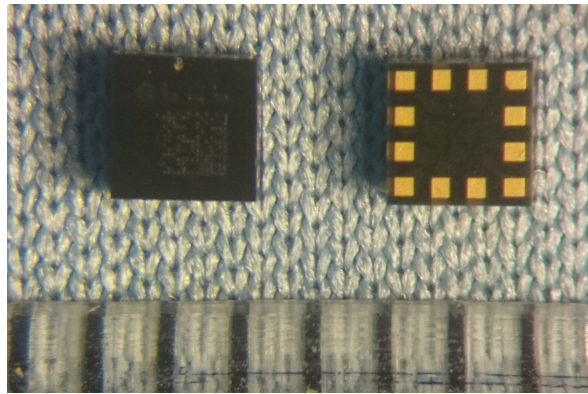


Figure 30: LIS2DH12 3-axis accelerometer from STMicroelectronics. A mm scale is for the reference at the bottom of the picture.

The LIS2DH12 communicates through I2C or SPI serial interface. The power supply voltage range is between 1.71 V and 3.6 V, and the power consumption is down to $2\ \mu\text{A}$. The accelerometer has user adjustable full scale of $\pm 2g/\pm 4g/\pm 8g/\pm 16g$.

The LIS2DH12 sensor has integrated three accelerometers, each for a single axis, as shown in Figure 31. It has three modes of operation: low-power mode with 8-bit data output, normal mode with 10-bit data output and high-resolution mode with 12-bit data output. The output data rate can be selected from 1 Hz to 5.376 kHz. The LIS2DH12 accelerometer has integrated temperature sensor and two programmable interrupts for wake-up/free-fall events and reaching of configured position.

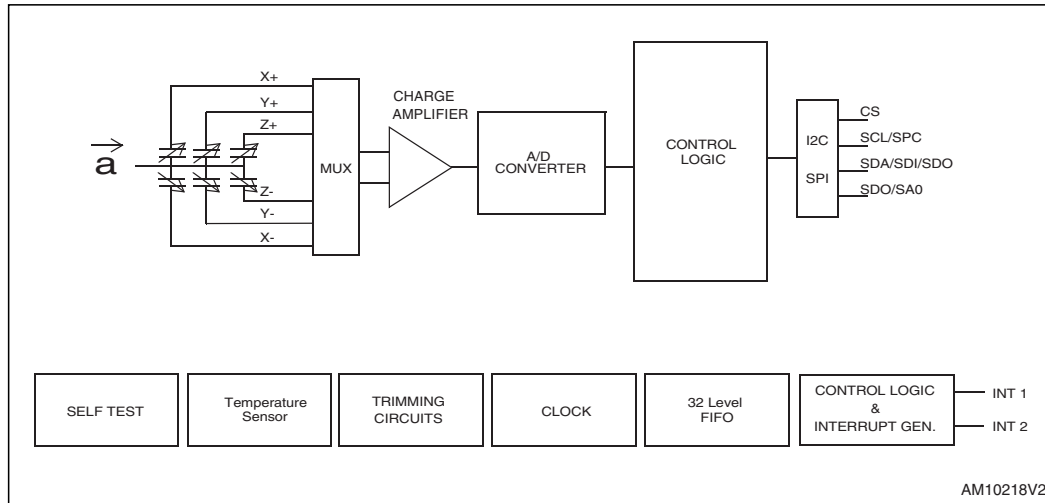


Figure 31: LIS2DH12 3-axis accelerometer's functional block diagram.

4.2.6 Universal inputs and outputs

As specified in the requirements, the device allows to connect up to two more I2C devices, four binary inputs and four PWM outputs. The I2C devices share the bus with the TMP006 IR temperature sensor and have to be configured with a different I2C address. The universal binary inputs are connected to 5 V tolerant inputs of the MCU, and the applied voltage must fulfil requirements for STM32F411VE microcontroller inputs. The universal PWM outputs can be configured using an advanced timer of the microcontroller (TIM1) and can generate the PWM with configurable duty cycle.

4.2.7 Memory card

The first scheme expected to use eMMC as a memory, which is integrated into the device. The advantage of this memory is a small BGA package and inability to remove it from the system. However, it was complicated to find where to buy such memory and also download adequate datasheet with necessary information about it. Therefore eMMC was substituted by microSD memory card, which is removable and bigger, but it has enough available documentation, and libraries support this standard.

One of the requirements for the device is a high sampling frequency of the analog-to-digital converter. Therefore, the memory card has to be fast enough to be able to save all the data in time. For this purpose the SD memory card class 10 was chosen, which allows writing speed up to 10 MB/s. The SD card requires a 3.3 V power supply. The card in microSD form has CMD signal, CLK signal and four data wires. The SDIO interface explained in Section 3.5.2 was used to obtain the speed as fast as possible.

4.2 COMPONENTS SELECTION

4.2.8 Wireless link

The wireless interface is used to set the measurement parameters and download files from the memory card. Firstly was chosen the Bluetooth Low Energy (BLE) module BlueNRG [35] from STMicroelectronics. The problem was the speed limitation of BLE, which is just 1 Mb/s. Therefore the Bluetooth was rejected at the expense of the Wi-Fi. Wi-Fi has higher speed, better range and configuration possibilities, as can be seen in Table 1.

The available Wi-Fi modules were CC3100 [36] from Texas Instruments Incorporated and one of the modules based on ESP8266 [37] from Espressif Systems. The CC3100 is shown in Figure 32 and its disadvantages are complicated configuration, a non-existing library for communication with STM32F4 microcontrollers and higher price. The disadvantage of ESP8266 modules is that it is from an unknown and potentially untrusted manufacturer. The advantage is low price and firmware with STM32F4 support. However, the firmware supports only UART data transmitting between the module and the main microcontroller and for SPI communication needs to be developed. ESP-07 based on ESP8266 was selected for simpler implementation, and it is shown in Figure 33.



Figure 32: Wi-Fi module CC3100 from Texas Instruments Incorporated.

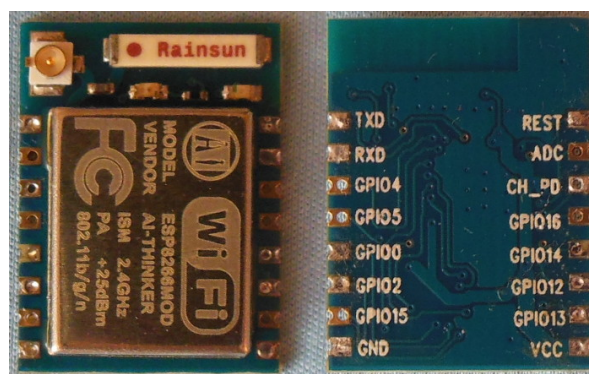


Figure 33: Wi-Fi module ESP-07 based on ESP8266 from Espressif Systems.

The ESP-07 supports protocol IEEE 802.11b/g/n with 2.5 GHz frequency band. There is integrated 32-bit MCU with 10-bit ADC, SDIO, SPI, UART, I2C, I2S, IRDA, PWM and GPIOs. The ESP-07 has 16 pins in total. The module allows the external antenna connection. The average operating current is 80 mA and operating voltage can be set between 3 V and 3.6 V. The MCU can be connected through SPI or UART interface [38]. The user can use a default firmware, which supports STA/AP/STA+AP operation modes. If the default firmware is not sufficient, the user can write his own firmware and flash it to the module using UART interface.

■ 4.2.9 Microcontroller

The microcontroller was elected to meet the requirements. The power consumption, availability of SDIO interface, the number of available buses and the number of GPIO inputs and outputs to be able to serve the circuits, were important. Another important parameter is a size of the integrated circuit to make the final device as small as possible. So, in the beginning, the microcontroller STM32F411RE was selected, which was in the LQFP64 package. This microcontroller eventually proved to be inadequate with its number of GPIO pins and the number of buses available for simultaneous use. For this reason the STM32F411VE microcontroller in LQFP100 package was selected. The STM32F411VE microcontroller has ARM 32-bit Cortex M4 core with FPU, and it provides 81 GPIOs, 16 channels of 12-bit ADC, 5 SPI buses, 3 I2C buses, 3 USART interface, SDIO interface and USB OTG FS interface, 7 Timers and one advanced-control Timer. The size of the Flash memory is 512 kB and the size of the SRAM is 128 kB. The maximum CPU frequency is 100 MHz and operating voltage range 1.7-3.6 V. The power consumption based on the datasheet should be in running mode 100 μ A/MHz [39], and the MCU is recommended for battery applications. In the Figure 34 is the final pin usage of the STM32F411VE microcontroller created with STM32CubeMX software [40].

■ 4.2.10 Real Time Clock

The microcontroller STM32F411VE includes a low power RTC [41, page. 423]. It is an independent counter, which in its register contains information about the real time in years, months, days, hours, minutes and seconds. RTC also provides a programmable alarm for wake-up and standby modes. An external power supply is needed to power the counter when the power supply of the microcontroller is turned off. So, the Lithium-ion battery CR1220 and external oscillator with nominal frequency 32.768 kHz were used to provide the clock signal.

4.2 COMPONENTS SELECTION

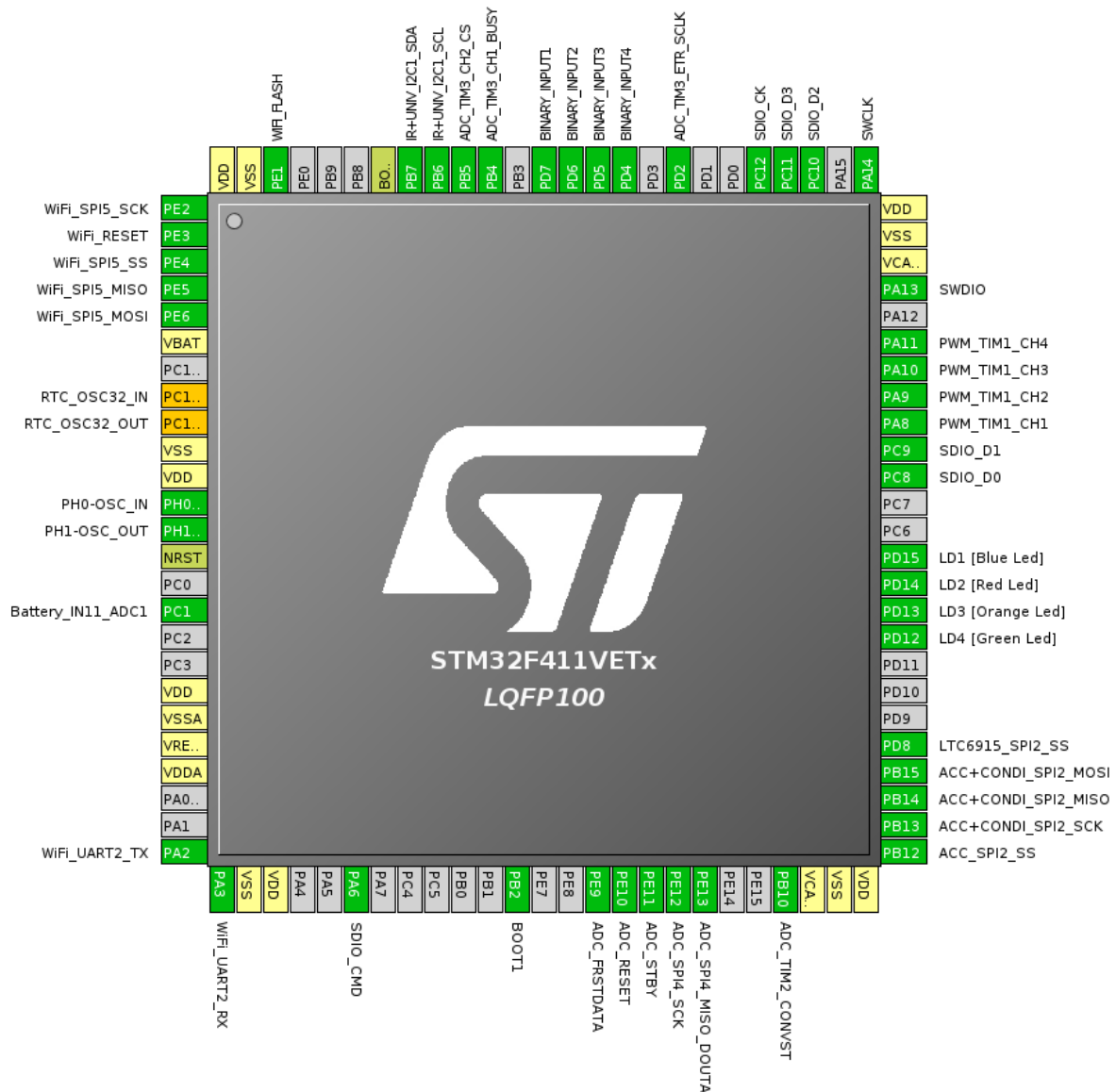


Figure 34: Pin usage of STM32F411VE microcontroller.

4.2.11 Lithium-Ion battery

The used battery is a rechargeable primary cell BAK 18650CA-2P-3J with a nominal voltage 3.7V [42]. The nominal capacity is 4500 mAh, the maximum continuous discharge current 2250 mA and the charge current 1100 mA. Inside the battery pack is integrated a small PCB with protection circuit. It includes NTC thermistor, over-current, overcharge and over-discharge protection, short circuit protection and self-discharge protection. The battery is charged from a 5V DC power source through a TP4056 1A standalone linear Li-Ion battery charger with thermal regulation [43]. This cheap charger in the SOP-8 package from the Chinese company NanJing Top

Power ASIC Corp. provides many advantages. It has programmable charge current up to 1 A, charge voltage 4.2 V, supply voltage range between 4 V and 8 V, temperature sense pin and easy connection. Red and green LEDs indicate the charge status.

The battery capacity is estimated from the battery voltage measured by the ADC integrated into a microcontroller. It is assumed that the discharge characteristic is linear. In the beginning, it was planned to measure the battery charge by an LTC2941 gas gauge communicating through the I2C interface. It was later dismissed because of unnecessary complexity.

■ 4.2.12 Power supply

All the components mentioned above needs to be powered by power supply required in their specification. The analog-to-digital converter, signal conditioners and programmable switch require a 5 V power supply. The signal conditioners and programmable switch require additional -5 V power supply. The microcontroller, digital sensors, SD card and Wi-Fi module require a 3.3 V power supply. All the components have to be powered by the battery, which produces an output voltage between 4.2 V and 2.75 V depending on the charge. So three regulators have to be used.

The 5 V power supply is generated from the battery output voltage by a step-up DC-DC converter MP1542 [44] in the MSOP8 package from Monolithic Power Systems. It is a cheap and high efficient regulator with output voltage programmable between 3 V and 22 V, switching frequency 700 kHz or 1.3 MHz and input voltage between 2.5 V and 22 V. The integrated power MOSFET has current limit 2 A, voltage 25 V and $R_{DS(on)} = 0.18 \Omega$.

The -5 V power supply is generated from the 5 V power supply by a step-down DC-DC converter MP1469 [45] from Monolithic Power Systems. The component has a small TSOT23-6 package. The converter has a wide operating input voltage range between 4.7 V and 16 V, switching frequency 500 kHz and output range between 4.7 V and $V_{in} - 3$ V. The converter is connected in inverting buck-boost topology to get the -5 V output voltage. The integrated power MOSFET half bridge has a total drain-source resistance $R_{DS(on)} = 0.415 \Omega$. The explanation of DC-DC converters operation is beyond the scope of this text.

The 3.3 V power supply is generated from the 5 V power supply by a low dropout voltage regulator TS1117BCW33 [46] from Taiwan Semiconductor. The low dropout performance is max. 1.5 V and output current up to 1 A. The regulator has TO-252 and SOT-223 package form.

The power supply for Lithium-Ion battery charger should have the output voltage between 4 V and 8 V. The battery can be charged through an accumulator or using wireless power transfer. There are many circuits for wireless charging on the market, for example from Texas Instruments Incorporated and STMicroelectronics. Most of these solutions use inductive power transfer and Qi standard described in Section 3.7. They usually provide many functions including the communication with the microcontroller. This unnecessary complexity led to a search for an easier solution, so a module from eBay [47] showed in Figure 35 was used.

4.3 TESTING BOARD

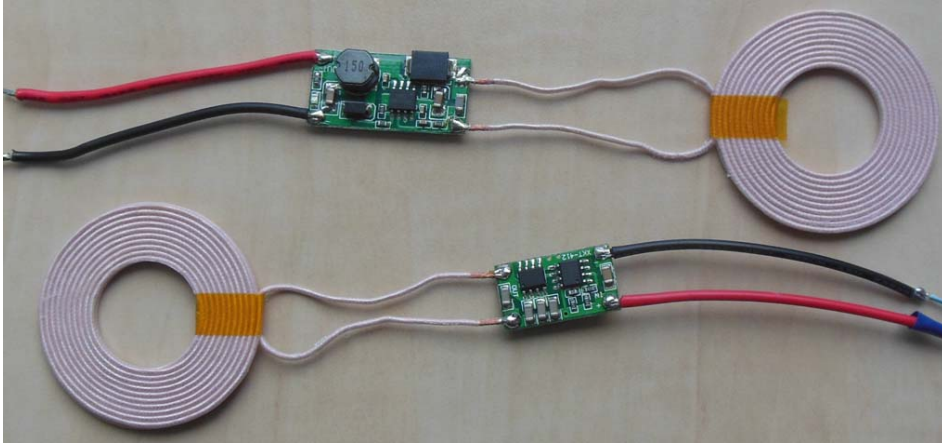


Figure 35: The inductive power receiver and transmitter.

■ 4.3 Testing board

The first experiments were with a breadboard connected to a NUCLEO-F411RE kit, which includes the STM32F411RE microcontroller. The components described in Section 4.2 are mostly SMD; therefore was necessary to place them to a THT reduction. The first tested component was the AD7606 converter described in Section 4.2.1 and the physical connection is shown in Figure 36. The electrical connection was very unreliable and disordered, so it was necessary to create a schematic and layout of the testing board.

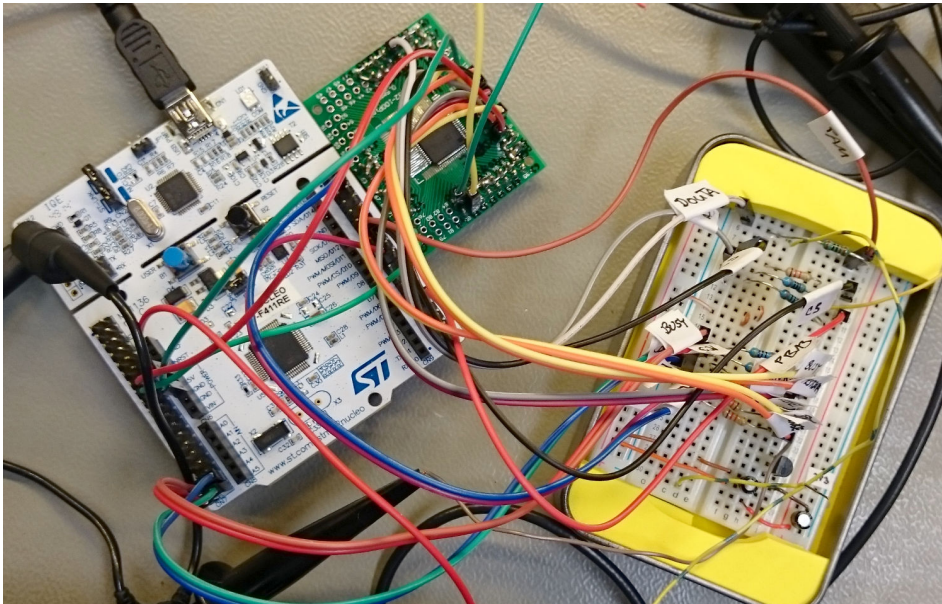


Figure 36: The AD7606 connected to STM32F411RE.

The testing device was split into two parts so that the probability of damaging a component is lower and smaller parts can be easier verified. The first board serves as a power supply; the second contains digital and analog components. The full schematics and layouts are attached in Appendix A.

4.3.1 Power supply board of the testing device

The power supply board showed in Figure 37 includes battery charging circuit, voltage regulators, gas gauge and battery connector. It contains power supply connector and many testing connectors.

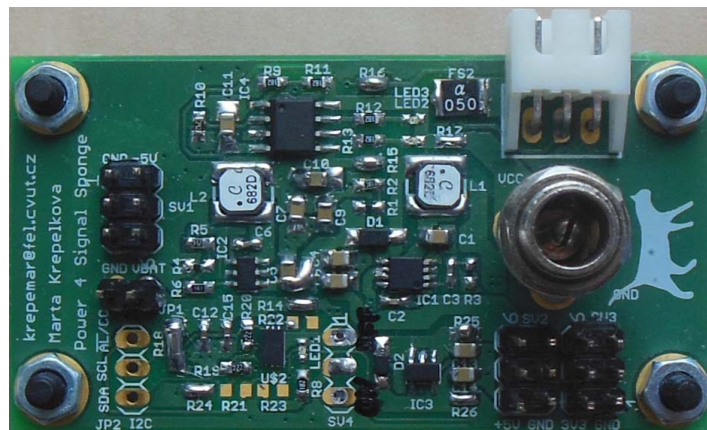


Figure 37: Power supply testing board.

The final device needs three voltage levels, as is mentioned in Section 4.2.12. Therefore there are three regulators. The step-up DC-DC converter MP1542 was connected according to the recommended application in the datasheet. The step-down DC-DC converter MP1469 was connected in inverting topology showed in Figure 38. The ground and the output voltage are swapped so that the buck converter can generate negative power supply.

The MIC5504 regulator was used to provide 3.3 V power supply. This simple regulator is not present in the final device because it produces a low output current. All the voltage regulators and battery charger worked correctly at the first attempt, so no further adjustments were needed.

The LTC2941 gas gauge with the I2C interface was soldered but lately was dismissed because it is unnecessary complex. Instead of the LTC2941 integrated circuit, the voltage divider was soldered on the back side of the board. The voltage can be directly sensed by an ADC pin of the microcontroller.

This board verified the reliability and suitability of the components and firmware implementation. It was possible to test the proposed schematic and consider further improvements suitable for the final device.

4.3 TESTING BOARD

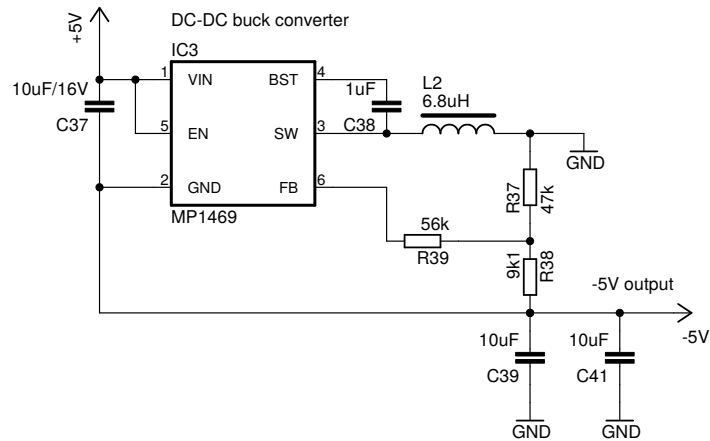


Figure 38: Schematic of inverting DC-DC step-down converter.

4.3.2 Testing board with analog and digital components

The board for analog and digital components testing is shown in Figure 37. The board contains these analog components: the analog-to-digital converter AD7606, signal conditioners MAX1454 and LTC6915 and current sources. All of them are described in Sections 4.2.1 to 4.2.3. The digital components are the microSD memory card, IR temperature sensor TMP006 described in Section 4.2.4 and accelerometer LIS2DH. The microcontroller STM32F411VE embedded on 32F411EDISCOVERY kit can be connected through connectors compatible with the discovery board.

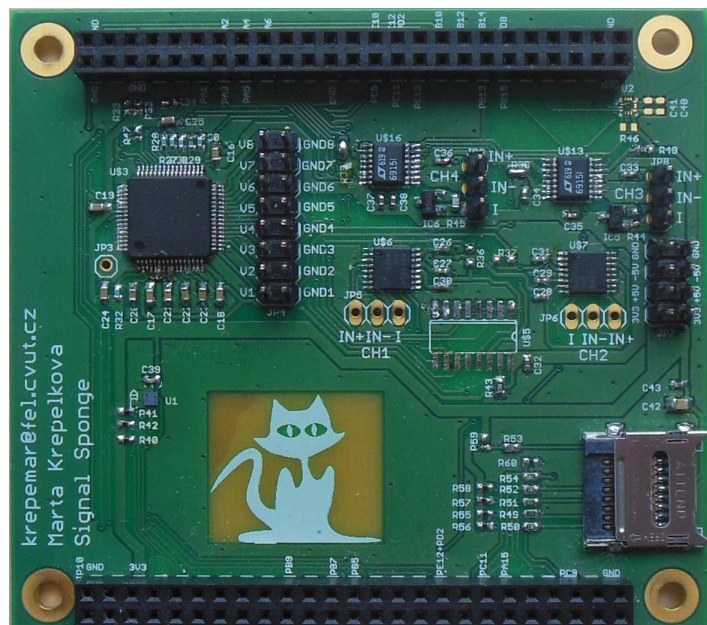


Figure 39: Testing board with analog and digital components.

The board mainly served for testing the functionality of the AD7606, which was connected according to the recommended application. The layout and recommended passive components are strictly complied to ensure the most accurate operation.

The board also includes two types of signal conditioners. Both were tested, compared, and the better one was chosen for the final board. The two MA1454 conditioners were connected. Each MAX1454 has to be configured through UART interface, which multiplexed an eight channel multiplexer 74HC4051. It allows to switch between the conditioners and to set each one with different parameters. Every MAX1454 provides a current source, so no more components excluding passive ones are needed. The schematic is showed in Figure 40.

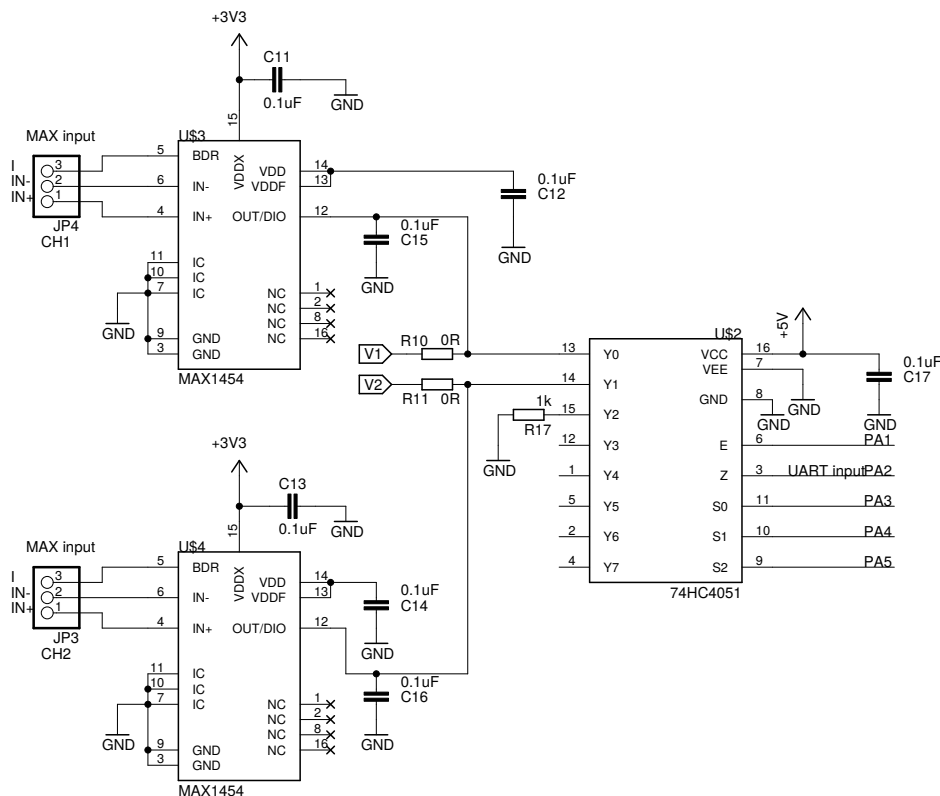


Figure 40: MAX1454 signal conditioner and 74HC4051 multiplexer electrical schematic.

For comparison were connected two LTC6916 conditioners. Every LTC6916 has to be configured through the SPI interface. The conditioners allow SPI daisy chaining as shown in Figure 41, so no more external components for their configuration were needed. The LTC6915 does not provide a current source, so the external source is necessary for every channel. Voltage regulator XC6206182MR was connected so it provided 0.5 mA constant current. Every current source has its regulator. This signal conditioning solution was selected for the final board due to better component parameters and easier operation.

4.3 TESTING BOARD

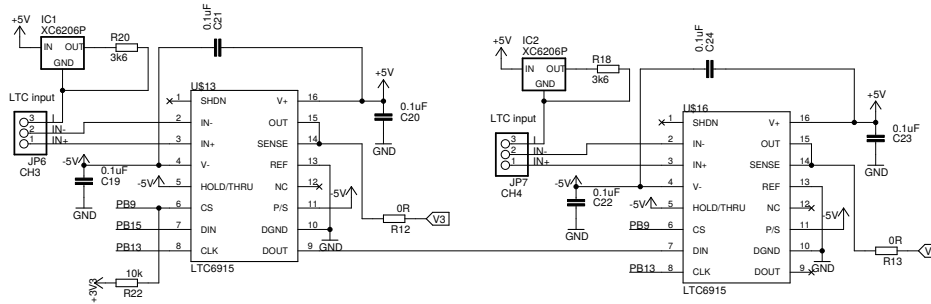


Figure 41: Electrical schematic of LTC6916 signal conditioner.

The attempt of mounting accelerometer was unsuccessful, as the package of LIS2DH and LIS2DH12 differs. Therefore, the ordered LIS2DH12 component did not fit into the LIS2DH footprint, which was discovered after unpacking.

The IR temperature sensor TMP006 was successfully soldered on a BGA rework station. The sensor has all the address pins connected to the ground, so the device's I2C address is 0x80. The TMP006 was tested and the internal registers including information about the device, die temperature and voltage were possible to read. Unfortunately, the register with the voltage contained an incorrect value. For this reason, the temperature calculated from the provided values was not correct. The computed temperature varied between 80°C and 90°C in the room. The improper functionality was due to failure to comply with the recommended layout.

The last component was the microSD card, which worked without issues.

4.3.3 External components connected to the testing boards

After experimenting with the testing board, additional parts were attached to the device. The external board STEVAL-MKI105V1 [48] with LIS3DH accelerometer showed in Figure 42 was connected and tested. The registers of the LIS3DH accelerometer can be programmed in the same way as LIS2DH12. Therefore, there was no issue with the code compatibility.

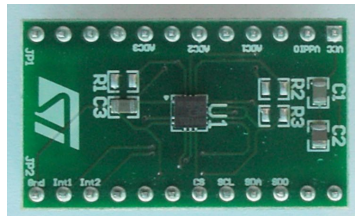


Figure 42: STEVAL-MKI105V1 adapter board with LIS3DH accelerometer from STMicroelectronics (source: [48]).

The 32F411EDISCOVERY board contains a microcontroller, which is linked to the testing board through a connector and wires. The discovery board does not include the battery and oscillator for the real-time clock, so they were additionally connected to the 32F411EDISCOVERY.

The last element connected to the testing boards was a LoLin V3 NodeMCU WIFI board with a Wi-Fi module ESP-12. The ESP-12 module differs from the ESP-07 only in antenna type, so the programming and connection were the same. The evaluation board was connected to the STM32F411VE MCU through UART interface. The final testing device is shown in Figure 43.

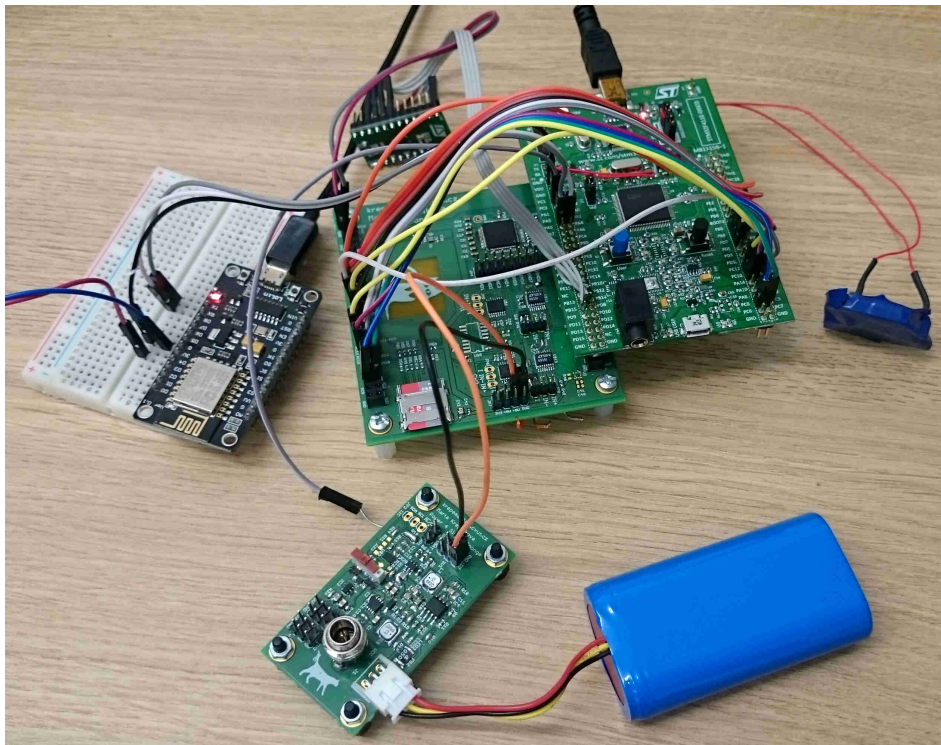


Figure 43: All parts of the testing device connected together.

The testing board allowed both to verify the functionality of the ADC7606 and to select a suitable signal conditioner as well as to test the footprints of the used components. The mutual communication between the components was also tested, and it showed shortcomings, which were later improved in the final version of the device. Those were, for example, a new footprint for the accelerometer, better layout for the temperature sensor TMP006, replacing the 3.3V regulator to the one with a higher output current, extension of current sources so they can be programmed, etc.

■ 4.4 Final board

The block diagram of the final device was mentioned in Section 4.1, and it corresponds to the final board. The only on-board sensor is the accelerometer, so the rest of the sensors are external. For example, the TMP006 IR temperature sensor needs to be placed in small hardly accessible places away from the main board. Therefore, a special board has been designed for it. The schematic and layout strictly follow the instruction in the datasheet. The complete schematic and layout are attached in Appendix B.

The final manufactured PCB showed in Figure 44 has all the components on a single 124.46 mm × 38 mm board. The board has four layers. The outer layers serve for signal paths and components, internal for power and ground planes. Multi-layer PCB allowed a higher level of miniaturisation of the final device. Most of the passive components are in the 0402 SMD package, which saves much space on the board. The board also includes many components for the final user. Besides the connector for the battery, the power adapter and the switch for the device power ON/OFF, the board is equipped with four test points, a connector for digital sensors and a connector for analog sensors. Eight LEDs indicate the state of the device.

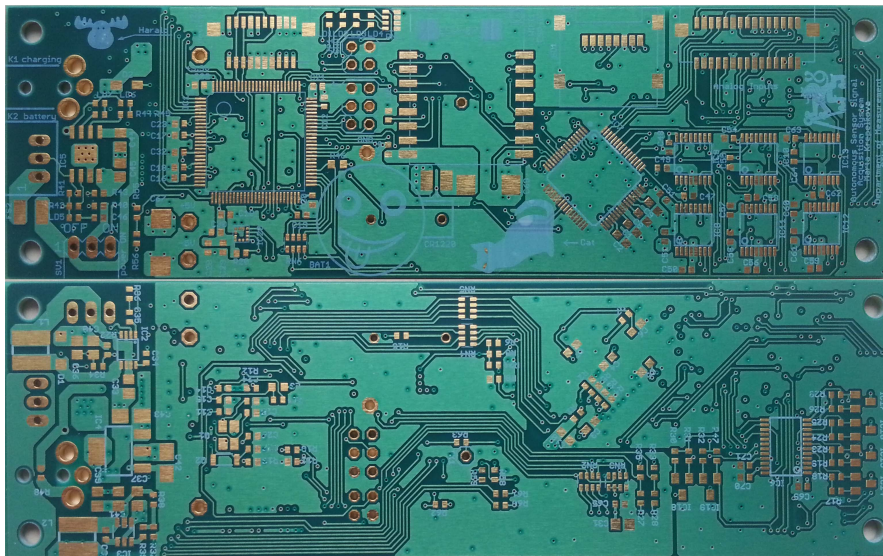


Figure 44: The TOP and the BOTTOM side of the final device's PCB.

The layout was designed with care about the interference between the components. The DC-DC regulators have to be placed as far as possible from the analog components. Otherwise, the accuracy of the analog components will be affected. Their accuracy can also affect the Wi-Fi module with RF antenna, which should also be placed as far as possible from the analog components. The antenna could also affect the DC-DC converters function. In the Figure 45 is the chosen block diagram of components position on the board.

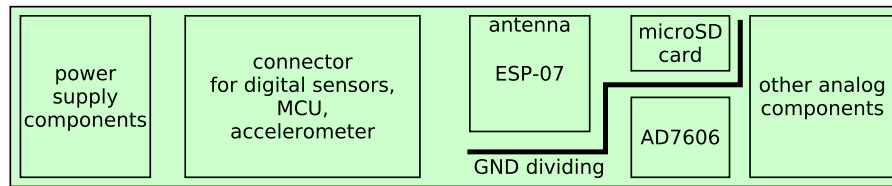


Figure 45: Final PCB's block diagram.

The following sections will describe the board in detail. During the testing, several changes were required, and they are mentioned in the description of the relevant parts. The schematic and layout of the final board including the corrections are attached in Appendix C.

4.4.1 Power part

The battery charging circuit and converters to $\pm 5\text{ V}$ use the same schematics as the testing board. The battery charger was connected accordingly to the recommended application to provide 0.5 mA charge current. The battery can be charged even if the device is powered off. Therefore, the switch for the device powering ON/OFF and its green LED indication is placed after the charging circuit. The green and red LEDs connected to the TP4056 battery charger indicate the charge status when the device is connected to an adapter. The charge voltage should be between 4 V and 8 V . The schematic of this part is in Figure 46.

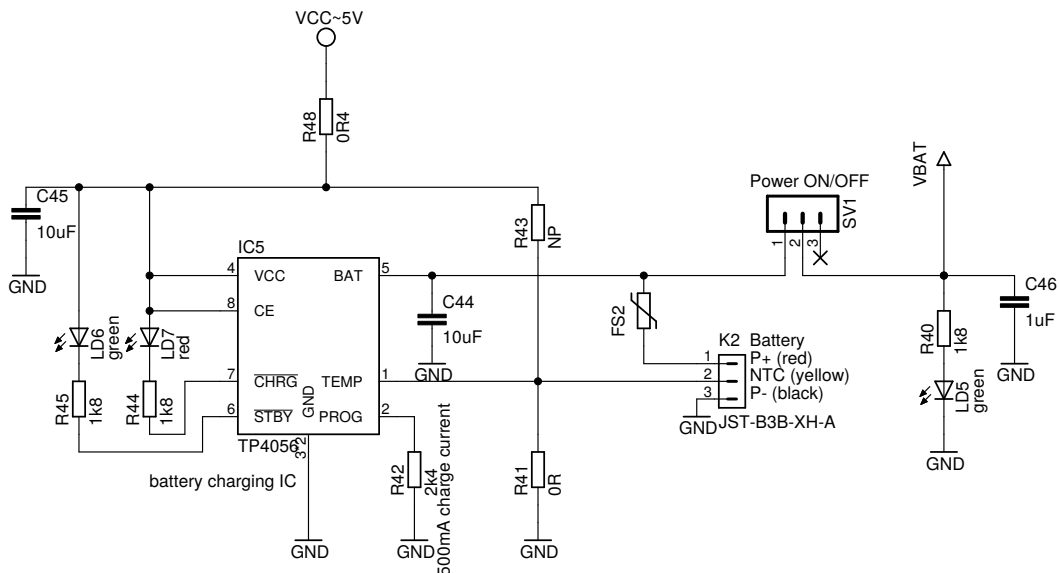


Figure 46: Battery charging circuit with power ON/OFF switch.

4.4 FINAL BOARD

The Li-Ion battery discharge curve is assumed to be linear. Hence the voltage can be directly measured and calculated to approximate the battery percentage. The maximum voltage range of the ADC included in the microcontroller is limited by the power supply voltage of the microcontroller. The full charged battery has the output voltage higher than the microcontroller's power supply. Therefore, the voltage divider was placed between the battery output and ADC pin to measure the whole battery output voltage range. The divider is shown in Figure 47 and its output voltage is approximately 0.75 times the input voltage.

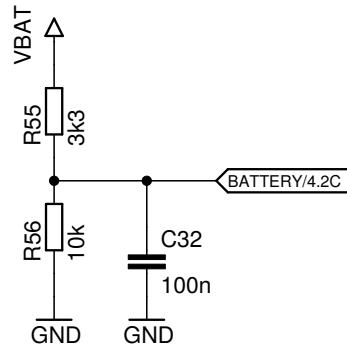


Figure 47: Voltage divider for battery voltage measuring.

The step-up and step-down DC-DC converters were already described in Section 4.3.1. Their final schematic does not differ from the testing schematic.

The 3.3 V voltage regulator MIC5504 was replaced by the TS1117BCW33 regulator, which has a larger output current. The higher current is necessary for the Wi-Fi modules based on ESP8266, which generates current peaks. They can cause a voltage drop and affect the function of other components in the circuit. The TS1117BCW33 regulator was connected according to the recommended application. Additionally, a niobium electrolytic capacitor was placed to the regulator's input. It stabilises sudden power changes because the 5 V converter would not be able to deal with them quickly. It would affect the analog components accuracy. The schematic is in Figure 48.

The power supply part included the first mistake. The power adapter was not connected according to the datasheet. The two pins of the connector were swapped, so it was necessary to swap them using an extra wire.

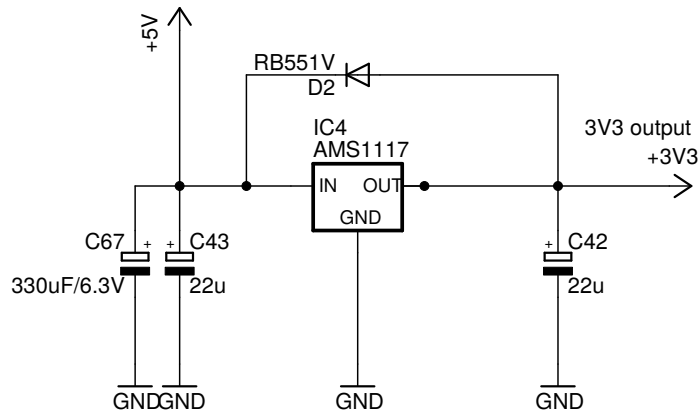


Figure 48: Electrical schematic of 3.3 V voltage regulator TS1117BCW33.

4.4.2 MicroSD memory card

The microSD memory card was connected according to the recommended application. The schematic is in Figure 49. The card is connected in four-wire SD data transfer mode with the SDIO pins of the microcontroller. The data are transferred through bidirectional D0-D4 pins. The clock signal is generated by the microcontroller and transferred to the CLK pin of the card. The CMD pin is a bidirectional command/response signal.

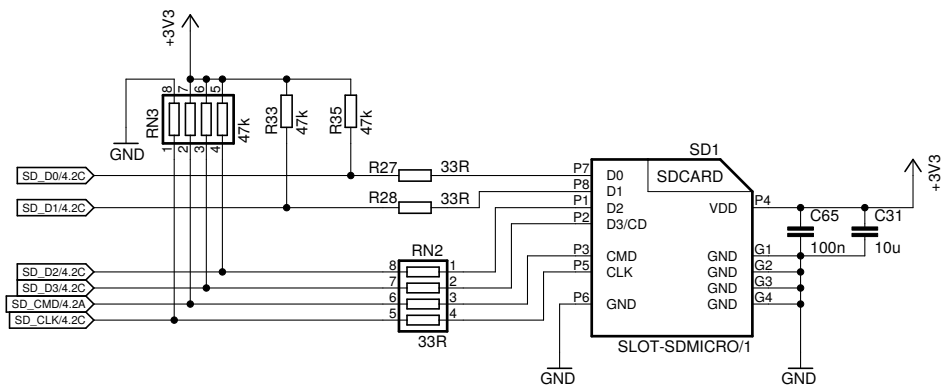


Figure 49: Electrical schematic of the microSD card.

4.4.3 Accelerometer LIS2DH12

The accelerometer LIS2DH12 was connected according to the datasheet, and the schematic is shown in Figure 50. This accelerometer allows communication through SPI and also I2C interfaces. The SPI bus was chosen for its higher data rate and is shared with the LTC6915 signal conditioners. The interrupt pins are not connected because they are useless in this application.

4.4 FINAL BOARD

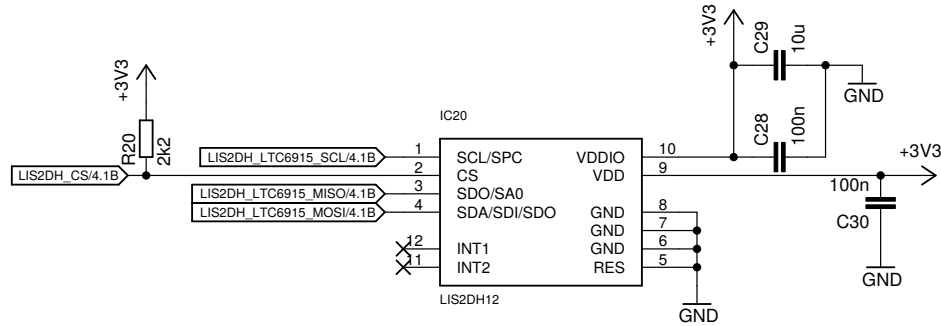


Figure 50: Electrical schematic of the LIS2DH12 accelerometer.

4.4.4 Wi-Fi module ESP-07

The schematic of the ESP-07 module is in Figure 51. The supply voltage of the module is filtered by the LC filter to avoid the interference of the 3.3 V power supply. The module has connected both the UART and SPI interfaces. The current module's firmware uses UART interface for the data transmission between the module and the microcontroller. However, the firmware can be replaced by the new one that would allow SPI data transmission, as the SPI interface has higher data rate. If the SPI is used, the GPIO15/SS pin should be pulled up.

The module includes two LEDs. The red one indicates that the module is powered up. The blue one is connected to the TX0 pin of the module and indicates the data transmission. A green external LED indicates the TX1 data transmission. The default UART state requires the green LED to be connected to a power supply. In the beginning, the LED was tied to ground, so it had to be corrected.

The Wi-Fi module is a source of interference, so it should be reflected in the layout. The final board has a ground plane below the antenna, which decreases the Wi-Fi range. For the next versions, the layout was fixed.

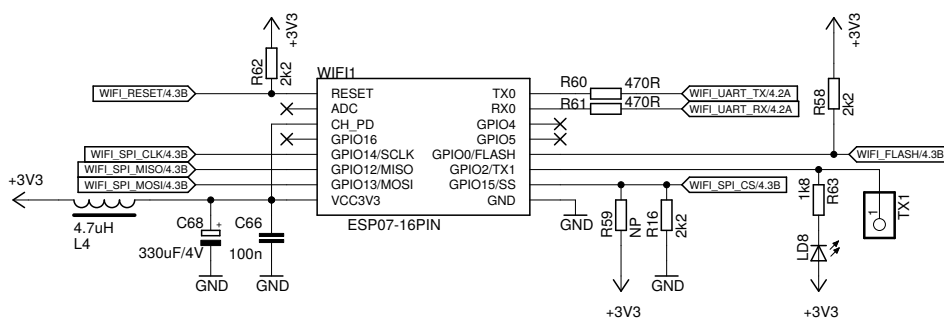


Figure 51: Electrical schematic of the ESP-07 Wi-Fi module.

4.4.5 Microcontroller STM32F411VE

The schematic of the microcontroller is in Figure 52, and it follows the recommended application. The battery BAT1 serves to power the real time clock. The JP1 is an SWD connector for programming and debugging the microcontroller. For an update of the microcontroller's firmware, the SWD pins have to be connected to the ST-LINK. The ST-LINK can be external [49] or embedded on any of STMicroelectronic's kit. The SWD pin arrangement on the final board is shown in Figure 53.

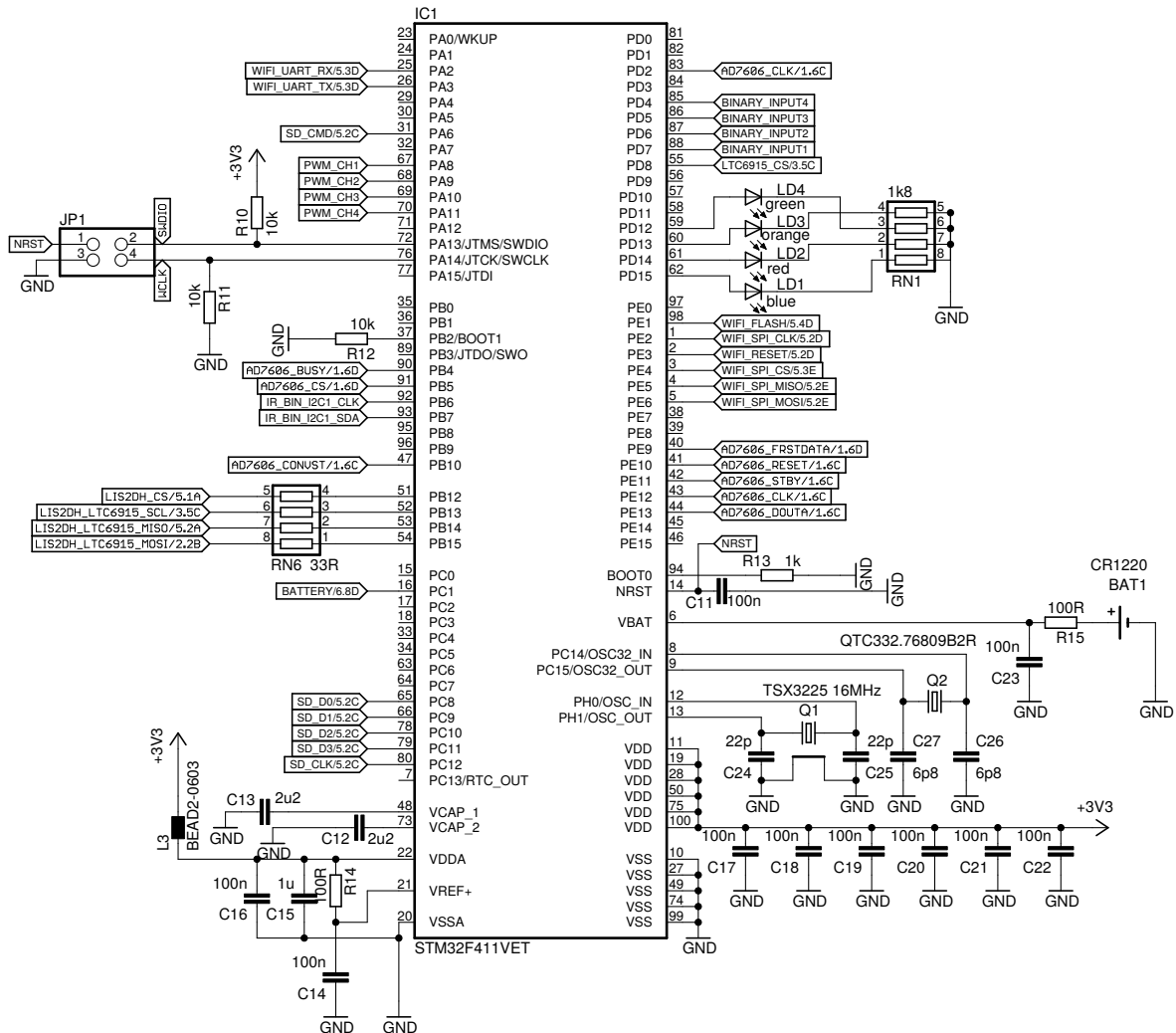


Figure 52: Electrical schematic of the STM32F411VE microcontroller.

4.4 FINAL BOARD

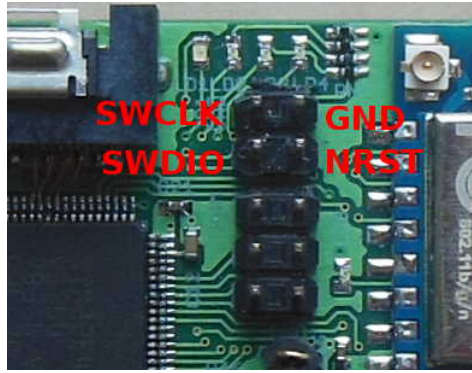


Figure 53: SWD pin arrangement on the final board.

■ 4.4.6 ADC AD7606

The converter and the associated passive components are shown in Figure 54 and they were connected according to the datasheet. The serial interface is selected by setting the pin $\overline{\text{PAR/SER/BYTE SEL}}$ to a logic one. Therefore, pins DB7/DOUTA and DB8/DOUTB serve for the transmission of measured data. The converted channels V1 to V4 appear on DB7/DOUTA pin simultaneously with the channels V5 to V8 on DB8/DOUTB. If the DB8/DOUTB is not being read, all the data appear on DB7/DOUTA pin. The DB[6:0] and DB[13:9] pins are present for the parallel interface, so they are tied to logic zero in this configuration. The RANGE pin is tied to logic zero, so the $\pm 5\text{V}$ range is set. The REF SELECT pin is set to logic one, and the internal reference is selected and enabled. The oversampling mode pins OS[2:0] are shorted together and tied to logic zero, so no oversampling is selected. Therefore, the maximum throughput is 200 kHz, and SNR is 89 dB.

Part of the AD7606 pins are connected to the microcontroller and can be configured. They serve to set the beginning of the conversion, read the data and get additional information about the state of the conversion. Their usage is the following:

$\overline{\text{STBY}}$ (Standby Mode Input) serves to place the AD7606 into the power-down mode by connecting the pin to logic zero.

RESET (Reset Input) serves to reset the converter after the power on.

CONVST (Conversion Start Input) serves to initiate conversions of the analog input channels. Both channels are sampled simultaneously, so the CONVSTA and CONVSTB are shorted together. The rising edge indicates the beginning of the conversion.

$\overline{\text{RD/SCLK}}$ (Parallel Data Read/Serial Clock Input) serves as a clock signal for the SPI interface.

$\overline{\text{CS}}$ (Chip Select Input) serves as a slave select for the SPI interface.

BUSY (Busy Output) indicates the proceeding conversion. The signal goes to logic zero when the conversion is finished.

FRSTDATA (First Data Output) indicates the first channel V1 is being read back.

DB7/DOUTA (Serial Interface Data Output Pin) is a serial output for converted data.

The network resistors are placed to improve the shape of transmitted signals. The AD7606 has eight inputs, where six can be in advance amplified by the signal conditioner, and two goes directly from the connector.

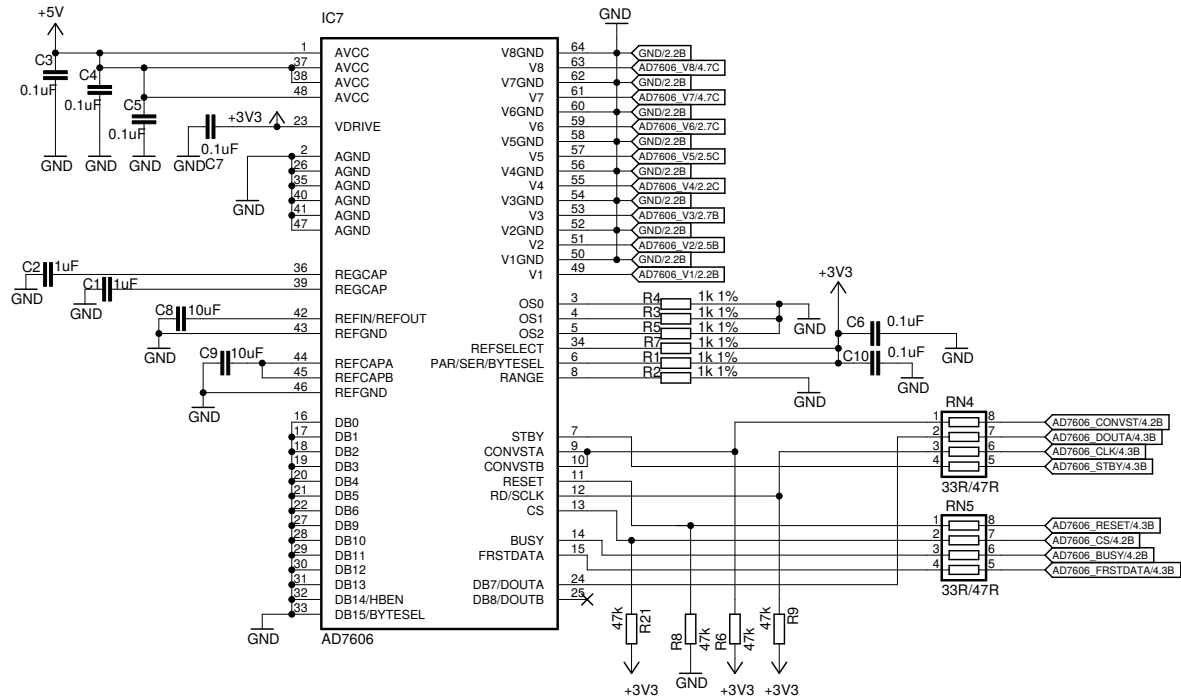


Figure 54: Electrical schematic of the analog-to-digital converter AD7606.

4.4.7 Signal conditioners LTC6915 and current sources

The six programmable signal conditioners LTC6915 are present on the board to amplify the AD7606 input signal. Their gain can be programmed through the SPI interface. They are connected in a daisy chain, so the data output of the first one is the data input of the next one. All of them have common clock signal and slave select signal. The schematic of one channel is in the Figure 55. The LTC6915 signal conditioner does not include any protection. Therefore, protective diodes should be connected to the inputs to protect the conditioner from voltages higher than the supply voltage. The diodes are not present in the final device, so the user must be careful not to connect a voltage higher than the supply voltage of the conditioner.

4.4 FINAL BOARD

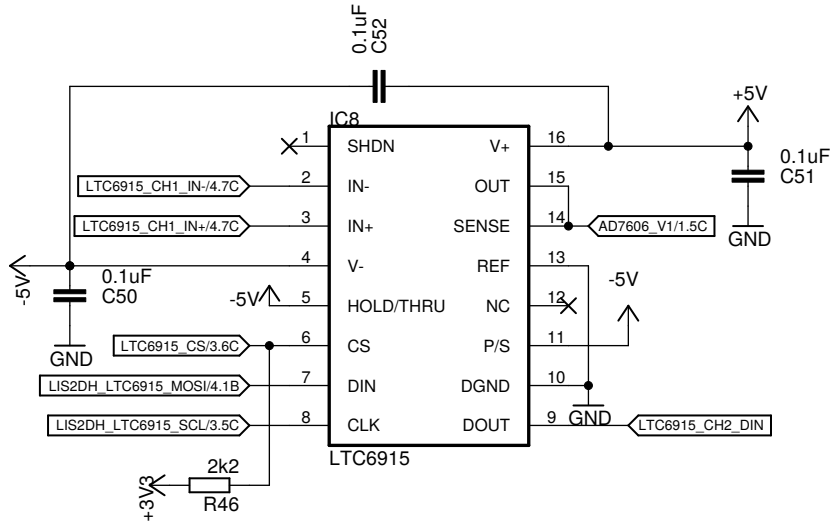


Figure 55: Electrical schematic of the first LTC6915 signal conditioner.

The signal conditioners do not provide any power source for the connected sensors. Therefore, the external programmable sources were created. Each current source is obtained from the voltage regulator XC6206182MR connected, so it provides a constant 0.5 mA or 0.2 mA current. The required output current is changed using the MAX335 programmable switch. By switching on a single MAX335 channel, the resistor connected in parallel to the switch is shorted, so the output current increases. The schematic of the programmable sources is in Figure 56.

Both LTC6915 conditioner and MAX335 programmable switch have the same SPI configuration. Therefore they can be configured in a single daisy chain. The data output of the sixth conditioner is connected to the input of the programmable switch MAX335. The SPI bus is also shared with the LIS2DH12 accelerometer, whose connection is in section Section 4.4.3. However, the SPI configuration of the accelerometer is different; therefore the interface has to be reinitialised. The reinitialisation is not an issue because the conditioners are initialised just once before the start of the measurement. So the reinitialisation during the measurement is not needed and does not affect the speed of the measurement.

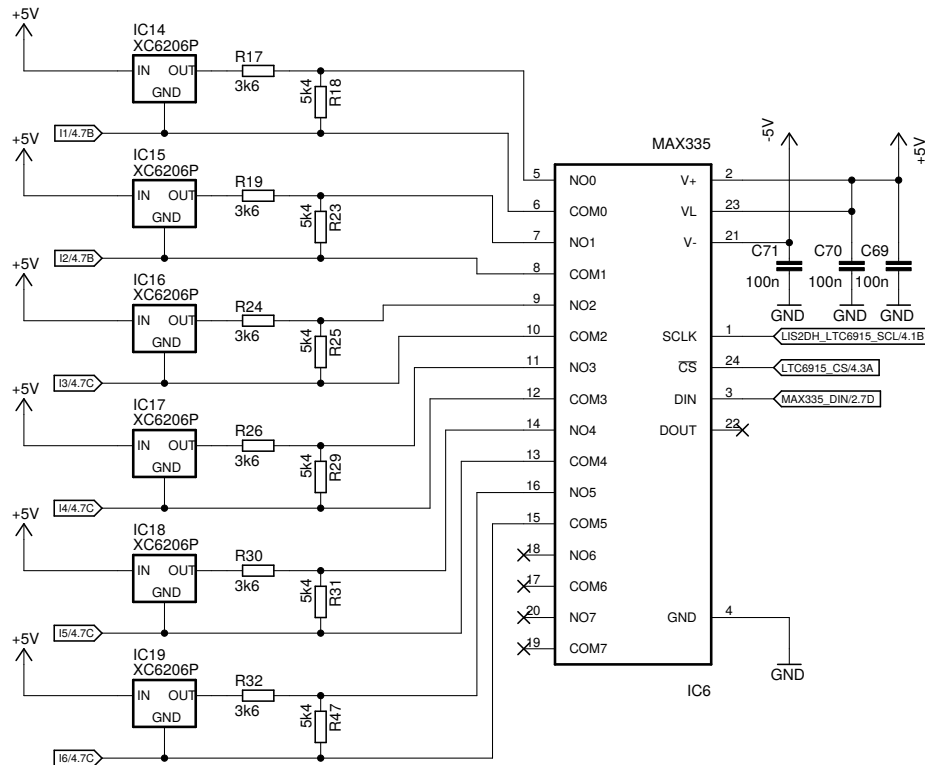


Figure 56: Electrical schematic of the current sources, which are switched using the MAX335 programmable switch.

4.4.8 User connectors

On the board three user connectors are available, schematics of which are shown in Figure 57. The user has to follow the connection to connect his device.

The PWM connector is optional and can be replaced by any 2.54mm header. The pin arrangement on the board is shown in Figure 58.

The second connector provides I2C interfaces and universal binary inputs. It is possible to connect up to three I2C devices with different addresses. All of them share the same I2C bus, which is connected to microcontroller's pins PB6 (SCL) and PB7 (SDA). The universal binary inputs are connected to the microcontroller's pins PD4-PD7.

The third connector serves for analog inputs and current sources output. Six inputs are going into signal conditioners, and six outputs of current source are intended to supply the analog components. Two more inputs are going directly to the analog-to-digital converter.

4.4 FINAL BOARD

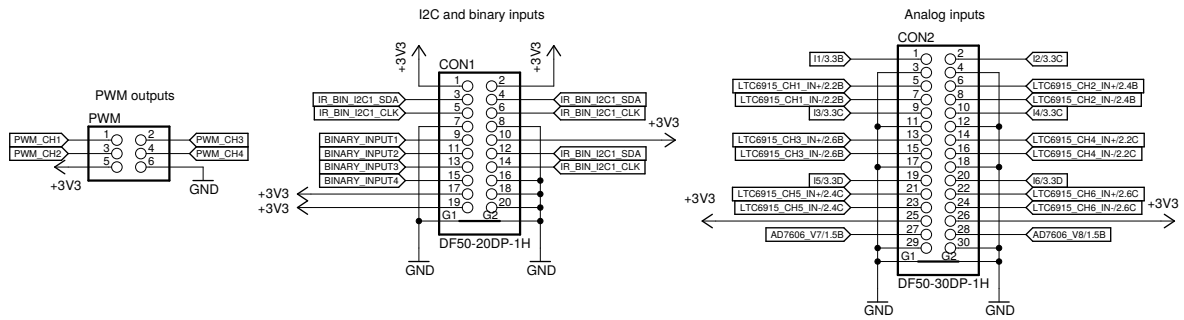


Figure 57: Electrical schematic of the user connectors.

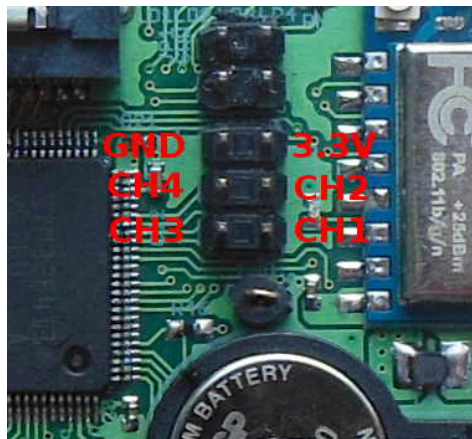


Figure 58: PWM pin arrangement on the final board.

4.4.9 Photo of the final board

The final board was successfully assembled and tested. The necessary changes mentioned in the text above were made and corrected in the final schematic and layout. The assembled board is shown in Figure 59.

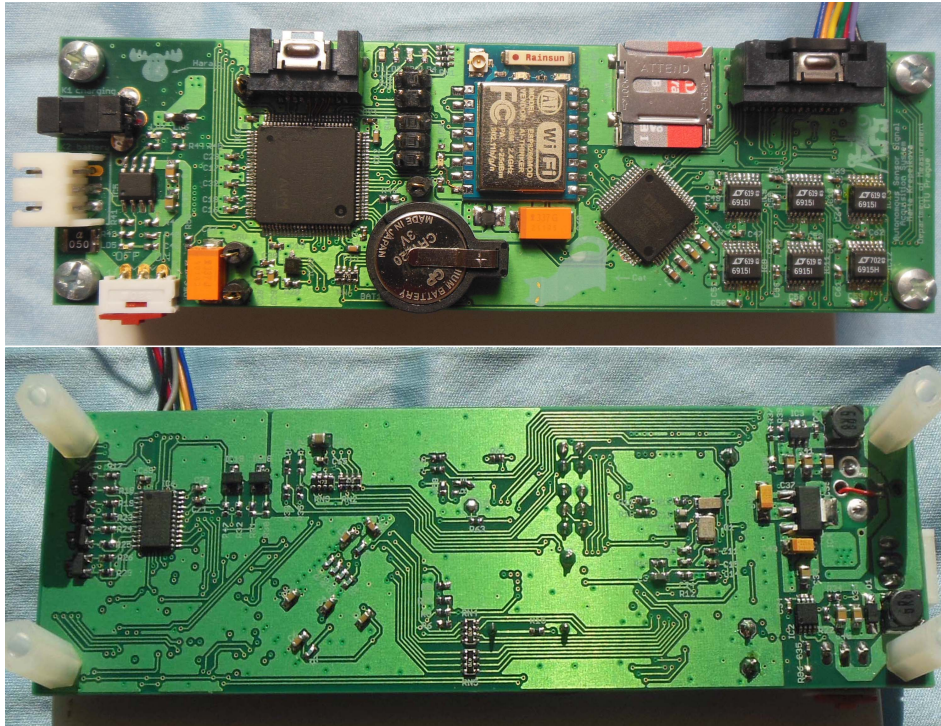


Figure 59: Assembled final board.

■ 4.5 STM32F411VE microcontroller's firmware

The important part of the device is a firmware programmed for the STM32F411VE microcontroller. The microcontroller is responsible for the following operations:

- Read the measured data from the AD7606 analog-to-digital converter.
- Set the gain of the LTC6915 signal conditioners.
- Set the state of the MAX335 programmable switch.
- Read the voltage of the battery and compute the approximate battery percentage from this information.
- Implement the functionality for the digital accelerometer LIS2DH12 and IR temperature sensor TMP006.
- Store the measured data to the card and also read them from the card.
- Delete data from the card.
- Cooperate with the microcontroller inside the Wi-Fi module to allow data transmission and measurement configuration.

The user can extend the code for custom devices and universal PWM outputs. How to upload a new firmware into the microcontroller is described in Section 4.4.5.

The main flow chart is in the Figure 61. After the device turns on, the microcontroller initiates all the components and tries to mount the microSD card. If the mounting is successful, it updates the state on the page, sent to the user by Wi-Fi. The state consists of approximate battery status and measurement state. In this initial moment,

4.5 STM32F411VE MICROCONTROLLER'S FIRMWARE

the measurement is not processing. If the microSD card mount is not successful, the program turns on the red LED and ends. The state on the page indicates the same by showing a fail message instead of a list of files on the card.

The battery status and state of the measurement is sent in an infinite loop every two seconds to the user. If the user starts the measurement through the Wi-Fi, the microcontroller goes to measurement function and runs the measurement. The measurement flow chart is in the Figure 62.

The data measured by the AD7606 converter are stored in a buffer with a defined number of rows, denoted as *samples in buffer*. A single AD7606 measurement consists of all eight measured channels and is considered as one sample saved in a single row. The data are stored via a cyclic buffer shown in Figure 60. It consists of two buffers that are cyclically switched. The actual position in a buffer is passed to the DMA RX stream. When the first buffer is being filled with new values, the second one is being saved on the microSD card. The data from digital sensors are measured from the AD7606 converter and saved just once per n samples.

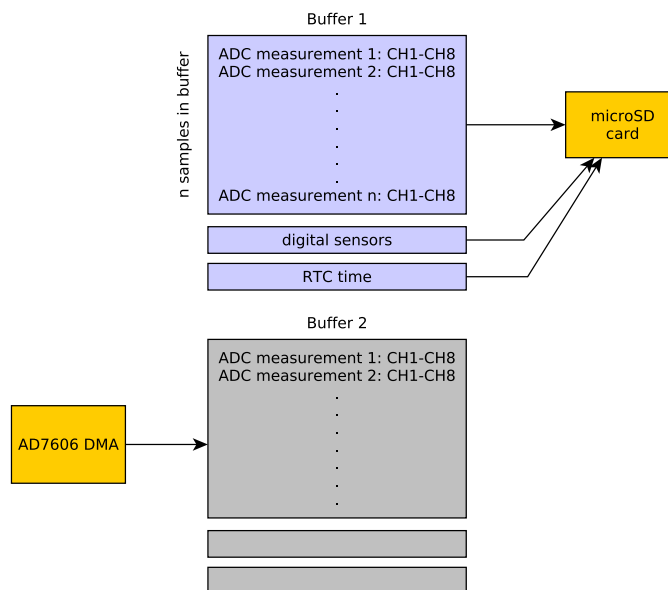


Figure 60: Cyclic buffer for the measurement.

The code is written in C language using STM32 Standard Peripheral Libraries [50]. Every component has its source and header file, as well as a configuration header file with GPIO pins definitions. In the following text, the code for each component is described in more detail.

4.5 STM32F411VE MICROCONTROLLER'S FIRMWARE

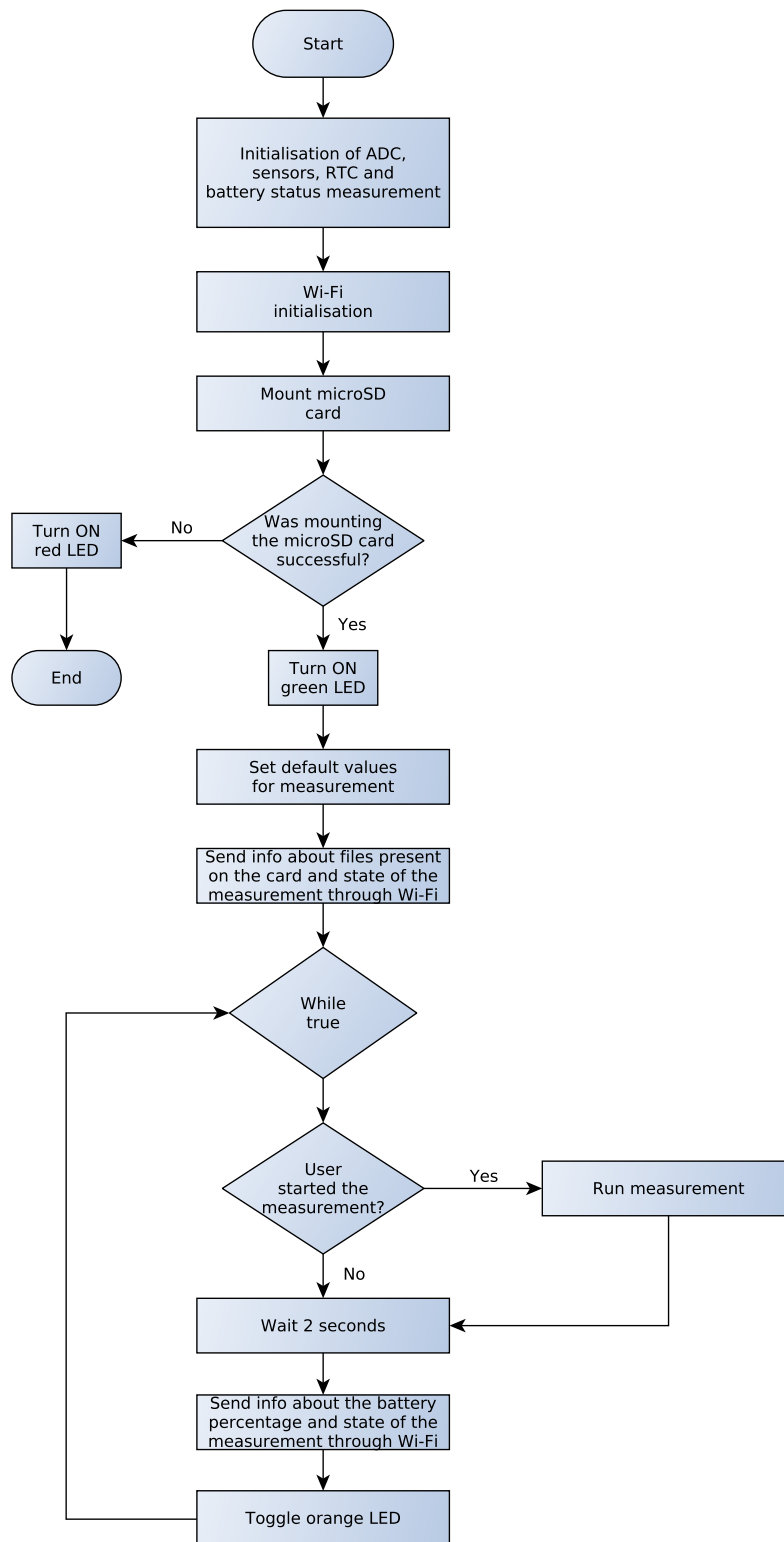


Figure 61: Main flow chart.

4.5 STM32F411VE MICROCONTROLLER'S FIRMWARE

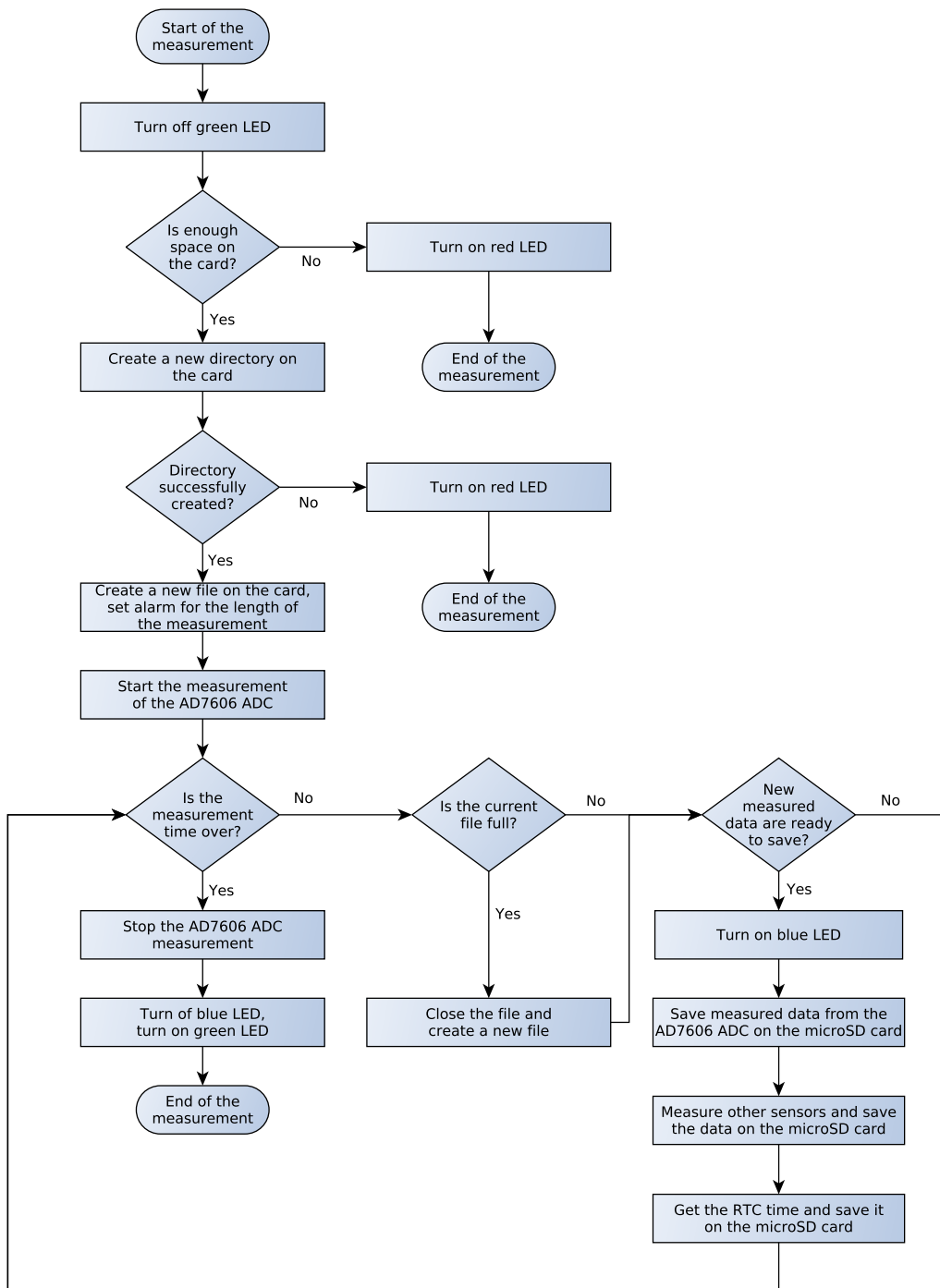


Figure 62: Measurement flow chart.

4.5.1 The AD7606 converter

The AD7606 converter has adjustable sampling frequency, and the measurement can be enabled and disabled. The data are transferred through the SPI interface using DMA, and two timers are used for the beginning of the conversion and the slave selection.

The AD7606 converter offers two reading modes: reading after a conversion and reading during a conversion. It was difficult to keep the desired timing diagram for the reading during a conversion, so the reading after a conversion shown in Figure 63 is used.

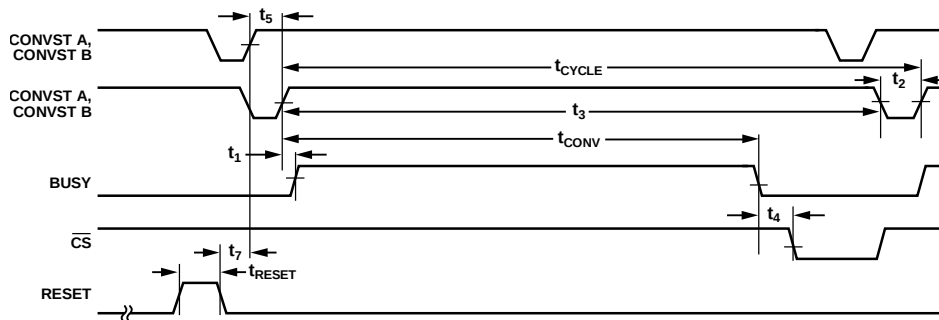


Figure 63: AD7606 ADC timing – reading after a conversion.

The reset of the converter is done after the device is switched on. When the user wants to start the measurement, the converter has to measure for a selected time automatically. Therefore, the following programming methods with the timing diagram shown in Figure 64 were chosen.

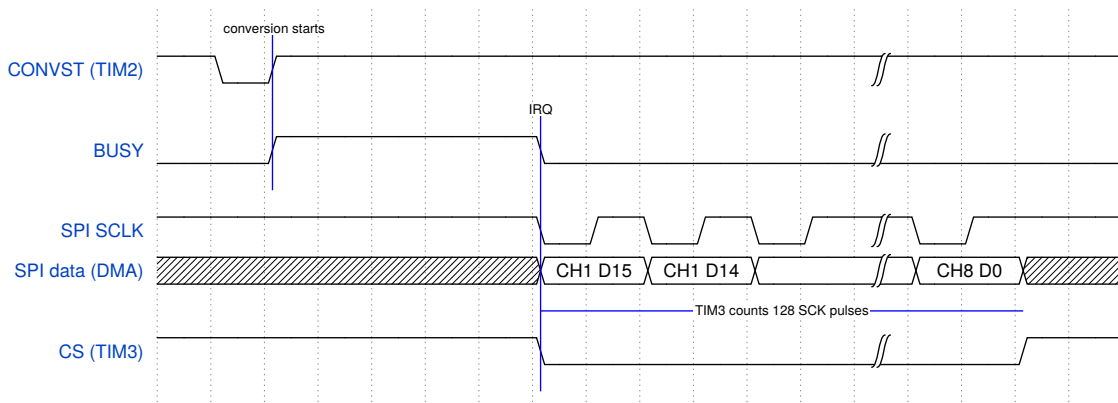


Figure 64: AD7606 ADC final timing diagram.

The CONVSTA and CONVSTB signals are shorted, so just one signal is necessary to generate the start of the conversion. The measurement has to be fully automatised. Therefore, the beginning of the measurement has to be generated automatically with the frequency given by the selected sampling frequency. The CONVST signal uses

4.5 STM32F411VE MICROCONTROLLER'S FIRMWARE

the TIM2. The timer has automatically reinitialised prescaler value and period based on the sampling frequency.

After the CONVST rising edge, the converter begins the measurement and the BUSY signal switches to a logic one. The signal is indicating the proceeding conversion. The data can be read back after the falling edge of the BUSY signal. The slave select signal needs to go to logic zero to read the data through the SPI. The rising edge of the slave select signal has to come exactly after all the data are transferred. However, when the data are saved through DMA, no signalisation for data transfer completion is present. The TIM3 with an external trigger on the falling edge of the BUSY signal was programmed for this purpose. Therefore, after the BUSY signal goes to logic zero, the TIM3 forces the slave select also to logic zero. The transmission takes exactly 128 clock pulses. The timer computes the clock pulses, and after the 128th pulse, the slave select signal goes back to logic one. The SPI data transfer is executed in an interrupt generated on the falling edge of the BUSY signal. The data are saved into a prepared buffer using DMA.

The data are saved on the microSD card as signed 16-bit integer in little endian format. The value can be transformed to the voltage using the Equation (22).

$$V = \frac{\text{int16 value}}{2^{15}} \cdot V_{REF}, \quad (22)$$

where the $V_{REF} = 5\text{ V}$ is converter's reference voltage.

■ 4.5.2 The LTC6915 signal conditioners and the MAX335 programmable switch

The signal conditioners have a programmable gain. Through a programmable switch the output current for the sensors can be changed. The conditioners and the switch are connected in a single daisy chain as is mentioned in the Section 4.4.7. Therefore, the data are sent in a row and all the devices are programmed after the SPI initialisation.

■ 4.5.3 The microSD card

The microSD card is formatted as the FAT32 file system. The existing library for STM32F4 microcontroller and FAT file system [51] was modified and used. The library is based on FatFs module by [52]. The library supports following operations: card initialisation, detection, mounting, writing on the card, reading from the card, etc. The library's source code is stored in extern source folder named SDIO.

The card is mounted via a four-wire SDIO interface with DMA configuration. The final device implements following functionalities (for the card): creating a new directory named after the current time, finding existing files on the card and formatting the card.

■ 4.5.4 The real time clock

The real time clock peripheral is configured only if the previous configuration is not present. The configuration is stored in the RTC backup register. The device's configuration consists of the current time and date, and it is stored using the battery and RTC oscillator connected to the microcontroller. Disconnecting the RTC battery discards the information about the date and time. When the new date and time needs to be set, it has to be configured again. The structures for the date and time should be filled with the current date and time information. These values are stored after the RTC configuration, setting the backup register as well. The folders and files names created on the microSD card are derived from the current time.

The RTC alarm is used to determine the measurement ending time. The alarm invokes an interrupt, and the measurement is stopped.

■ 4.5.5 Battery percentage measurement

The battery voltage is measured through an ADC inside the microcontroller. The measurement is performed via DMA. The approximate battery percentage is derived from the arithmetic mean of defined number of samples of the voltage. The knowledge of the maximum and the minimum voltage values and resistors values in the voltage divider are necessary for the battery percentage calculation.

■ 4.5.6 The LIS2DH12 digital accelerometer

The selected accelerometer can use both SPI and I2C interfaces. The SPI interface was selected for its higher data rate. The accelerometer is configured after the SPI initialisation. The configuration includes, for example, the data rate, resolution mode and SPI mode. The user can also specify the range of the accelerometer. The range is set up in a function, which writes the adequate values into the control register of the accelerometer. The x , y , and z acceleration axes are obtained by reading the output registers of the accelerometer.

■ 4.5.7 The IR temperature sensor TMP006

The TMP006 infrared sensor communicates through the I2C interface. The sensor needs just the I2C initialisation. The manufacturer ID, device ID, local temperature and sensor voltage can be read from the sensor's registers. An algorithm for computation of the temperature from the local temperature and sensor voltage is described in Section 4.2.4.

The I2C interface uses acknowledgements, which can be a disadvantage. When the TMP006 temperature sensor is not connected, the code for the registers writing should not be executed. Otherwise, the program will be waiting for the device's response, which never comes.

■ 4.5.8 Placeholders for the custom code

Inside the code are present placeholders, where some extra code can be inserted. Every component has to be usually initialised and in a measuring loop periodically measured. The measured data can be saved into the microSD card. A recommended example of the code implementation for more sensors are the source and header files of the IR temperature sensor. The user functions can be called from the prepared parts of the `main.c` source file. The parts are specified by comments in the code.

■ 4.5.9 The Wi-Fi module

The Wi-Fi module is intended to provide a user interface for the end user. The current firmware inside the ESP-07 Wi-Fi module supports the UART interface for the communication with the STM32F411VE microcontroller. On the STM32F411VE microcontroller's side, the UART for the Wi-Fi module has to be initialised with the same parameters, as was initialised in the module. The TinyFrame library [53] for building and parsing frames over a serial interface was used for the communication. Both the STM32F411VE microcontroller and the module's microcontroller include this library, so they can easily cooperate using the library's API. The type of the request from the module is recognised, and the required code in the STM32F411VE microcontroller is executed. The communication between both microcontrollers is in more detail described in Section 4.6.

The communication from the STM32F411VE to the Wi-Fi user interface includes following messages:

- Battery status: the approximate battery percentage.
- Measurement status: it determines, if the measurement is proceeding or not.

The Wi-Fi module can send the following requests to the STM32F411VE microcontroller:

- Set the measurement parameters: the STM32F411VE microcontroller receives the new measurement parameters, which are saved into a prepared structure and STM32F411VE sets the components. The STM32F411VE microcontroller does not respond to this request.
- Start the measurement: the STM32F411VE microcontroller sends back to the Wi-Fi module the beginning measurements status. The STM32F411VE microcontroller sends another measurement status to the Wi-Fi module after having finished the measurement.
- Get the names of the files on the microSD card: the STM32F411VE microcontroller lists all the files present on the card and sends a list as a response to the Wi-Fi module.

■ 4.6 The ESP8266 microcontroller's firmware

The Wi-Fi module ESP-07 comes with a default AT-command firmware [54]. The module communicates with the microcontroller via AT-commands. The initial implementation used a finite state automaton to parse the commands together with the HTTP1.1 GET requests for the user control. This solution was later dismissed as it was complex to maintain all possible commands and the firmware was slow.

The final device required firmware capable of more advanced control. A new firmware was created in cooperation with Ondřej Hruška, who already tested existing examples. He created a working solution available from his GitHub page [55]. Ondřej Hruška also created the TinyFrame library [53] for building and parsing frames that are being sent over a serial interface.

The necessary modifications were made to fit the Ondřej Hruška's firmware on this device. The UART baud rate is set to 460 800, which is the highest value ensuring reliable data transfer. An appropriate web page was implemented and is shown in Figure 65. The web page uses the styles from the project example and provides to the user the following features:

- Wi-Fi configuration (took from the example project).
- Display a project overview page (also took from the example project).
- See the approximate battery percentage. It is not being actualised when the measurement is in progress.
- Set the measurement parameters.
- Start the measurement. It is not allowed if there are more than 30 files on the microSD card. In such case, the user must erase the card.
- Display files present on the microSD card. The files are displayed only if the measuring is not in progress.
- Delete the files from the microSD card.

The parts of the web page are dynamically changed using JavaScript and JSON, and the frames are transferred using TinyFrame library. The web page can be visible on the 192.168.4.1 address after connecting to the ESP-07 Wi-Fi.

■ 4.6.0.1 The TinyFrame library

The TinyFrame library [53] allows the frame identification using a unique ID. The frames can be protected against unintended modifications by a checksum (XOR, CRC16 or CRC32). The frame structure is shown in Figure 66. Every frame consists of:

- SOF (Start of Frame): one bit 0x01.
- ID (Identifier): a unique frame identifier. The MSB is the peer bit.
- LEN (Length): the number of data bytes in the frame.
- TYPE: the message type used for Type Listeners.
- HEAD_CKSUM: header checksum.
- DATA: the transferred data consist of LEN bytes.
- DATA_CKSUM: checksum, implemented as XOR of all preceding bytes in the message.

4.6 THE ESP8266 MICROCONTROLLER'S FIRMWARE

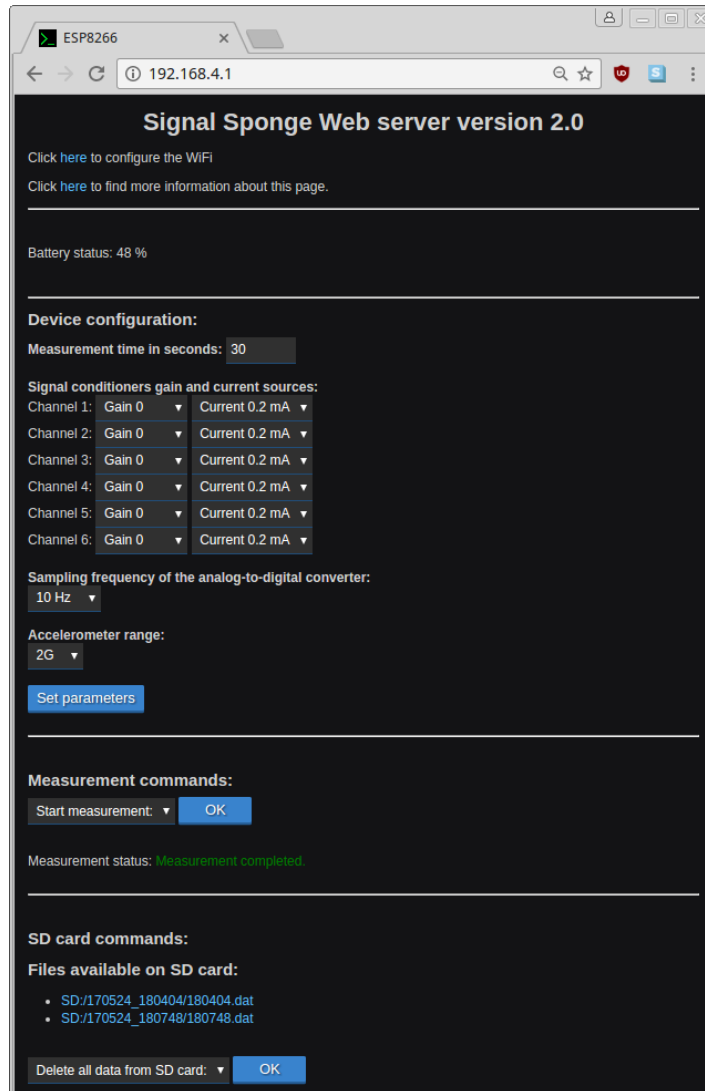


Figure 65: The web user interface.

The library allows an initialisation as a Master or a Slave device. The data can be transferred using a sending or a respond function. The three types of listeners can be created: Generic listener, Type listener and ID listener.

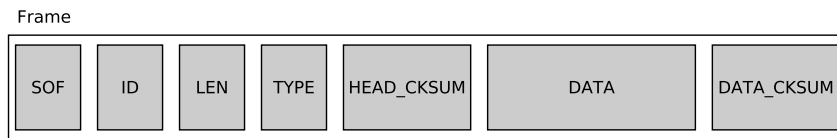


Figure 66: The TinyFrame structure.

■ 4.6.0.2 Implementation of the TinyFrame library

The TinyFrame library is implemented in both ESP-07 module and STM32F411VE microcontroller. The ESP-07 module is configured as a Master and the STM32F411VE microcontroller as a Slave. There are seven message types:

- MSG_param: to set the measurement parameters.
- MSG_start: to start the measurement.
- MSG_SDdelete: to delete the files on the microSD card.
- MSG_SDsend: to download the file from the microSD card.
- MSG_battery: to get the information about approximate battery percentage.
- MSG_measurementEnd: to get information whether the measurement is proceeding or not.
- MSG_fileNames: to get a list of files present on the microSD card.

The data are received using three Type listeners. The first is for battery percentage, the second for information about the measurement (proceeding or not) and the third for getting the file names presented on the microSD card. If the message from the STM32F411VE microcontroller comes, it is parsed by the message type and executed by an adequate listener. The adequate part of the web page can be updated by the listener to inform the user about battery status, measurement status and available files.

The measurement parameters are set by the (HTTP 1.1) GET method. The parameters are proceeded in a httpd function inside the ESP8266 microcontroller and sent to the STM32F411VE microcontroller. The message is parsed inside the STM32F411VE microcontroller by the message type and executed by an adequate listener.

The command for the start of the measurement and command for the card erase is performed by sending a frame that includes just the message type. The adequate code is proceeded by the type listener inside the STM32F411VE microcontroller.

The request for the file download is sent as a message including the message type and the file name. The STM32F411VE microcontroller's listener proceeds the code for reading the file from the microSD card. The file is sent in parts using the respond function. The frame includes the message type, data and also an acknowledgement containing either that there is more data to be sent, or the transmission of the whole file has finished.

When the web page is loaded, a request for files available on the microSD card is sent automatically. The listener inside the STM32F411VE microcontroller finds the files and sends the names in a respond.

Chapter 5

Results

the final device has been tested, so its full functionality is ensured. The hardware part required several modifications, mentioned in the text in Figure 59. These modifications were made and corrected in the schematic and layout for the further production. Several changes can be further made to improve the device durability. For example, the input protective diodes can be placed to the inputs of the signal conditioners protecting them from accidental high voltage application. Another improvement may be rewriting the WiFi firmware for the SPI communication.

The firmware was implemented to support all the required functionalities of used components. The device's power consumption was measured, and it meets the requirements for a low consumption. The consumption is around 0.2 A when the measuring is not in progress, so the battery can last for 21 hours. The final acquisition system is shown in Figure 67.

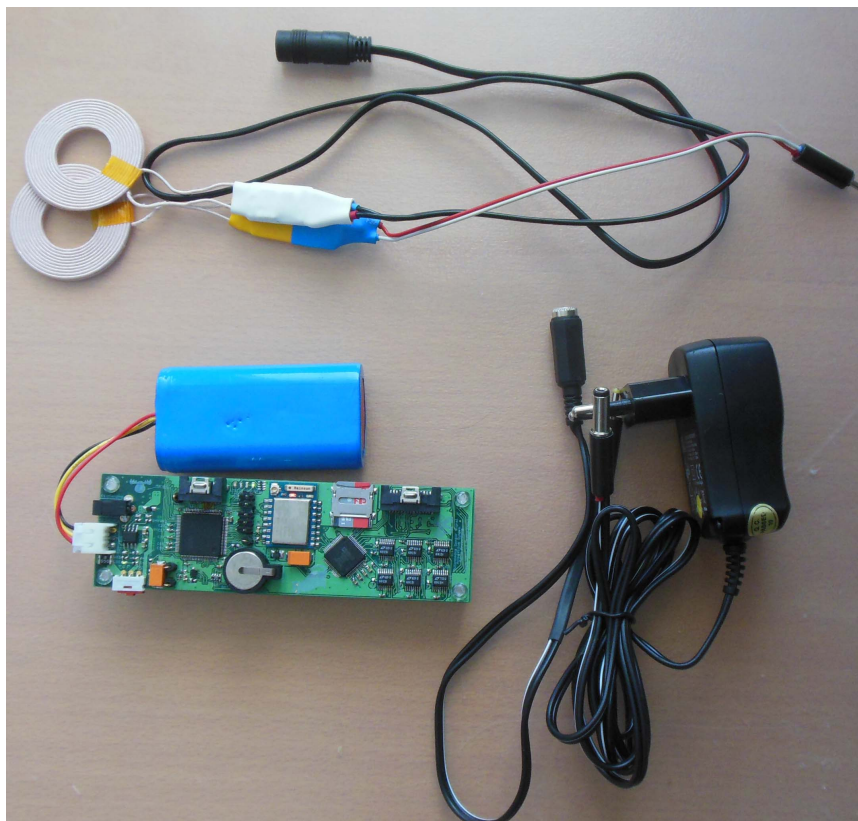


Figure 67: The developed sensors acquisition system.

The system supports to measure up to eight analog inputs. The analog-to-digital converter is programmed to allow selectable adjustable frequency from 10 Hz to 20 kHz. In the future, the code is prepared to support sampling frequency up to 100 kHz. The current sampling frequency is limited by the speed of the microSD card. Two of the analog inputs go directly to the converter. Six of the analog inputs can be gained by a signal conditioner where the gain can be selected from 0 to 4096. The system also provides six current sources for the analog sensors with the adjustable output current.

The system includes an onboard accelerometer, which communicates through the SPI interface and its range can be configured between $\pm 2\text{G}$ and $\pm 16\text{G}$.

The system allows to connect four binary inputs and up to three I2C devices. For example, the IR temperature sensor is supported. the PCB layout of the IR temperature sensor for later manufacturing was prepared, and firmware support created. the prepared board initiates the I2C address of the temperature sensor to 0x80. The user can add extra I2C sensors and other binary inputs. For this purpose, it is necessary to write the appropriate code. The places for adding the user code are highlighted in the main.c file with a comment. These placeholders are located in the initialisation part of the components and in the part of storing data into the microSD card. The user must take into account that the I2C bus uses message acknowledgements. Therefore, it is always necessary to execute the code only when the device is connected. Otherwise, the system gets stuck while waiting for the data, and the measurement is not performed. The system also includes PWM outputs that can be configured with TIM1.

The measured data are saved into the microSD card, where the names of the files and folders are derived from the real time.

The user can control the device using an easy web interface. After connecting to the Wi-Fi ESP-A270C4, the web page can be visible on the 192.168.4.1 address. The web page is divided into five sections:

Control part: Contains the Wi-Fi configurations and the project overview page.

Battery part: Displays the approximate battery percentage. It is not being actualised when the measurement is in progress.

Device configuration: the configuration of the measurement parameters:

- Measurement time in seconds: the minimum measurement time is 30 s, the maximum 86 400 s, which corresponds to 24 h.
- Signal conditioners gain and current sources: This part allows to configure the gain of the signal conditioners. This gain can be set from 0 (the output of the conditioner is off) to 4096. The current sources are present to power the analog sensors. They can provide 0.2 mA or 0.5 mA output current.
- Sampling frequency of the analog-to-digital converter: the sampling frequency can be set between 10 Hz and 20 kHz. The other sensors are measured once the cycling buffer with analog values is full. For more information see the Figure 60. The number of *samples in buffer* is for different sampling frequencies shown in the Table 2.

5.1 FORMAT OF THE OUTPUT DATA

Sampling frequency	Samples in the buffer
10 Hz	100
20 Hz	200
50 Hz	500
100 Hz	500
200 Hz	500
500 Hz	500
1 kHz	500
2 kHz	1000
5 kHz	1000
10 kHz	1000
20 kHz	1000

Table 2: Size of the buffer dependent on the sampling frequency.

- **Accelerometer range:** the range of the accelerometer can be set to $\pm 2\text{G}/\pm 4\text{G}/\pm 8\text{G}/\pm 16\text{G}$.

Measurement commands: the start of the measurement can be set. It is not allowed if there are more than 30 files on the microSD card. In such case, the user must erase the card. After the measurement started, the information about proceeding measurement is displayed to the user.

SD card commands: the user can see the names of files present on the microSD card. The files are displayed only if the measuring is not in progress. The file is downloaded by clicking on its name. The microSD card can be also erased in this section.

As the system allows high sampling rate and also wireless communication, there are two modes available. In the stand-alone mode, the system measures for given time and with given setting. The measured data are saved into the microSD card, where the file names are derived from the real time. In transfer mode, the system can be configured through the web page, and the files with measured data can be downloaded.

The battery can be charged using an inductive charger. The inductive charger's transmitting part needs an input voltage between 9 V and 12 V. The device can also be charged using a normal power adapter with 5 V output voltage. The user has to take into account the different input voltages and not to connect more than 5 V supply voltage to the device. Otherwise, the device will be damaged.

■ 5.1 Format of the output data

The measured data format is shown in Figure 60. The data from the analog-to-digital converter are saved in the 16-bit little endian format. All n samples in buffer contains all eight channels, and they are stored behind each other. The output example is in Figure 68. The voltage can be obtained by computing the Equation (22). The data from all three axes of the accelerometer are saved after the data from the converter. They

are placed in order x , y , z and they are in 16-bit little endian format. Behind the accelerometer, the values from the IR temperature sensor can be saved. The measured values are two, the first is the die temperature and the second is the voltage. The values are saved in float format with two decimal places. The temperature can be computed from the Equation (21). Following the temperature sensor, the code for more sensors can be placed. The entry ends with the timestamp including year, month, date, hours, minutes and seconds. The output file does not include any ending character, such as a new line.

```

00000000 | 10 01 17 01 DE 02 13 01 01 01 18 01 03 00 41 2F | .....A/
00000010 | 12 01 18 01 BC 02 12 01 FE 00 17 01 02 00 3E 2F | .....>/
00000020 | 10 01 18 01 CD 02 11 01 02 01 17 01 03 00 0B 2F | ...../
00000030 | 13 01 18 01 F7 01 12 01 01 01 18 01 03 00 10 2F | ...../
00000040 | 10 01 19 01 7F 02 12 01 00 01 18 01 02 00 0A 2F | ...../
00000050 | 11 01 17 01 98 01 13 01 00 01 18 01 02 00 FE 2E | .....
00000060 | 10 01 17 01 F6 00 11 01 00 01 16 01 02 00 31 2E | .....1.

```

Figure 68: Example of the measured data.

5.2 LEDs usage

The PCB includes four LEDs (LD1-LD4) shown in Figure 69, which are configurable by the firmware. The LD1 is blue and is switched on when the measuring is in progress. The LD2 is red and is switched on when the error occurs. It is usually on when the microSD card was not mounted or the when it is not possible to write the data on it. The LD3 is orange, and this LED signals that the device is in transfer mode by changing its state every two seconds. In the stand-alone mode, the last state of the LD3 persists. The LD4 is green and is powered on when the measurement has been successfully completed.

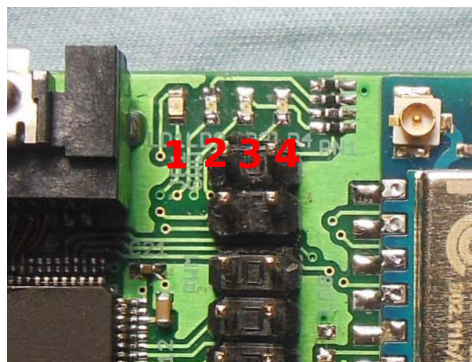


Figure 69: LEDs configurable by the firmware.

5.3 Measured data

The device was tested for a strain measurement using strain gauges. The sensors were attached to a beam, as shown in Figure 70.

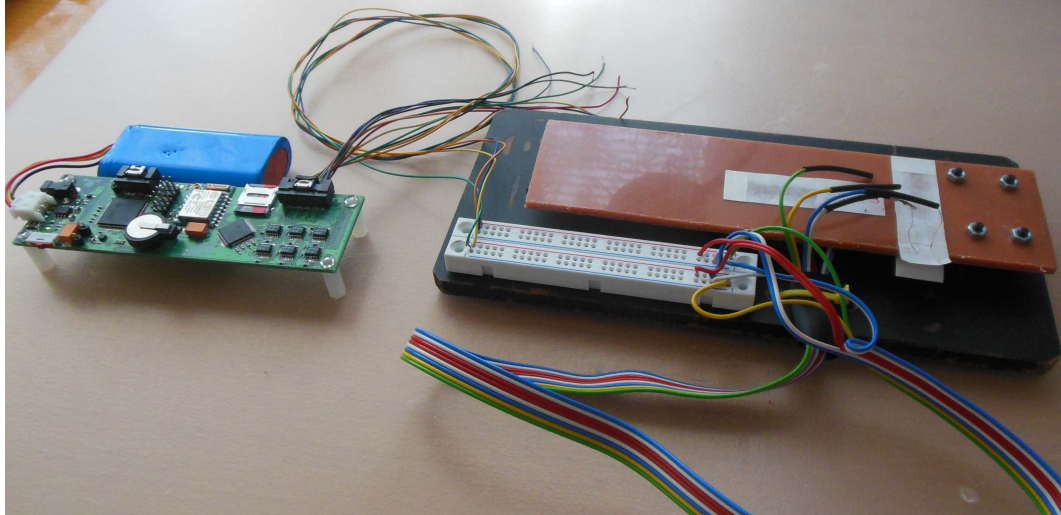


Figure 70: Measurement with the strain gauges connected to the acquisition system.

The strain gauges were connected to the full Wheatstone bridge. Two of the strain gauges were measuring, and the remaining two were compensating. The schematic is shown in Figure 72. the sampling rate was set to 1 kHz, current source 0.5 mA and gain of the LTC6915 conditioner was 4096.

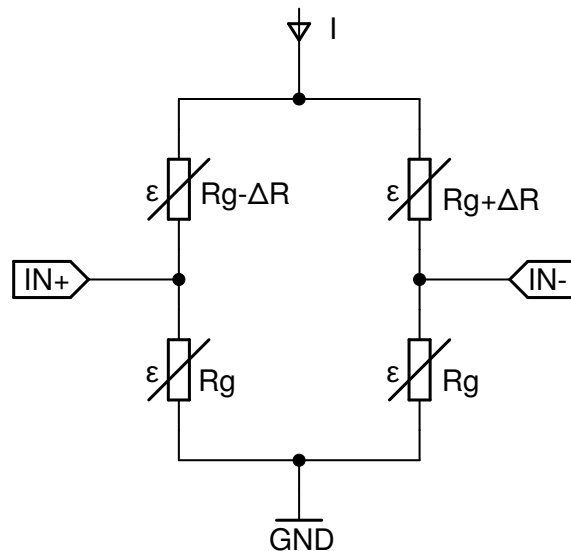


Figure 71: Electrical schematic of the strain gauges connected to the acquisition system. For the simplicity, the balancing resistor is not present.

When the beam is deflected, one of the measuring strain gauges is extended and the second one is shorted causing the bridge's output voltage change. The measured data are shown in a Figure 72. It is obvious that the measured values contain a lot of noise. The reason is a great amplification, which amplifies not only the useful signal but also the noise. Therefore, averaging the signal for 20 times was applied to eliminate the noise.

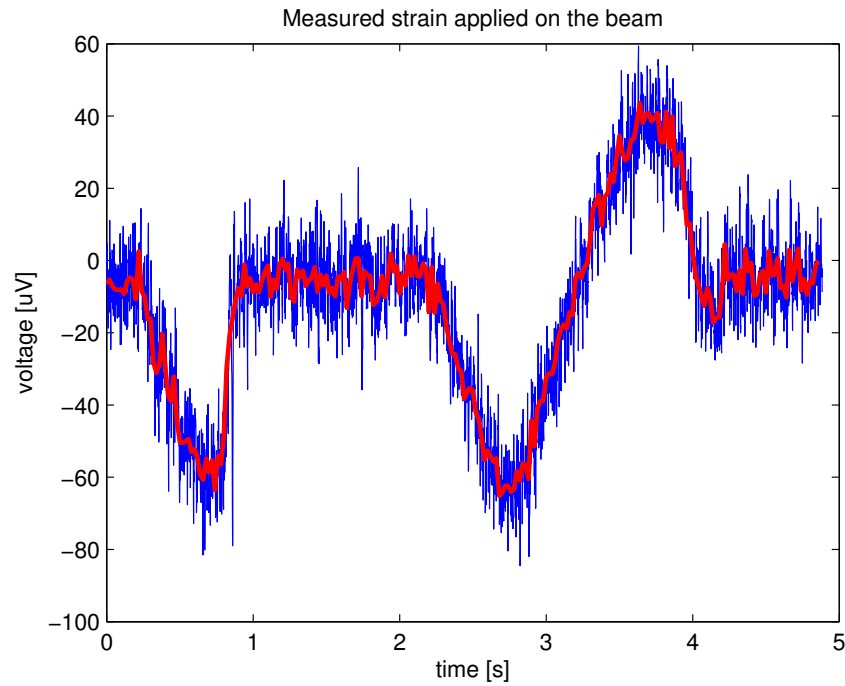


Figure 72: Measured strain applied on the beam.

5.3 MEASURED DATA

The second tested sensor was an onboard accelerometer. The device was mounted on a rotating chair, and all three acceleration components were scanned. The physical application is shown in Figure 73.

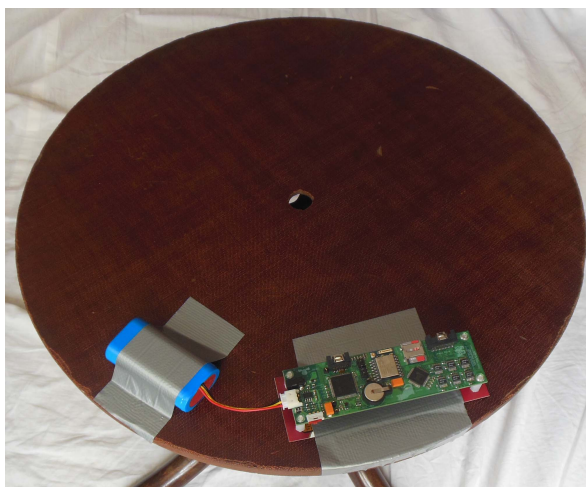


Figure 73: Measurement with the onboard accelerometer.

The acceleration was set to $\pm 2G$, and the chair was spun at the highest speed. The measured data are in Figure 74. The axis x is tangential, axis y radial and axis z axial part of the acceleration. The fluctuation at the first half of record is related to the start of the rotating movement.

Additionally, the hand movement was recorded using the accelerometer. This time, the device was rotated by hand. When the device was moved from up to down, the board was turned upside down, so it caused the change of the acceleration sign in the z axis. The measured dynamic effect is shown in Figure 75.

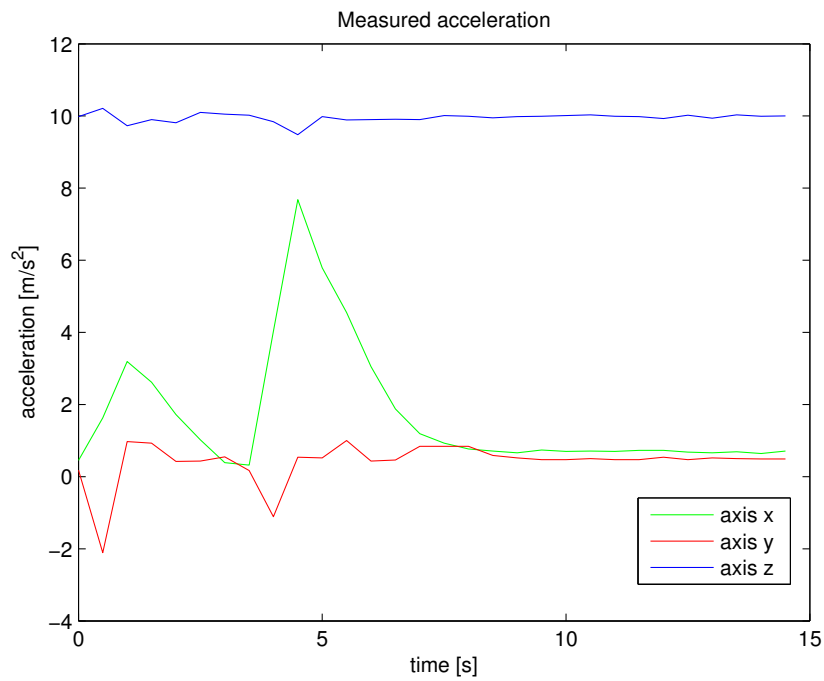


Figure 74: Measured acceleration on the rotating chair. Fluctuations are caused by hand initiating the rotation.

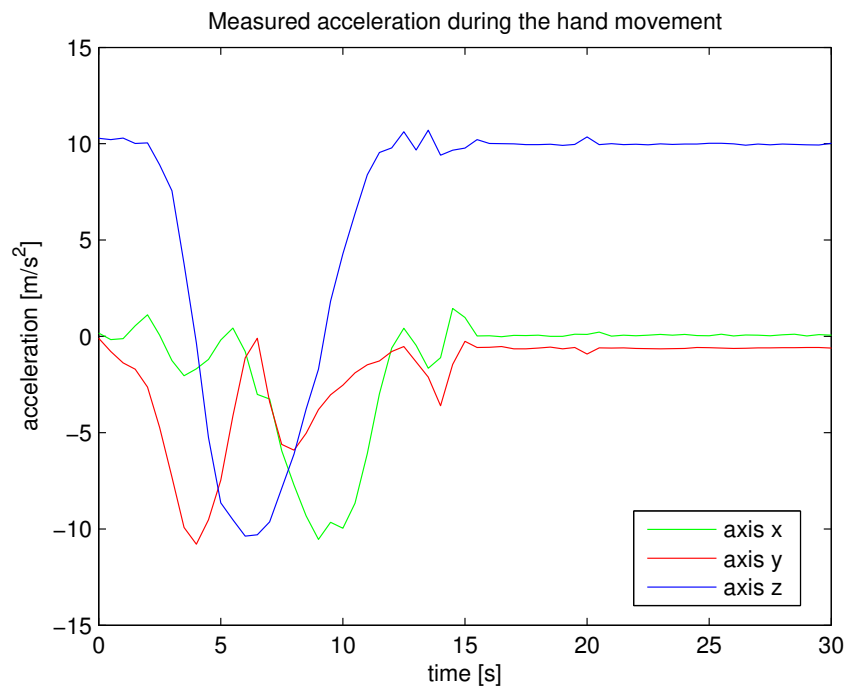


Figure 75: Measured acceleration caused by hand movement.

Chapter 6

Conclusion

the aim of this work was to create a sensor acquisition system that can be used for the measurement of the dynamic effects. Such a device can be used, for example, for testing the connecting rod in a combustion engine or for testing the wheels of the forklift trucks. The requirements for the device were the following:

- Small size.
- Battery powered device.
- Eight analog channels.
- Signal conditioning of analog signals (strain gauges and RTDs).
- High sampling rate (in tens of kHz).
- Support for digital sensors.
- Internal memory for offline data storage.
- Wireless communication.
- Inductive charging.

The requirements led to the choice of the concept where the device works in two modes. In the stand-alone mode, the system measures with specified settings for given time. The measured data are saved into the microSD card. In the transfer mode, the system uses wireless communication. The device can be configured, and the files with measured data are available for download.

It turned out that such a device does not exist on the market. Some of the existing systems do not support wireless communication, while others do not allow offline data storage. There exist various large systems for strain measurement, which cannot be placed directly on the measured object. Therefore, the device described in this work is innovative.

This work went through the device design and implementation. First, it was necessary to design a concept and select the components. An eight channel analog-to-digital converter AD7606 was chosen to convert the analog signals. This converter supports high sampling frequency and the choice of both parallel and serial output. The device is controlled by STM32F411VE microcontroller, providing a sufficient number of peripherals and a low power consumption.

A prototype device for testing and further design plans was build from the selected components. The initial schematics and layouts were designed for the prototype boards. These boards were used to test the selected components and to decide whether they could be suitable for the final device. The testing boards also served to find the weak points of the proposed concept. After checking the functionality of the most parts of the device, the final device's schematic and layout was designed.

The final acquisition system is designed for a higher level of miniaturisation

on a four-layer PCB. The used components were selected in as small package as possible, but big enough to be still soldered manually. The analog components, DC-DC regulators and Wi-Fi module were placed on a single PCB, so it was designed with care about the components interference. The proposed PCB required later some modifications which are mentioned in the text. After these corrections, the device worked as expected and met the requirements. These changes were corrected in the final schematic and PCB layout attached to this thesis.

An important part of the device was the firmware which was created simultaneously with the hardware design. The firmware for the STM32F411VE microcontroller had to support all the selected components and allow their cooperation. The microcontroller also cooperated with the microcontroller included inside the Wi-Fi module ESP-07 providing a user-friendly interface for the end user. The default firmware inside the ESP8266 microcontroller included in the ESP-07 Wi-Fi module was not suitable for this device. Hence, the custom firmware was created.

A web page served as the end user interface. It was visible after logging to the device's Wi-Fi. The user could set the measurement parameters through the interface, start the measurement, see and download the files present on the microSD, erase the card and see the approximate battery percentage.

The full wireless operation of the device was ensured by the possibility of connecting an inductive charger. Therefore, it was not necessary to disconnect the device even for the battery charging.

The device was tested for measurement with the strain gauges and the onboard accelerometer. Some of the tests were mentioned in the Chapter "Results". The tests verified that the device measured at the required sampling frequency, so the measurement of dynamic effects was possible. Furthermore, the device's sensitivity outperformed estimates. Even with a large amplification of the analog signal, the measured signal was large enough to be recognised from the noise.

References

- [1] J. Barton, J. Vcelák, J. Torres-Sanchez, B. O'Flynn, C. O'Mathuna, and R. V. Donahoe, "A miniaturised arrow ballistic measurement system", in *Sensors, 2011 IEEE*, IEEE, 2011, pp. 1289–1292.
- [2] Texas Instruments Incorporated. (2017). SimpleLink™ Bluetooth low energy/Multi-standard SensorTag, CC2650STK, [Online]. Available: <http://www.ti.com/tool/cc2650stk> (visited on 2017-05-21).
- [3] Micro-Measurements. (2017). System 7000 Data Acquisition System, [Online]. Available: <http://www.vishaypg.com/micro-measurements/instruments/system-7000-list/> (visited on 2017-05-21).
- [4] IR Telemetrics. (2017). IR Telemetrics products, [Online]. Available: <http://www.irtelemetrics.com/products> (visited on 2017-05-23).
- [5] J. Fraden, *Handbook of modern sensors*. Springer, 2010, vol. 5, ISBN: 978-3-319-19302-1 (Print) 978-3-319-19303-8 (Online).
- [6] K. Walt, "Analog-digital conversion", *Analog Devices Inc*, p. 675, 2005.
- [7] J. G. Webster and H. Eren, *Measurement, instrumentation, and sensors handbook: Electromagnetic, optical, radiation, chemical, and biomedical measurement*. CRC press, 2014, ISBN: 978-1-4398-4893-7.
- [8] V. Haasz and M. Sedláček, *Elektrická měření: Přístroje a metody*. Vydavatelství ČVUT, Praha, 1998, ISBN: 80-01-01717-6.
- [9] S. Ďádo and M. Kreidl, "Senzory a měřicí obvody", ISBN 80-010-1500-9, Tech. Rep., 1996, p. 315.
- [10] VISHAY micro - measurements. (Mar. 2008). Strain Gage Rosettes: Selection, Application and Data Reduction, [Online]. Available: http://www.u.arizona.edu/~kcolavit/strain_rosette.pdf (visited on 2017-02-18).
- [11] National Instruments. (Aug. 1998). Strain Gauge Measurement – A Tutorial. Application Note 078, [Online]. Available: http://elektron.pol.lublin.pl/elekp/ap_notes/NI_AN078_Strain_Gauge_Meas.pdf (visited on 2017-02-21).
- [12] John. (Aug. 2011). Accelerometer, [Online]. Available: <http://www.instrumentationtoday.com/accelerometer/2011/08/> (visited on 2017-02-24).
- [13] M. Andrejašič and I. Poberaj, "MEMS accelerometers", in *Seminar, Dept. of Phys, Univ. of Ljubljana, Ljubljana, Slovenia*, 2008.
- [14] C. Aszkler. (2005). The Principles of Acceleration, Shock, and Vibration Sensors, [Online]. Available: <http://www.sensorsmag.com/components/principles-acceleration-shock-and-vibration-sensors> (visited on 2017-05-03).
- [15] Analog Devices. (2017). Accelerometer Specifications - Quick Definitions, [Online]. Available: <http://www.analog.com/en/products/landing-pages/001/accelerometer-specifications-definitions.html> (visited on 2017-02-25).
- [16] P. Ripka and A. Tipek, *Modern sensors handbook*. John Wiley & Sons, 2013, ISBN: 978-1-905209-66-8.

- [17] KELLER HCW GmbH. (2017). Principles of Non-Contact Temperature Measurement, [Online]. Available: <http://www.keller-msr.com/application/principles-infrared-temperature-measurement.php> (visited on 2017-03-20).
- [18] Wikipedia, *Serial Peripheral Interface Bus* — *Wikipedia, The Free Encyclopedia*. [Online]. Available: https://en.wikipedia.org/w/index.php?title=Serial_Peripheral_Interface_Bus&oldid=776789750 (visited on 2017-04-23).
- [19] *SPI Block Guide V03.06*, Motorola, Inc., 2003. [Online]. Available: <https://web.archive.org/web/20150413003534/http://www.ee.nmt.edu/~teare/ee3081/datasheets/S12SPIV3.pdf> (visited on 2017-04-23).
- [20] Technical Committee SD Card Association, *SD Specifications, Part 1, Physical Layer, Simplified Specification*, 2013. [Online]. Available: https://members.sdcard.org/downloads/pls/simplified_specs/part1_410.pdf (visited on 2017-04-23).
- [21] *SD Specifications, Part E1, SDIO Simplified Specification*, Technical Committee SD Card Association, 2007. [Online]. Available: https://www.sdcard.org/developers/overview/sdio/sdio_spec/Simplified_SDIO_Card_Spec.pdf (visited on 2017-04-23).
- [22] NXP Semiconductors, *UM10204 - I2C-bus specification and user manual*, 2014. (visited on 2017-04-23).
- [23] A. Lundgren. (2012). Software Development Tools Optimize ZigBee Performance, IAR Systems, [Online]. Available: <https://www.wirelessdesignmag.com/blog/2012/09/software-development-tools-optimize-zigbee-performance> (visited on 2017-04-23).
- [24] AIR802. (2017). IEEE 802.11 Standards, Facts & Channels, [Online]. Available: <https://www.air802.com/ieee-802.11-standards-facts-amp-channels.html> (visited on 2017-04-29).
- [25] I. Poole. (2017). Qi Wireless Charging Standard, Adrio Communications Ltd, [Online]. Available: <http://www.radio-electronics.com/info/power-management/wireless-inductive-battery-charging/qi-wireless-charging-standard.php> (visited on 2017-04-23).
- [26] Wikipedia, *Inductive charging* — *Wikipedia, The Free Encyclopedia*. [Online]. Available: https://en.wikipedia.org/w/index.php?title=Inductive_charging&oldid=776565265 (visited on 2017-04-23).
- [27] W. P. Consortium. (2017), [Online]. Available: <https://www.wirelesspowerconsortium.com> (visited on 2017-04-23).
- [28] Analog Devices, Inc. (). AD7606, 8-Channel DAS with 16-Bit, Bipolar, Simultaneous Sampling ADC, [Online]. Available: <http://www.analog.com/en/products/analog-to-digital-converters/precision-adc-10msps/simultaneous-sampling-ad-converters/ad7606.html#product-overview> (visited on 2017-05-06).
- [29] STMicroelectronics. (2008). AN2790 Application note, TFT LCD interfacing with the high-density STM32F10xxx FSMC, [Online]. Available: http://www.st.com/content/ccc/resource/technical/document/application_note/85/ad/ef/0f/a3/a6/49/9a/CD00201397.pdf/files/CD00201397.pdf/jcr:content/translations/en.CD00201397.pdf (visited on 2017-05-07).
- [30] Maxim Integrated. (2017). MAX1454 product page, Precision Sensor Signal Conditioner with Overvoltage Protection, [Online]. Available: <https://www.maximintegrated.com/en/products/analog/sensors-and-sensor-interface/MAX1454.html> (visited on 2017-05-07).
- [31] Linear Technology. (2004). LTC6915 product page, Zero Drift, Precision Instrumentation Amplifier with Digitally Programmable Gain, [Online]. Available: <http://www.linear.com/product/LTC6915> (visited on 2017-05-07).
- [32] Maxim Integrated. (2003). MAX335 product page, Serial Controlled, 8-Channel SPST Switch, [Online]. Available: <https://www.maximintegrated.com/en/products/analog/analog-switches-multiplexers/MAX335.html> (visited on 2017-05-07).

- [33] Texas Instruments Incorporated. (2017). TMP006 product page, Infrared Thermopile Contactless Temperature Sensor in WCSP Package, [Online]. Available: <http://www.ti.com/product/TMP006> (visited on 2017-04-30).
- [34] STMicroelectronics. (2017). LIS2DH12 product page, MEMS digital output motion sensor: ultra low-power high performance 3-axes femto accelerometer, [Online]. Available: <http://www.st.com/en/mems-and-sensors/lis2dh12.html> (visited on 2017-05-01).
- [35] —, (2017). BlueNRG product page, Bluetooth® low energy wireless network processor, [Online]. Available: http://www.st.com/content/st_com/en/products/wireless-connectivity/bluetooth-low-energy/bluenrg.html (visited on 2017-04-30).
- [36] Texas Instruments Incorporated. (2017). CC3100 product page, SimpleLink™ Wi-Fi® Network Processor, Internet-of-Things Solution for MCU Applications, [Online]. Available: <http://www.ti.com/product/CC3100> (visited on 2017-04-30).
- [37] Espressif Systems. (2017). ESP8266 product page, [Online]. Available: <https://espressif.com/en/products/hardware/esp8266ex/overview> (visited on 2017-04-30).
- [38] AI-Thinker team. (2015). ESP-07 WiFi Module, Version1.0, [Online]. Available: <http://www.exp-tech.de/pdf/products/ESP-07/Ai-thinker%20ESP-07%20WIFI%20Module-EN.pdf> (visited on 2017-04-30).
- [39] STMicroelectronics. (2017). STM32F411VE product page, High-performance access line, ARM Cortex-M4 core with DSP and FPU, 512 Kbytes Flash, 100 MHz CPU, ART Accelerator, [Online]. Available: <http://www.st.com/en/microcontrollers/stm32f411ve.html> (visited on 2017-04-30).
- [40] —, (2017). STM32CubeMX product page, STM32Cube initialization code generator, [Online]. Available: http://www.st.com/content/st_com/en/products/development-tools/software-development-tools/stm32-software-development-tools/stm32-configurators-and-code-generators/stm32cubemx.html (visited on 2017-04-30).
- [41] —, (2014). RM0383 Reference manual, STM32F411xC/E advanced ARM ® -based 32-bit MCUs, [Online]. Available: http://www.st.com/content/ccc/resource/technical/document/reference_manual/9b/53/39/1c/f7/01/4a/79/DM00119316.pdf/files/DM00119316.pdf/jcr:content/translations/en.DM00119316.pdf (visited on 2017-05-02).
- [42] BAK. (2017). BAK 18650CA-2P-3J product page, Rechargeable Battery, 3.7 V, Lithium Ion, 4.5 Ah, [Online]. Available: <http://uk.farnell.com/bak/18650ca-2p-3j/battery-lithium-ion-3-7v-4500mah/dp/2401853> (visited on 2017-05-06).
- [43] NanJing Top Power ASIC Corp. (2017). Tp4056 datasheet, 1A Standalone Linear Li-Ion Battery Charger with Thermal Regulation in SOP-8, [Online]. Available: <https://dlmnh9ip6v2uc.cloudfront.net/datasheets/Prototyping/TP4056.pdf> (visited on 2017-05-06).
- [44] Monolithic Power Systems. (2011). MP1542 product page, 700kHz/1.3MHz Boost Converter with 2A Switch, [Online]. Available: [https://www.monolithicpower.com/Products/Product-Detail/368/Step-up\(Boost\)/SwitchingRegulators/DC-DCPowerConversion/Non-Synchronous/MP1542](https://www.monolithicpower.com/Products/Product-Detail/368/Step-up(Boost)/SwitchingRegulators/DC-DCPowerConversion/Non-Synchronous/MP1542) (visited on 2017-05-06).
- [45] Monolithic Power Systems. (2013). MP1469 product page, High-Efficiency, 1.5A, 16V, 500kHz Synchronous, Step-Down Converter In 6 Pin SOT 23, [Online]. Available: [https://www.monolithicpower.com/Products/Product-Detail/174/Step-down\(Buck\)/SwitchingRegulators/DC-DCPowerConversion/Converters/MP1469](https://www.monolithicpower.com/Products/Product-Detail/174/Step-down(Buck)/SwitchingRegulators/DC-DCPowerConversion/Converters/MP1469) (visited on 2017-05-06).
- [46] Taiwan Semiconductor. (2017). TS1117BCW33 product page, 1A Low Dropout Positive Voltage Regulator, [Online]. Available: <http://www.taiwansemi.com/en/products/details/TS1117BCW33> (visited on 2017-05-06).
- [47] eBay Inc. (2017), [Online]. Available: <http://www.ebay.com/> (visited on 2017-05-06).

- [48] STMicroelectronics. (2016). STEVAL-MKI105V1 product page, LIS3DH adapter board for standard DIL 24 socket, [Online]. Available: http://www.st.com/content/st_com/en/products/evaluation-tools/product-evaluation-tools/mems-motion-sensor-eval-boards/steval-mki105v1.html (visited on 2017-05-08).
- [49] —, (2016). ST-LINK/V2, ST-LINK/V2 in-circuit debugger/programmer for STM8 and STM32, [Online]. Available: <http://www.st.com/en/development-tools/st-link-v2.html> (visited on 2017-05-11).
- [50] —, (2017). STM32 Standard Peripheral Libraries, [Online]. Available: <http://www.st.com/en/embedded-software/stm32-standard-peripheral-libraries.html?querycriteria=productId=LN1939> (visited on 2017-05-13).
- [51] Tilen Majerle. (2014). Library 21- Read SD card with FatFs on STM32F4, [Online]. Available: <http://stm32f4-discovery.net/2014/07/library-21-read-sd-card-fatfs-stm32f4xx-devices/> (visited on 2017-05-14).
- [52] ChaN. (2017). FatFs - Generic FAT File System Module, [Online]. Available: http://elm-chan.org/fsw/ff/00index_e.html (visited on 2017-05-14).
- [53] O. Hruška. (2017). TinyFrame on GitHub, A minimalist library for building and parsing data frames for serial interfaces (like UART / RS232), [Online]. Available: <https://github.com/MightyPork/TinyFrame> (visited on 2017-05-15).
- [54] Espressif Inc. (2017). ESP8266 AT Instruction Set. version 2.1.0, [Online]. Available: https://www.espressif.com/sites/default/files/documentation/4a-esp8266_at_instruction_set_en.pdf (visited on 2017-05-17).
- [55] (2017). ESP8266 Remote Terminal project, [Online]. Available: <https://github.com/MightyPork/esp-vt100-firmware> (visited on 2017-05-17).

- A Testing board schematic and layout
- A.1 Power supply board of the testing device

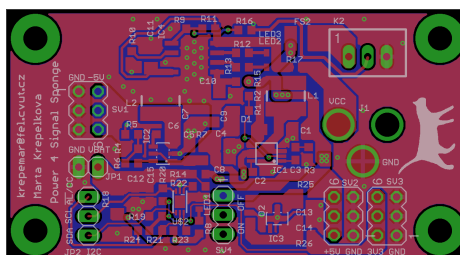
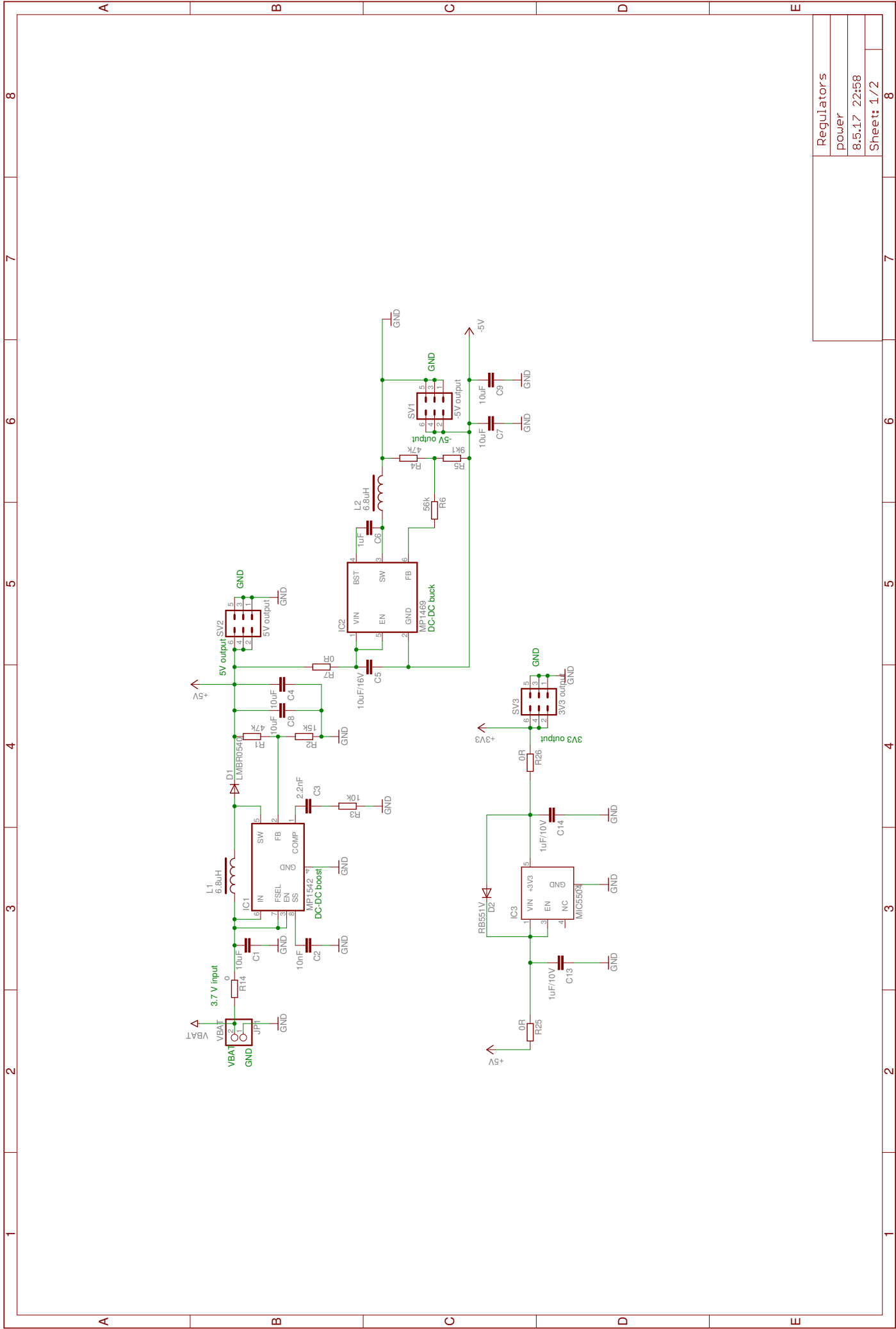
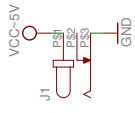
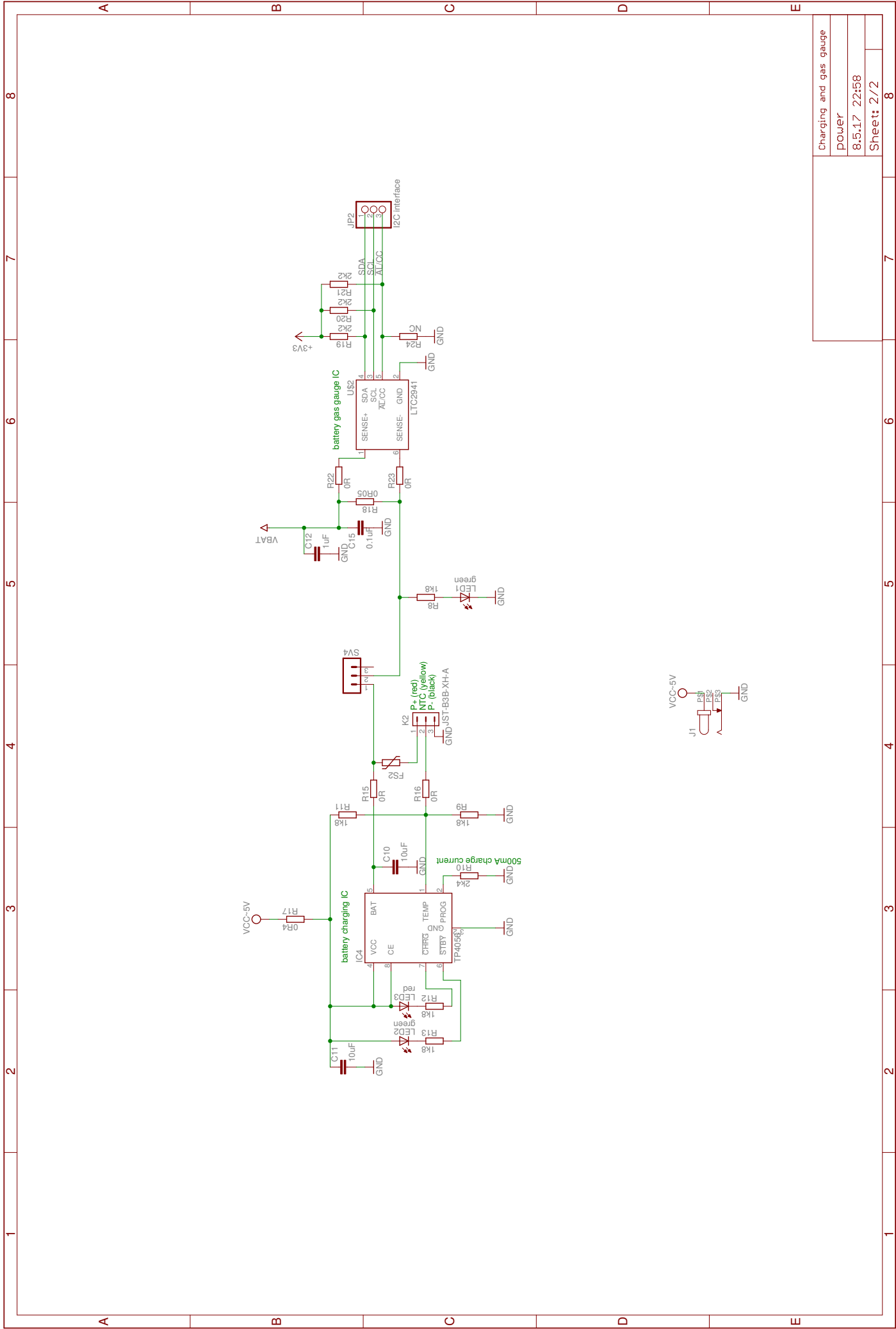


Figure 76: Real-size PCB image of the power supply board.



Regulators	
power	
8.5.17 22:58	
Sheet: 1/2	



Charging and gas gauge
power
8.5.17 22:58
Sheet: 2/2

■ A.2 Testing board with analog and digital components

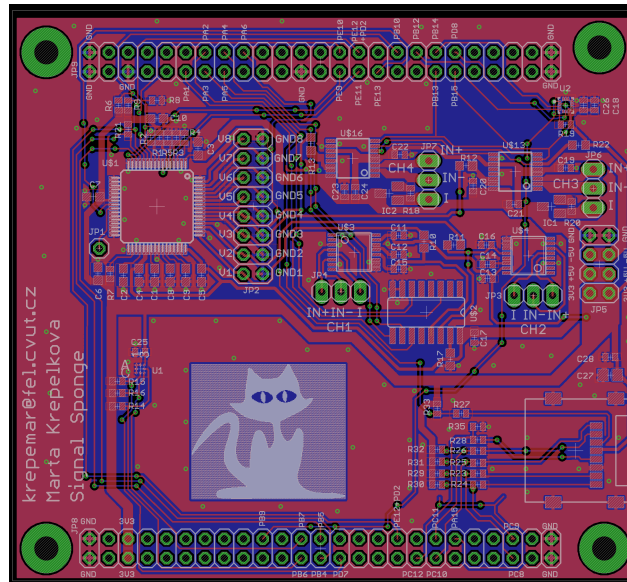
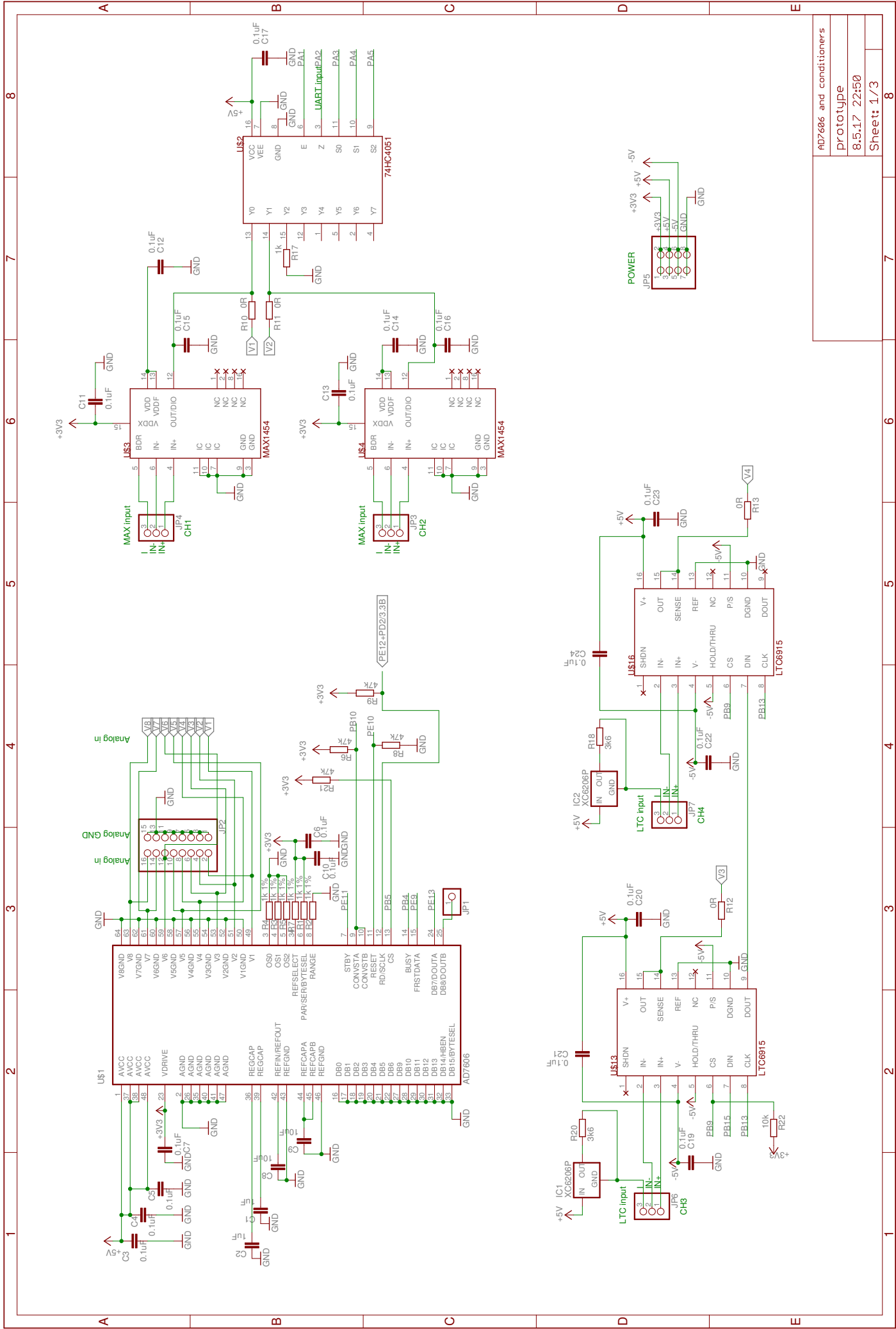
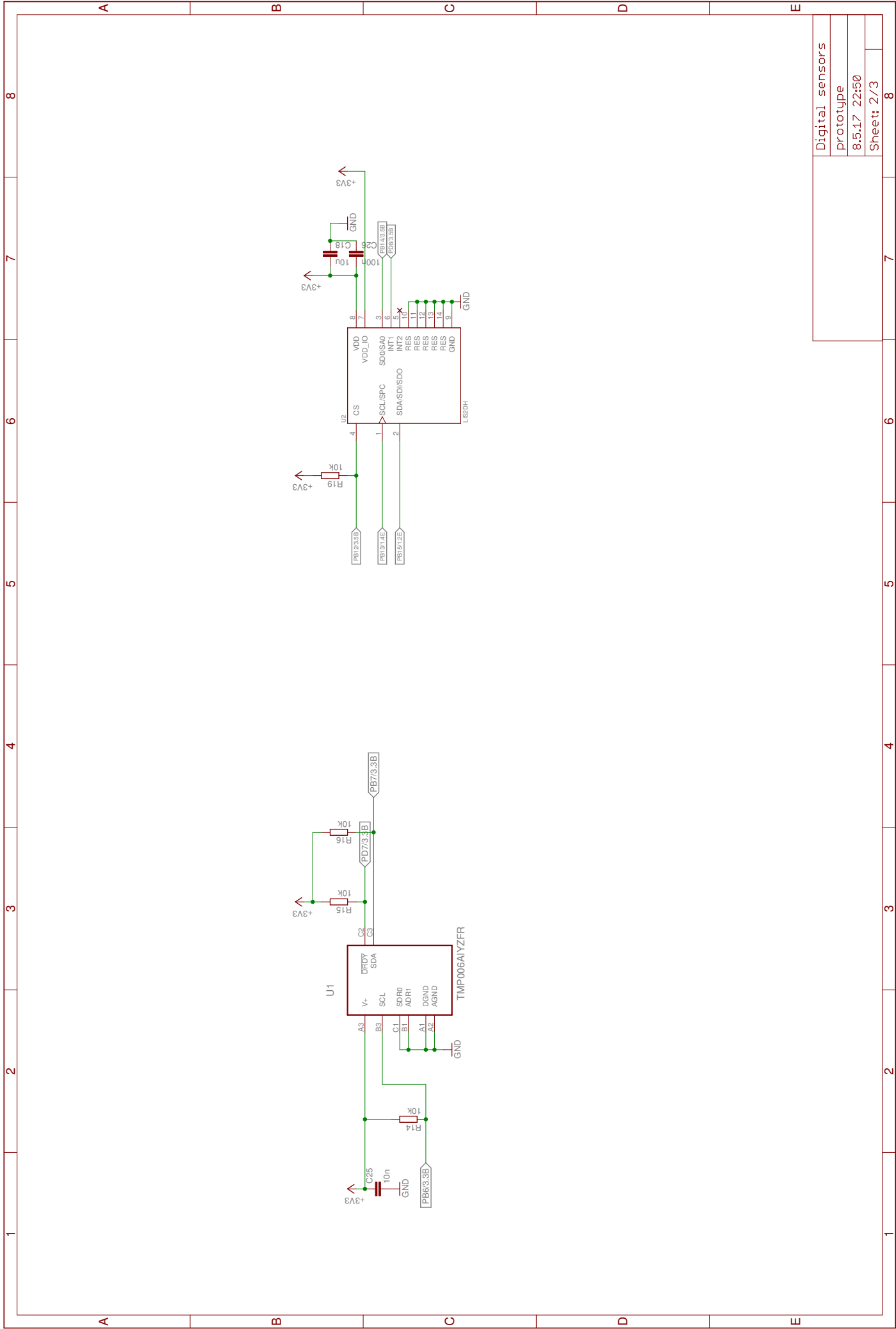


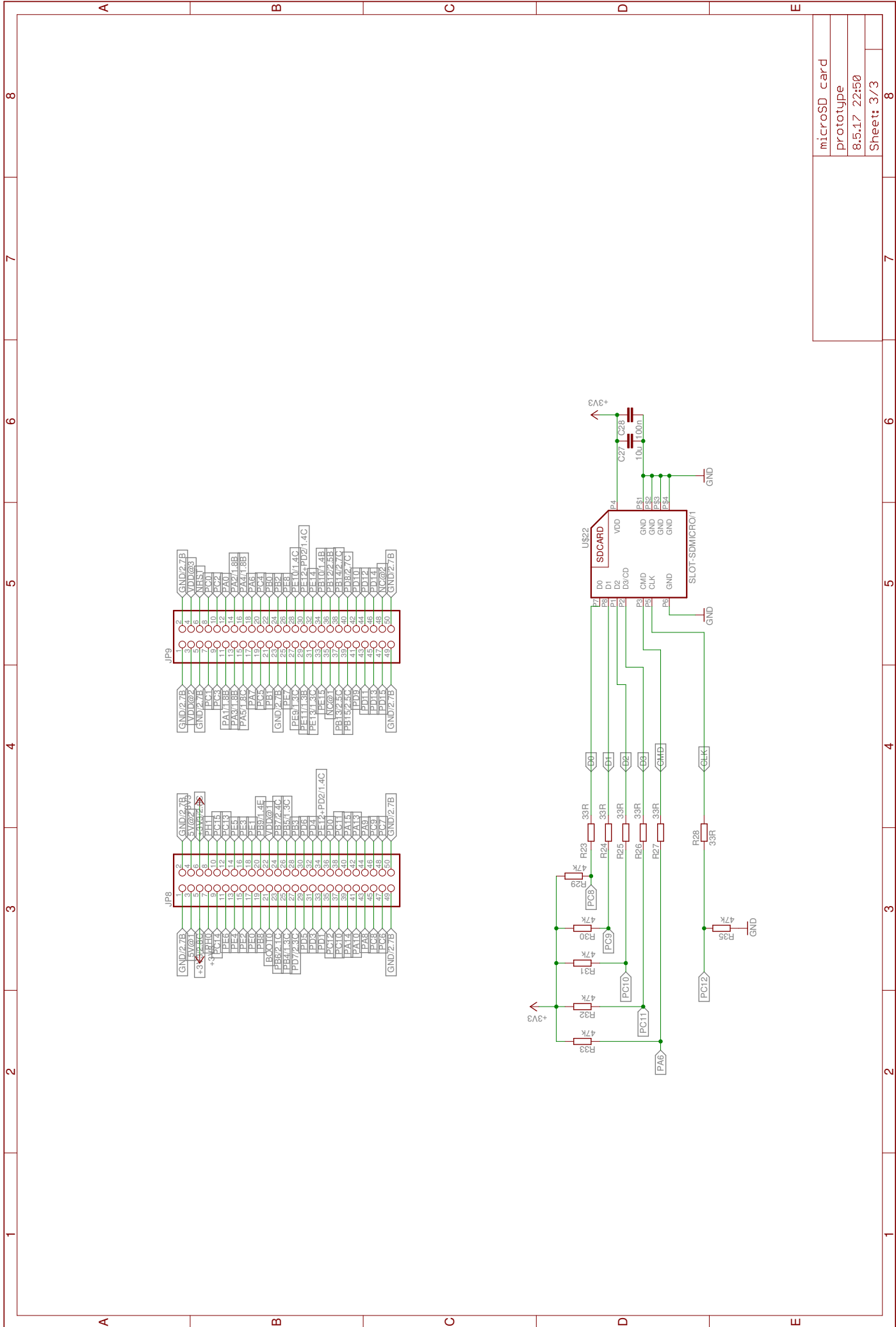
Figure 77: Real-size PCB image of the testing board.



AD7606 and conditioners
 prototype
 8.5.17 22:50
 Sheet: 1/3



Digital sensors	
prototype	
8.5.17 22:50	
Sheet: 2/3	



microSD card	
prototype	
8.5.17 22:50	
Sheet: 3/3	

■ B TMP006 schematic and layout

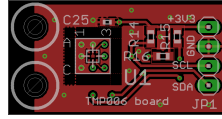
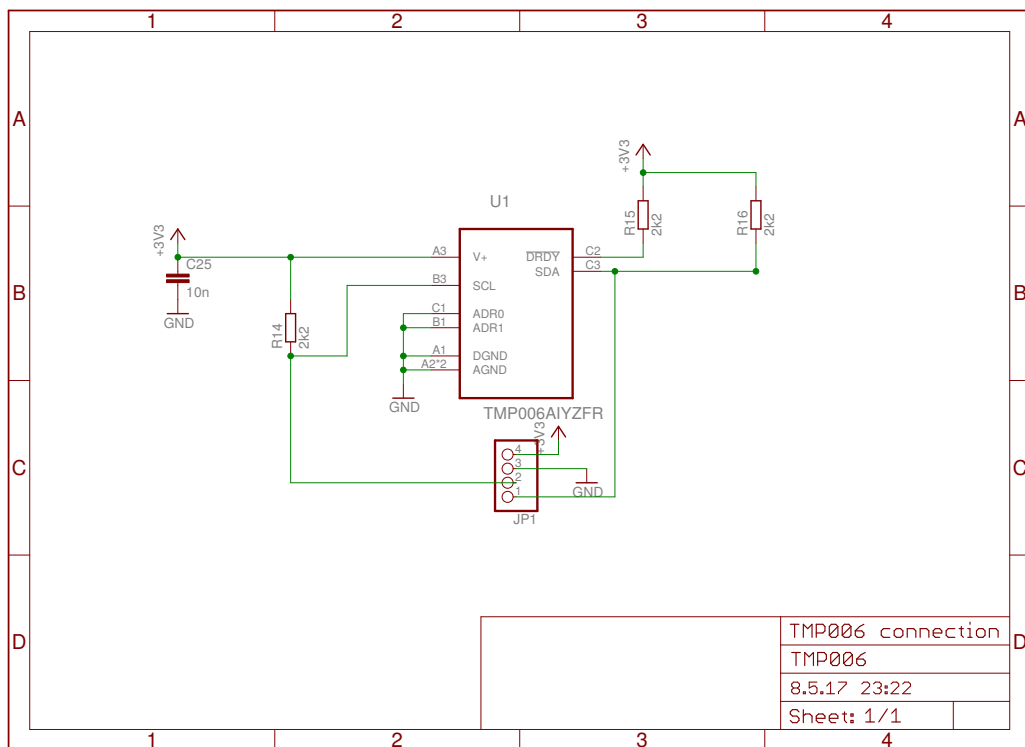


Figure 78: Real-size PCB image of the TMP006 board.



C Final device schematic and layout

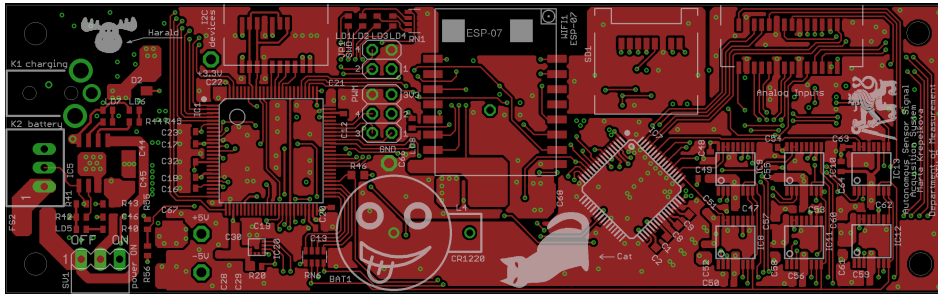


Figure 79: Real-size PCB image of the final board - TOP side.

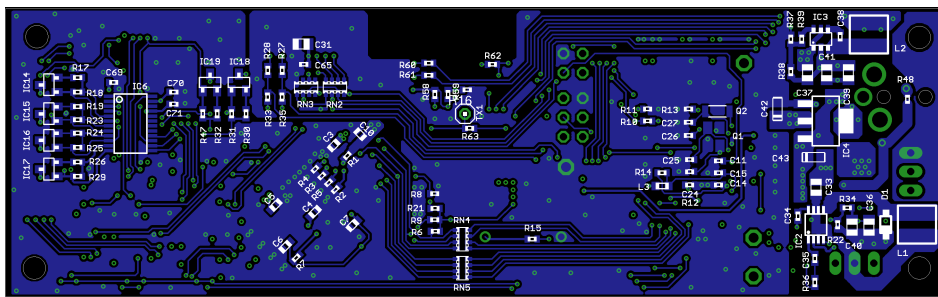


Figure 80: Real-size PCB image of the final board - BOTTOM side (mirrored).

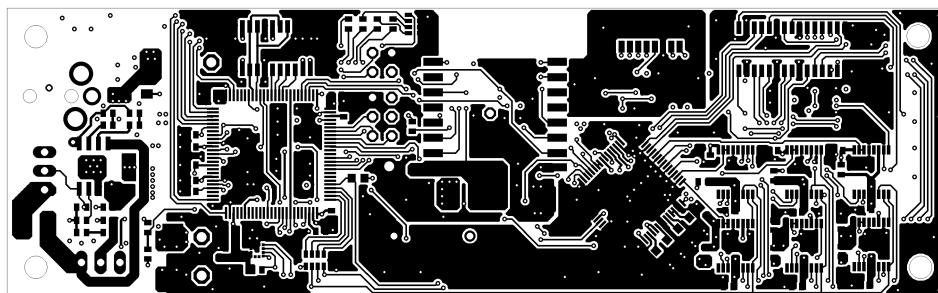


Figure 81: Final device: the TOP layer of the PCB.

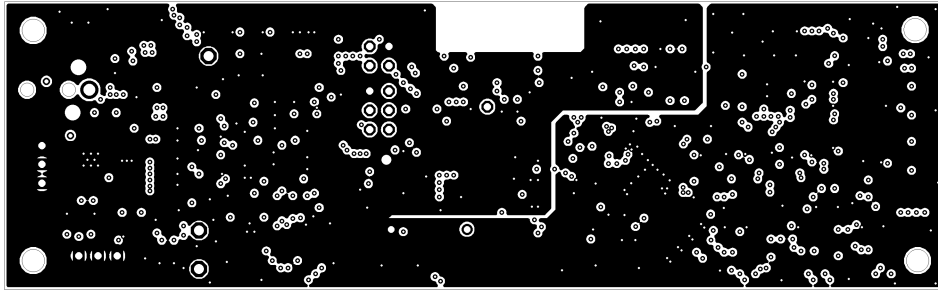


Figure 82: Final device: the second layer of the PCB.

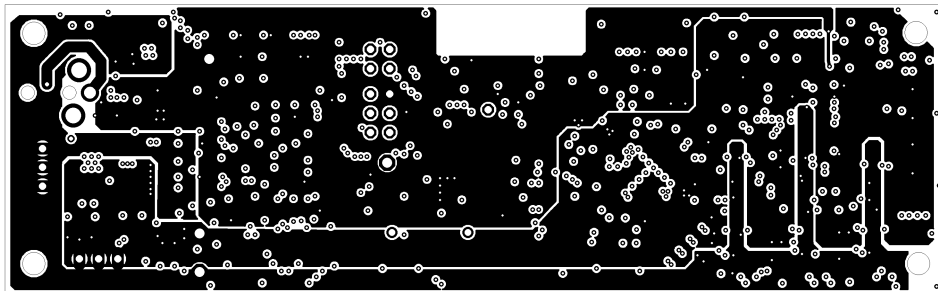


Figure 83: Final device: the third layer of the PCB.

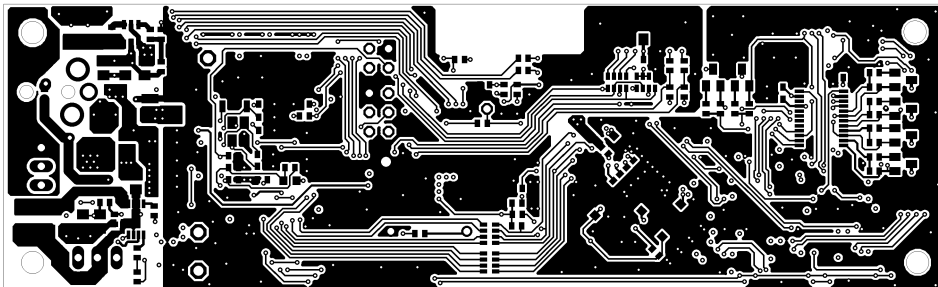
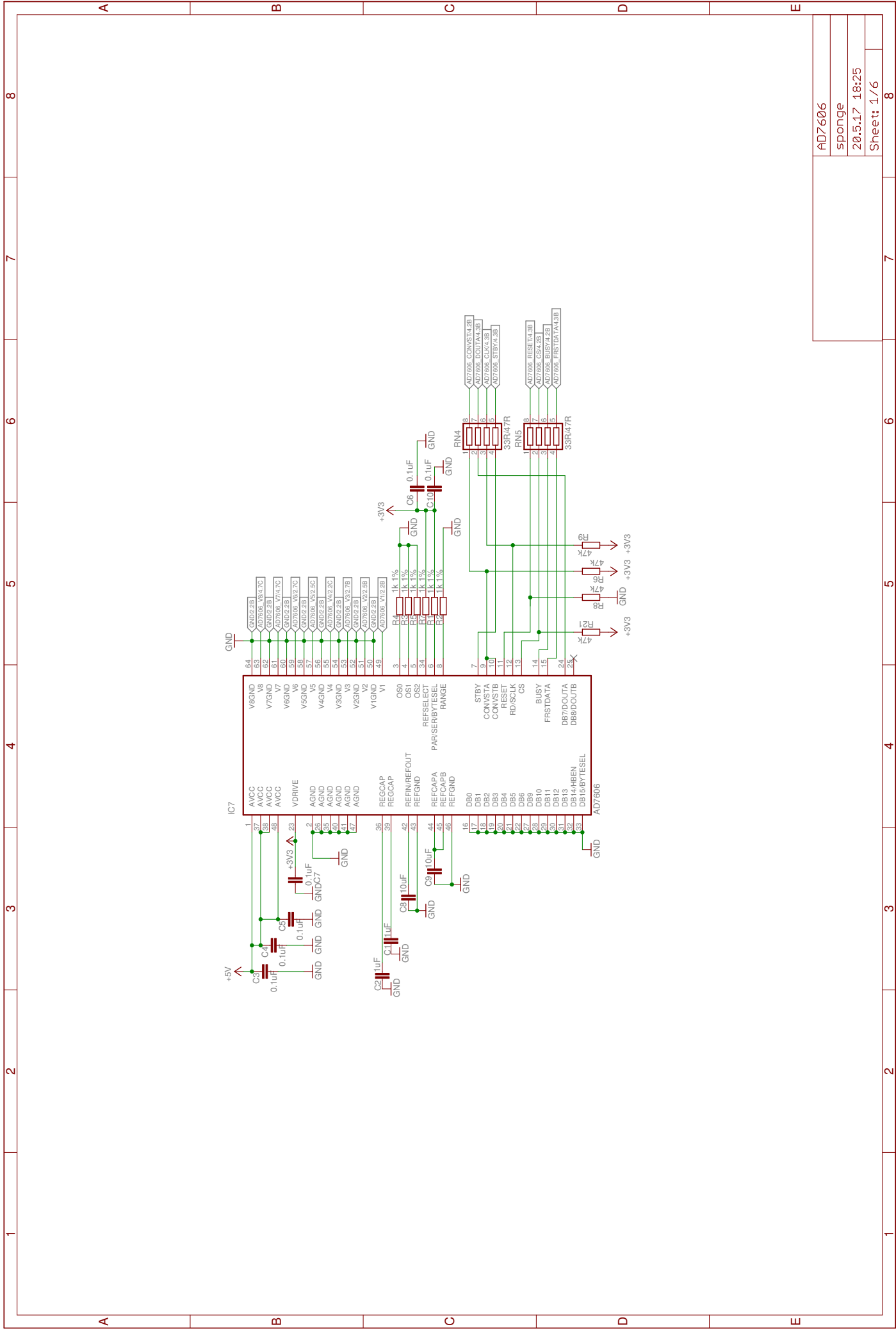


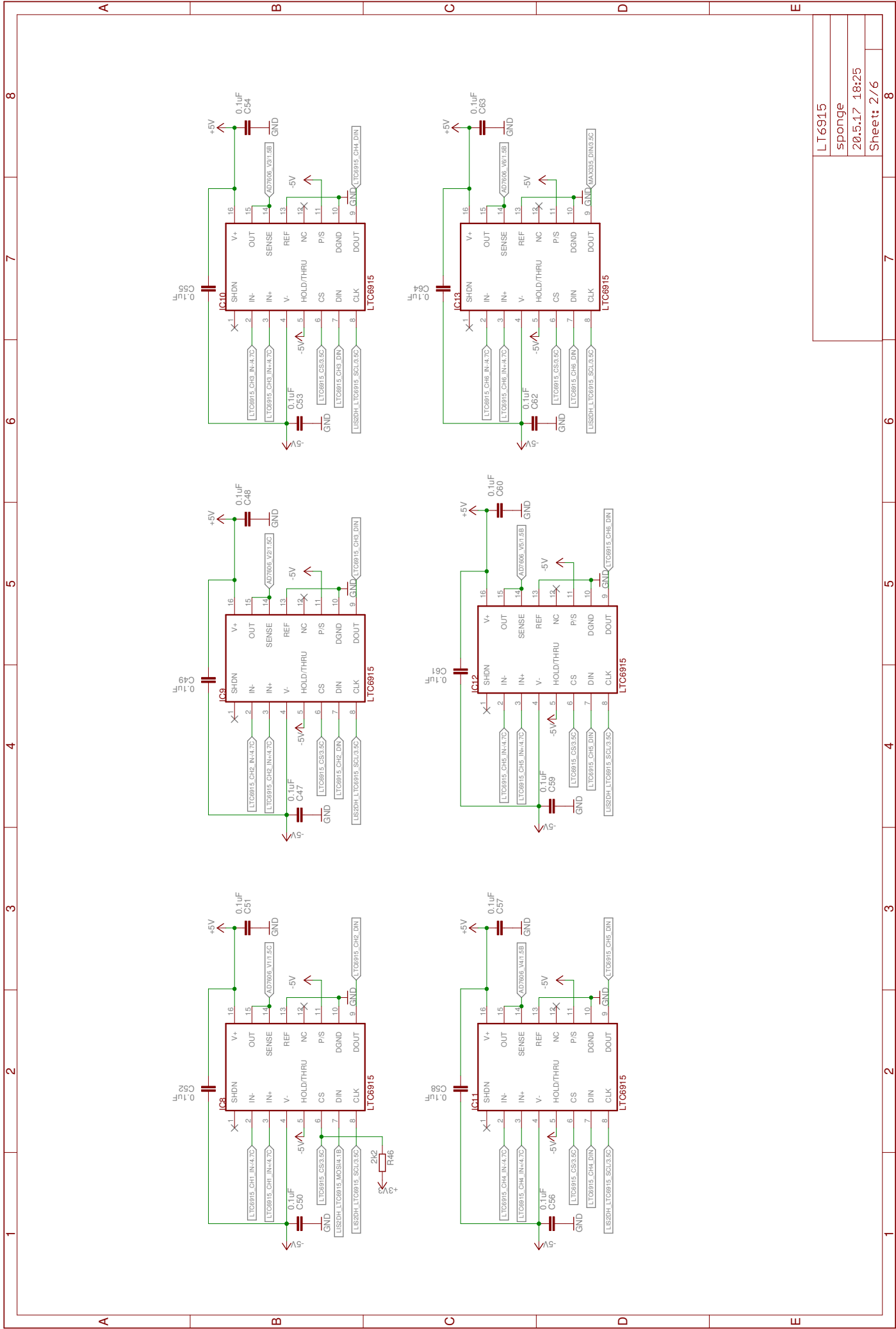
Figure 84: Final device: the BOTTOM layer of the PCB.



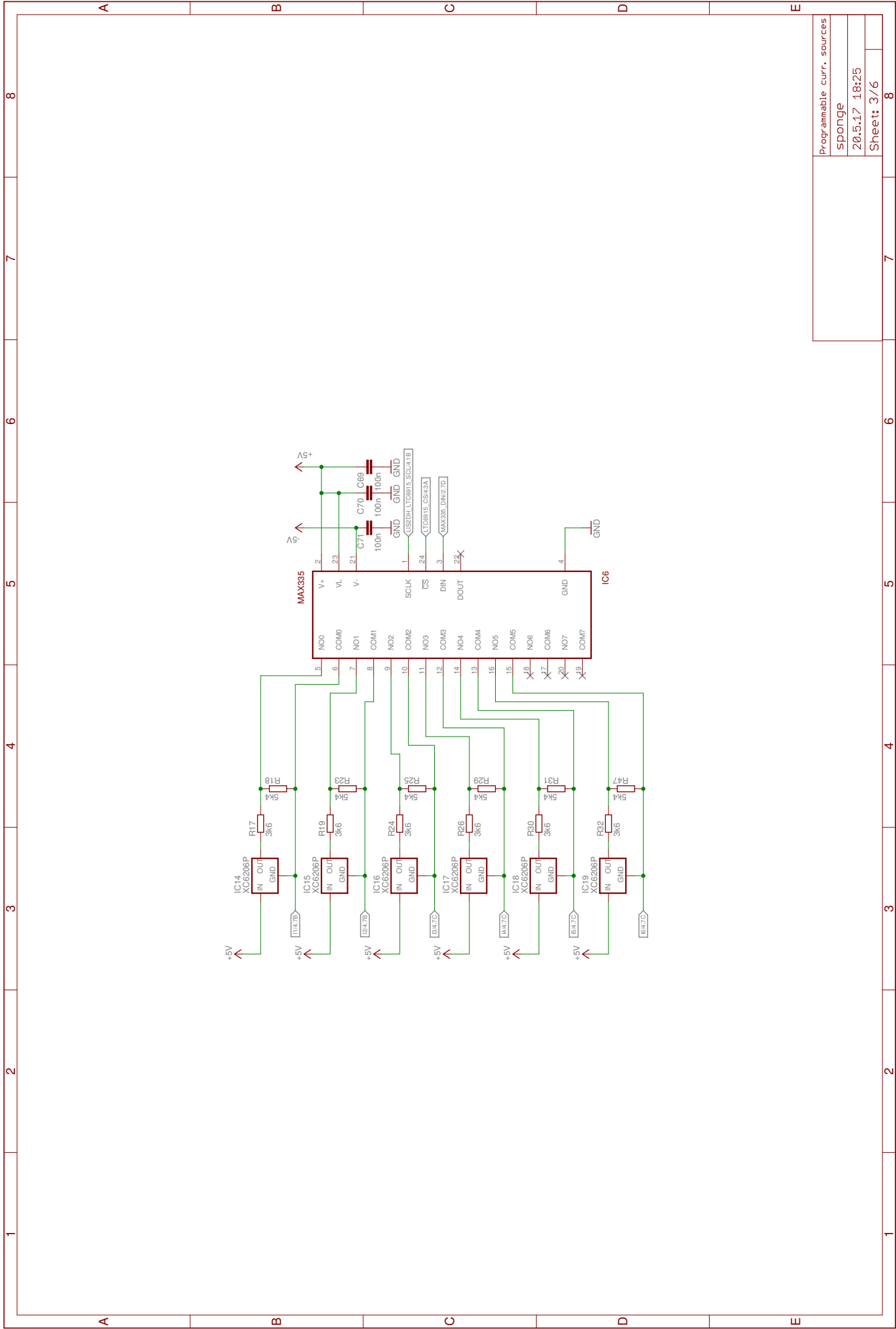
AD7606
sponge
20.5.17 18:25
Sheet: 1/6

1 2 3 4 5 6 7 8

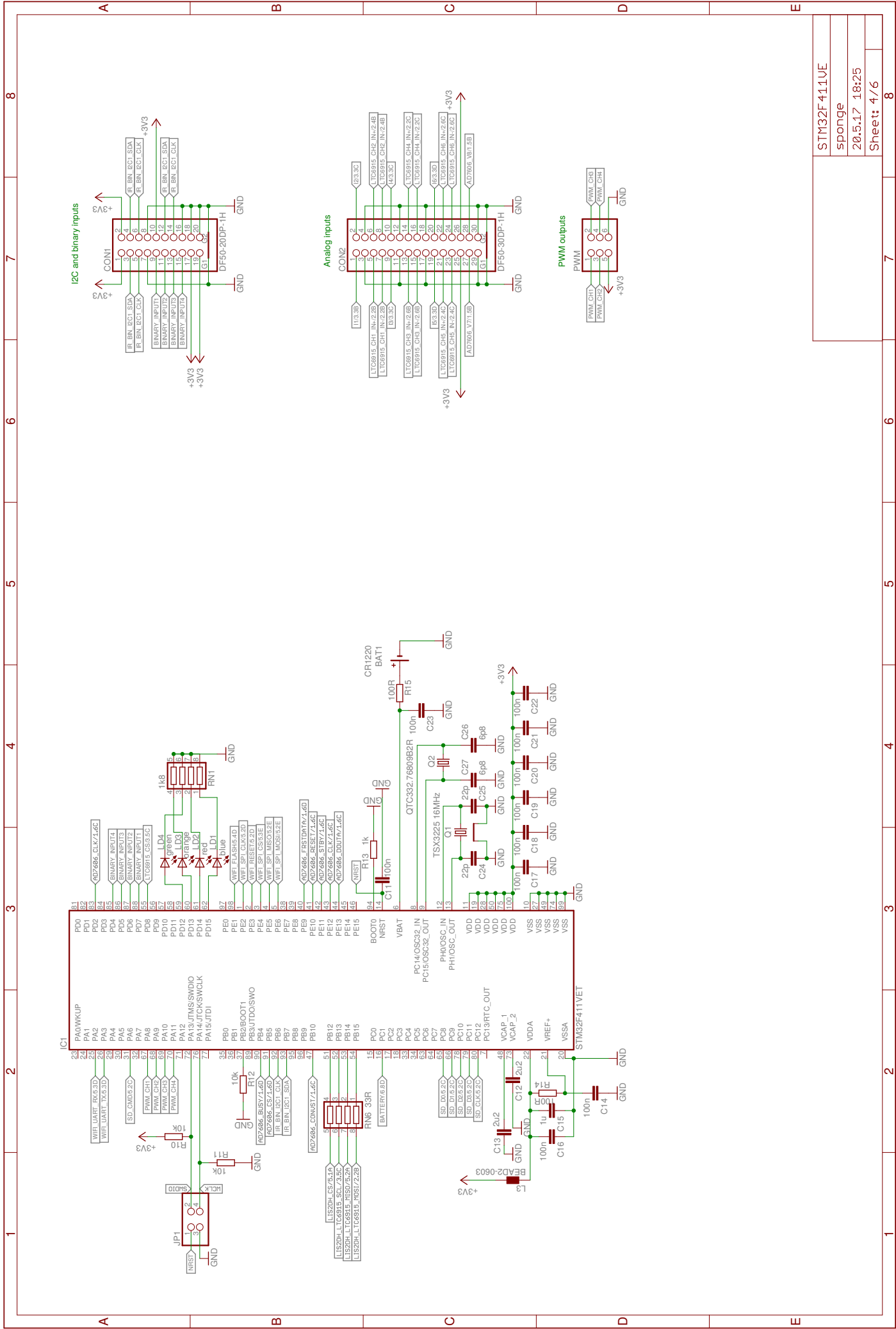
A B C D E



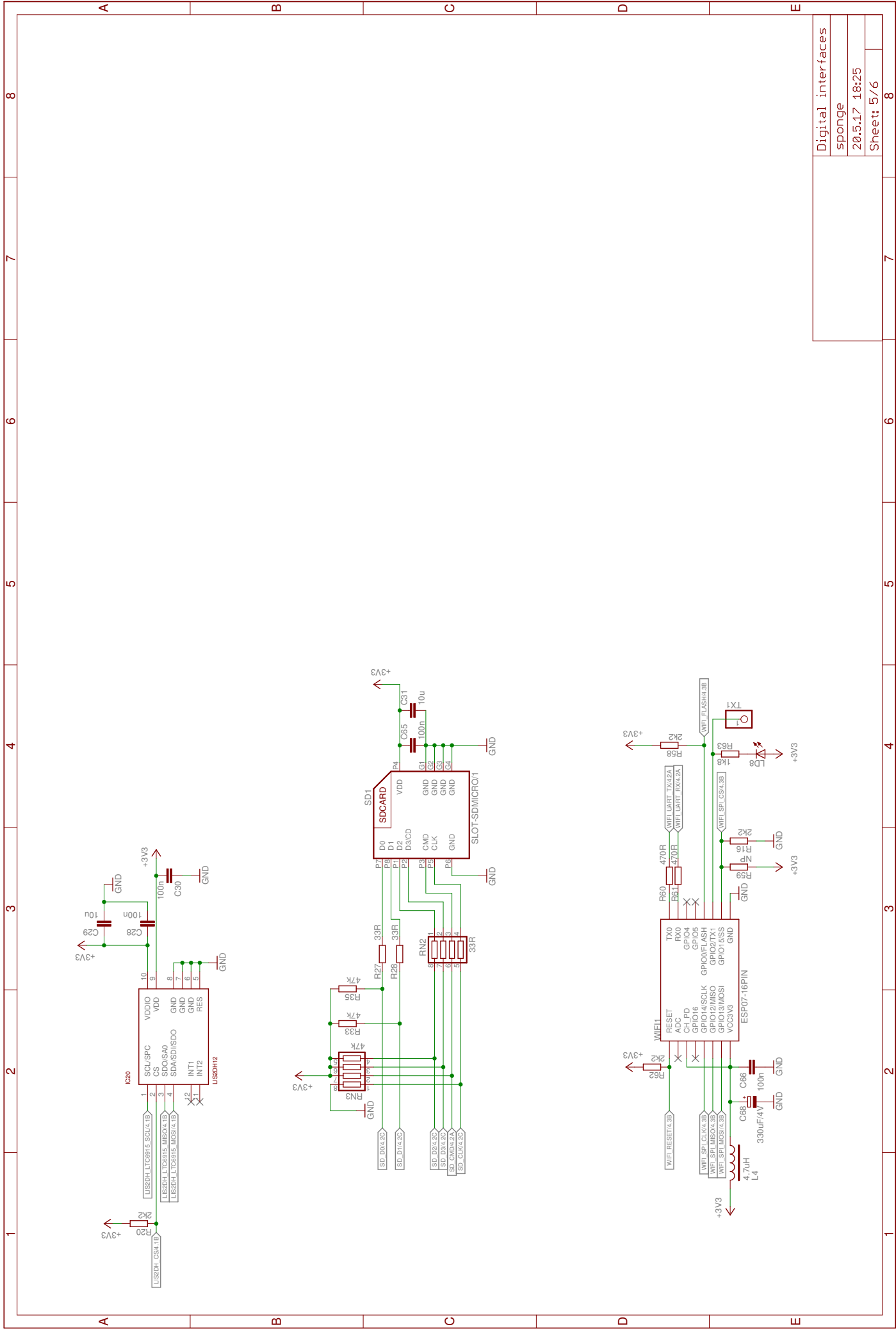
LTC6915
sponge
20.5.17 18:25
Sheet: 2/6



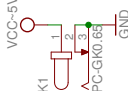
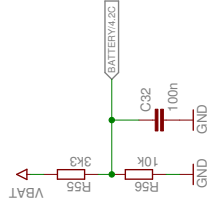
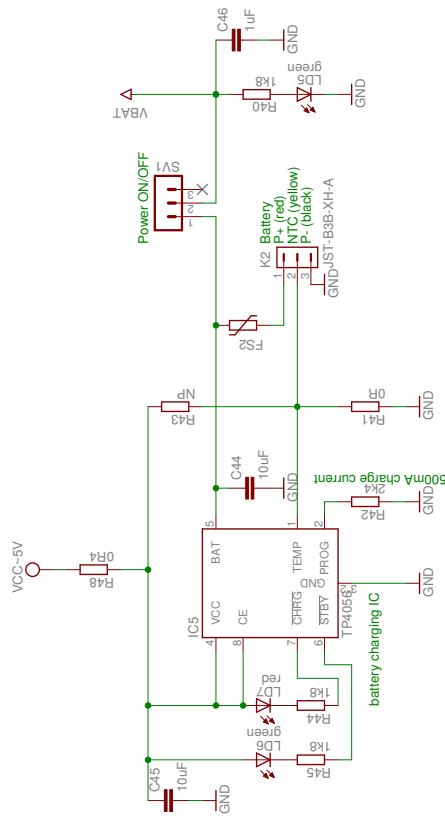
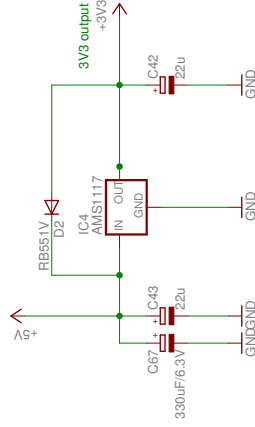
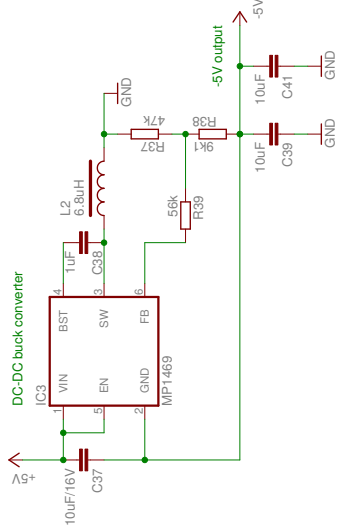
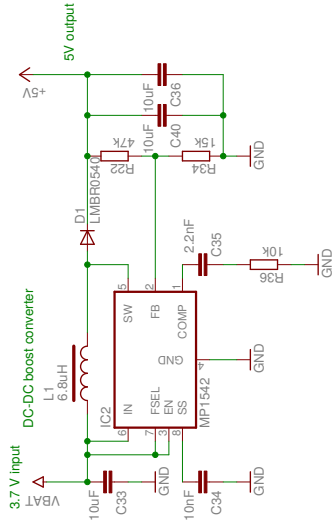
Programmable curr. sources
 sponge
 20.5.17 18:25
 Sheet: 3/6



STM32F411UE
sponge
20.5.17 18:25
Sheet: 4/6



Digital interfaces	
sponge	
20.5.17 18:25	
Sheet: 5/6	



■ D Content of the CD

- Datasheets: datasheets of the used components.
- Board: schematic and layout in the Eagle software.
- TMP006: schematic and layout of board for IR temperature sensor in the Eagle software.
- STM32F411VE: firmware for the STM32F411VE microcontroller (in the AC6 software).
- ESP8266: firmware for the ESP8266 microcontroller.
- Text: the text of the thesis.